

Copyright
by
Seunghyun Chun
2011

**The Dissertation Committee for Seunghyun Chun Certifies that this is the approved
version of the following dissertation:**

**Analysis of Classical Root-Finding Methods Applied to Digital
Maximum Power Point Tracking for Photovoltaic Energy Generation**

Committee:

Alexis Kwasinski, Supervisor

W. Mack Grady

Mircea Driga

Gary Hallock

Jaesoo Byoun

**Analysis of Classical Root-Finding Methods Applied to Digital
Maximum Power Point Tracking for Photovoltaic Energy Generation**

by

Seunghyun Chun, B.S.; M.S.

Dissertation

Presented to the Faculty of the Graduate School of
The University of Texas at Austin
in Partial Fulfillment
of the Requirements
for the Degree of

Doctor of Philosophy

The University of Texas at Austin

August 2011

Dedication

This work is dedicated to my wife Hyejin Oh, son Jason Chun, daughter Joanna Chun, and my loving parents Dr. Chang Hwan Chun and KeeWha Lee

Acknowledgements

How can I begin to thank the numerous amounts of people that have helped me in so many different ways in supporting and encouraging my studies. It's with great pleasure I take this space to thank you all for making this possible and a dream come true.

First and foremost I'd like to express my sincere gratitude to my Ph.D advisor Professor Alexis Kwasinski for his assistance and guidance through my doctoral studies. What I have achieved academically would not have been possible without the kind and sometimes well needed kick in the right direction comments and encouragements he provided. He not only saw the potential in me but never stopped believing in me and also continuously encouraged me to do better. I am grateful and honored to have been his student.

Next I wish to thank the members of my committee who served on my Ph.D dissertation committee; starting with Professor. W. Mack Grady who I would like to thank for the encouragement and suggestions in the area of solar power and also for the awesome courses I took, coming from a different area other than the energy systems area, taught by him where I gained a great amount of insight of power systems. Also I am thankful that he allowed me to use his solar arrays for many experiments I had to do while we were installing ours on the roof of ENS. I'd also like to thank Professor Mircea Driga for the discussions we had and the advises he provided in finding optimization methods to the proposed MRFM method. I also would like to thank him for his electric

machine course I took which provided a platform for my future research interests. Special thanks to Professor Gary Hallock who let me supervise a few students of his to help me test and compare my DMPPT method with the one used by the UT Solar Car Project. Also the help he provided during the personally difficult semesters I had while I was his Teaching Assistant. And the last member of my dissertation committee Dr. Jaesoo Byoun whom I had the privilege of knowing personally during my studies at UT. I am deeply grateful for his guidance and encouragement during the most difficult times of my grad school period. You were truly a God send. I will never forget the selfless help you provided, the many late hour discussions we had and the great memories our families shared together.

I'd also like to thank Professor Anthony Donaldson and the faculty of the School of Engineering at California Baptist University for sharing their vision and passion with me and giving me the opportunity to join them to continue to educate Christian engineers and leaders with a God given purpose in life.

I would also like to acknowledge and thank National Instruments for the support provided in my research and experiments and especially Eric Dean, for the continued technical support and discussions we shared about cool ideas for engineering education.

My deepest thanks also goes out to my friends and colleagues of the Power Electronics Research Group. They have been the ones who not only provided help in my research but their friendship and support whenever I needed a time away from it all. Thank you Dr. Chimaobi Onwuchekwa, Sheng Yang Yu, Ruichen Zhao, Harsha Kumar, Vaidyanathan Krishnamurthy, Amir Toliyat and Vaibhav Sule. And also to the members

of UT Energy Systems Track Korean Students Association I'd like to extend a special thanks to Jin Hur, Dr. Seung Hoon Choung, Cheol Hee Cho, Dr. Wonjin Cho, Heejung Park, Sungwoo Bae, Juyoung Jung, Junsuk Song, Doohee Lee, Jihoon Yoon, Young Sung Kwon, Joohyun Jin, Joon Hyun Kim and Han Kang. Special thanks to my good friend Sanmi Koyejo who has been there from the beginning through it all with me. And to Melanie Gulick. How can I forget the guidance and encouragement you provided during the most difficult times of my academic years at UT. I believe the ECE department at UT is so much a better place with you helping the students with grad school life. Thank you!

Also I'd like to express my gratitude to Pastor Keeyoung Jung and the members of Evergreen Gospel Church of Austin for their constant prayers for not only my studies but also everything else I needed prayer in my life in Austin. Especially the leaders Won Lee, Japil Lee, Byung Jeong Min, Seungmin Lee and Yonghan Kang who were always there to encourage and pray and serve me and my family. I am truly grateful and humbled by your love and commitment.

And finally I want to thank my loving family, my parents Chang Hwan Chun, KeeWha Lee and my sister Dahyun Chun. Thank you for always loving, praying and supporting me through this difficult Ph.D degree process. I can only hope to be as good parents like you and to support and raise my children with love like you did for me. Also I'd like to thank my parents-in-law Taikgil Oh and Meeyoung Kim for their support, love and prayers. And special thanks to my brother-in-law Euisang (Sean) Oh for all the fun we had during the breaks between my work. And to the love of my life, my wife Hyejin

Oh thank you for always being there for me and believing in me, praying for and supporting me during the good and bad times. Also I thank you for all the hardships you had to endure while raising our beautiful children alone when I was away in the lab. Your love and support is invaluable to me. And to the great joy of my life, my son Jason and daughter Joanna. I thank you for the many days and nights you all had to sacrifice and manage without your father to play with, or call out to when you needed help or tuck you in to bed. I am thankful and sorry. And last of all I give all my praise and utmost thanks, all honor and glory to God who brought me this far faithfully with a purpose for my life and continues to guide my every step every day. Hallelujah!!

Analysis of Classical Root-Finding Methods Applied to Digital Maximum Power Point Tracking for Photovoltaic Energy Generation

Seunghyun Chun, Ph. D

The University of Texas at Austin, 2011

Supervisor: Alexis Kwasinski

This dissertation examines the application of various classical root finding methods to digital maximum power point tracking (DMPPT). An overview of root finding methods such as the Newton Raphson Method (NRM), Secant Method (SM), Bisection Method (BSM), Regula Falsi Method (RFM) and a proposed Modified Regula Falsi Method (MRFM) applied to photovoltaic (PV) applications is presented. These methods are compared among themselves. Some of their features are also compared with other commonly used maximum power point (MPP) tracking methods. Issues found when implementing these root finding methods based on continuous variables in a digital domain are explored. Some of these discussed issues include numerical stability, digital implementation of differential operators, and quantization error. Convergence speed is also explored. The analysis is used to provide practical insights into the design of a DMPPT based on classical root finding algorithms. A new DMPPT based on a MRFM is proposed and used as the basis for the discussion. It is shown that this proposed method is faster than the other discussed methods that ensure convergence to the MPP. The

discussion is approached from a practical perspective and also includes theoretical analysis to support the observations. Extensive simulation and experimental results with hardware prototypes verify the analysis.

Table of Contents

List of Figures	xiii
Chapter 1: Introduction	1
1.1 Overview	1
1.2 Scope of this Research	9
1.3 Dissertation Organization	9
Chapter 2 : Photovoltaic Module Model.....	11
2.1 Introduction.....	11
2.2 Photovoltaic Cell Mathematical Model	11
2.3 Photovoltaic Characteristic	14
Chapter 3 : Root Finding Algorithms	19
3.1 Introduction.....	19
3.2 Open Methods.....	20
3.2.1 Newton Raphson Method (NRM).....	20
3.2.2 Secant Method (SM).....	22
3.3 Bracketing Methods.....	24
3.3.1 Bisection Method (BSM).....	24
3.3.2 Regula Falsi Method (RFM)	25
Chapter 4 : Modified Regula Falsi Method(MRFM).....	29
4.1 Introduction.....	29
Chapter 5 : Analog Algorithms Application to Digital MPPT	33
5.1 Introduction.....	33
5.2 Numerical Analysis.....	33
5.2.1 Numerical Stability	34
5.2.2 Quantization Error	34
5.2.3 Discretization Error.....	36
5.3 Application to MRFM DMPPT	36
5.4 Simulation-Based Result.....	47

5.4.1 Simulation-base comparison.....	57
Chapter 6 : Experimental Results	60
6.1 Experiment System	60
6.1.1 Photovoltaic Module.....	61
6.1.2 DC-DC Converter	61
6.1.3 Control System.....	62
6.2 Experimental Results	64
Chapter 7 : Shading Effects	71
7.1 Introduction.....	71
7.2 Multiple Input Converter	76
7.3 DMPPT using MIC	77
7.3.1 Simulation Results	81
Chapter 8 : Conclusion.....	83
8.1 Summary	83
8.2 Future Work	85
Appendix A.....	86
A.1 Matlab Code.....	86
A.2 LabVIEW vi's	104
References.....	108
Vita	117

List of Figures

Figure 1.1 : Technical Advances made in PV Model [3]	1
Figure 1.2 : PV System Capital Cost [5].....	2
Figure 1.3 : Voltage Feedback System Configuration.....	4
Figure 1.4 : Power Feedback System Configuration	5
Figure 1.5 : Concept comparison between (a) conventional MPPT method and (b) Root.....	7
Figure 2.1: Ideal PV cell[29]	12
Figure 2.2 : Practical PV cell electrical model [29].....	13
Figure 2.3: Irradiance effect on P-V Characteristic at Constant Temperature (25°C)	15
Figure 2.4: Irradiance effect on I-V Characteristic at Constant Temperature (25° C)	16
Figure 2.5: Temperature Effect on P-V Characteristic at constant irradiance (1000W/m ²).....	16
Figure 2.6: Temperature Effect on I-V Characteristic at constant irradiance (1000W/m ²).....	17
Figure 2.7: Maximum Power Point for different curves of a PV module.....	17
Figure 3.1: NRM x^* is represented by the cross.....	21
Figure 3.2: NRM (wrong initial value choice).....	22
Figure 3.3: Secant Method (SM)	23
Figure 3.4 : Bisection Method(BSM)	25
Figure 3.5: Regula Falsi (RFM).....	26
Figure 4.1 : Number of iterations required to reach 99.9% of the root of	30

$f(x) = \ln(x)$ for different weight(γ) factors	30
Figure 4.2 : Modified Regula Falsi (MRFM) DMPPT	31
Figure 4.3 : MRFM Flow Chart.....	32
Figure 5.1: Termination condition comparison between two irradiance levels.....	38
Figure 5.2: dP/dV , d^2P/dV^2 , and d^3P/dV^3 of PV module at 200W/m^2 , 25°C	42
Figure 5.3: dP/dV , d^2P/dV^2 , and d^3P/dV^3 of PV module at 1000W/m^2 , 25°C (STC).....	43
Figure 5.4: Error caused by a small ΔV value	45
Figure 5.5 : Perturb & Observe Method MPPT @ 1000W/m^2	49
Figure 5.6 : Perturb & Observe Method MPPT in Dynamic Environment	50
Figure 5.7 : INC MPPT @ 1000W/m^2 ($\Delta D=0.01$)	50
Figure 5.8 : INC MPPT in Dynamic Environment ($\Delta D=0.01$)	51
Figure 5.9 : INC MPPT @ 1000W/m^2 ($\Delta D=0.005$)	51
Figure 5.10 : INC MPPT in Dynamic Environment ($\Delta D=0.005$)	52
Figure 5.11 : Secant Method MPPT @ 1000W/m^2 (Initial Point near MPP).....	52
Figure 5.12 : Secant Method MPPT in Dynamic Environment (Initial Point near MPP)	53
Figure 5.13 : Secant Method MPPT Initial Point far from MPP	53
Figure 5.14 : Bisection Method MPPT @ 1000W/m^2	54
Figure 5.15 : Bisection Method MPPT in Dynamic Environment	54
Figure 5.16 : Regula Falsi Method MPPT @ 1000W/m^2	55
Figure 5.17 : Regula Falsi Method MPPT in Dynamic Environment	55
Figure 5.18 : Modified Regula Falsi Method MPPT @ 1000W/m^2	56
Figure 5.19 : Modified Regula Falsi Method MPPT in Dynamic Environment ...	56
Figure 5.20 : Comparison of the Root Finding Methods DMPPT through simulations	57

Figure 6.1 : Experiment system setup	60
Figure 6.2 : Close up of experimental setup	61
Figure 6.3 : Boost Converter Circuit with a PV module as a source	62
Figure 6.4: DMPPT Experimental Setup for DMPPT	64
Figure 6.5 : DPWM signal from the FPGA	67
Figure 6.6 : Experimentally generated results for the P&O DMPPT	67
Figure 6.7 : Experimentally generated results for the INC DMPPT, $\Delta D=0.01$	68
Figure 6.8 : Experimentally generated results for the INC DMPPT, $\Delta D=0.005$	68
Figure 6.9 : Experimentally generated results for the SM DMPPT	69
Figure 6.10 : Experimentally generated results for the BSM DMPPT	69
Figure 6.11 : Experimentally generated results for the RFM DMPPT	70
Figure 6.12 : Experimentally generated results for the MRFM DMPPT	70
Figure 7.1 : PV module divided into 4 subsections	71
Figure 7.2 : (A) PV Module Divided into Subsections (B) Partially shaded PV Module w/o Bypass Diode (C) Partially shaded PV Module w/ Bypass Diode.....	72
Figure 7.3 : I-V Plot for Unshaded & Partially Shaded Case w/o Bypass Diode..	73
Figure 7.4 : P-V Plot for Unshaded & Partially Shaded Case w/o Bypass Diode.	75
Figure 7.5 : I-V Plot for Unshaded & Partially Shaded Case w/ Bypass Diode....	75
Figure 7.6 : P-V Plot for Unshaded & Partially Shaded Case w/ Bypass Diode...	76
Figure 7.7 : Multiple Input Boost Converter connected to subsections of a PV Module	77
Figure 7.8 : DMPPT System with Partial Shading	79
Figure 7.9 : DMPPT System with Partial Shading utilizing Multiple Input Boost Converter.....	80

Figure 7.10 : P-V plot of simulated PV module with partial shading.....	81
Figure 7.11 : Simulation result of MRFM DMPPT for the system in Fig. 7.8.....	82
Figure 7.12 : Simulation result of MRFM DMPPT for the system in Fig. 7.9(MICs)	82
Figure A2.1 : VI of MRFM DMPPT	104
Figure A2.2 : VI of Monitoring the Generated Power, Panel Voltage and Panel Current	105
Figure A2.3 : VI of PV Module I-V sweep	106
Figure A2.4 : VI of DPWM generating code that is embedded in FPGA of NI CompactRIO	107

Chapter 1: Introduction

1.1 OVERVIEW

The world's energy demand is projected to increase 1.5% yearly between 2007 and 2030 [1]. Yet, since fossil fuels remain the world's main energy source, there is increased concern on how to address the dilemma of meeting this expected energy demand without affecting the environment. It is expected that increased utilization of sustainable energy sources will help to address this issue [2]. In particular, technical advances [3] in PV energy generation shown in Fig. 1.1, as one of the main sustainable

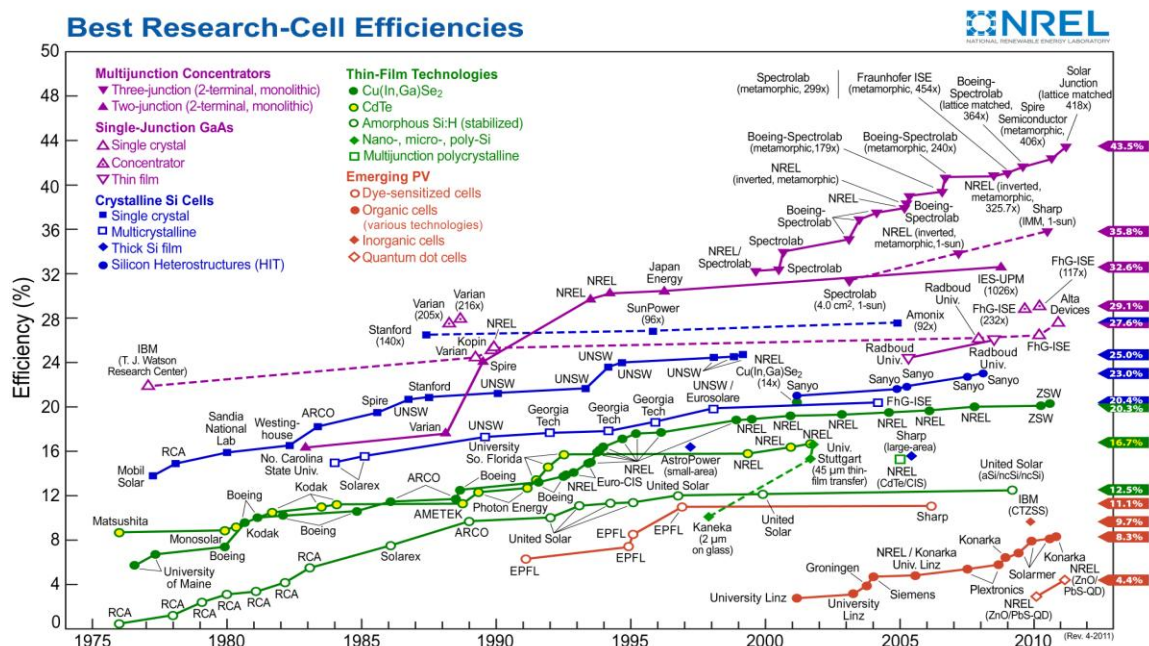


Figure 1.1 : Technical Advances made in PV Model [3]

energy sources, have made it a potentially attractive solution for this issue [4]. However, PV modules' high installation and capital costs as shown in Fig. 1.2 still create some barriers that limit their application as a widespread solution that would convert predominately resource-consuming present electric generation sources into a power generation base with sustainable characteristics.

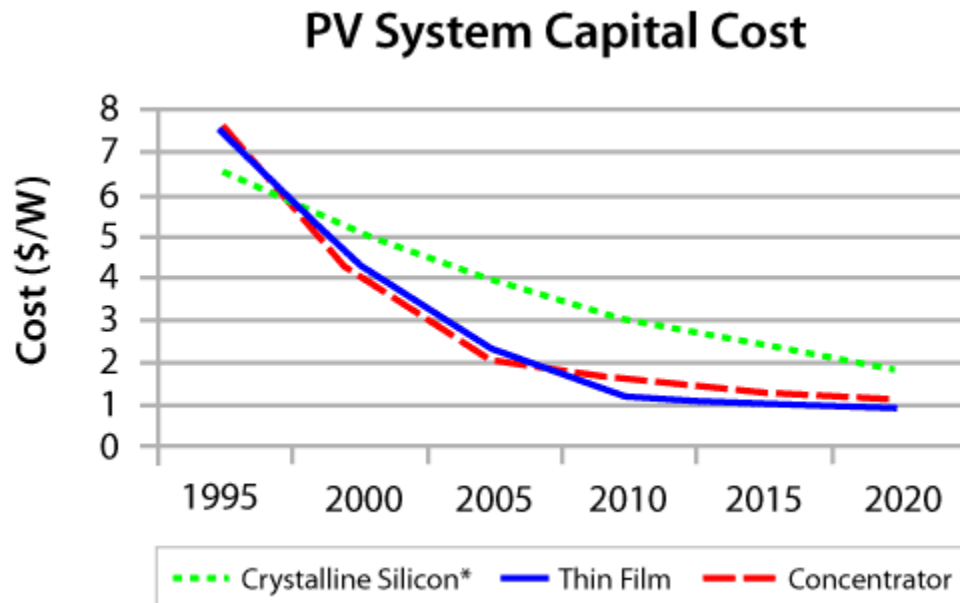


Figure 1.2 : PV System Capital Cost [5]

Hence, in order to make PV generation a truly attractive sustainable choice that contributes to meet future energy demands, it is necessary to maximize its utilization. In order to obtain the maximum possible power output from PV modules, it is necessary to operate them at their absolute maximum power point (MPP) where the derivative of the output power with respect to the output voltage—i.e., dP/dV — is zero. However, PV sources have an output current – voltage (I-V) characteristic that is nonlinear and varies

with different irradiance, temperature and load conditions. Our optimization problem and motivation for this work is to track and find this MPP and to force the PV panel to operate at this point in the fastest and more stable way possible.

In recent years numerous MPPT methods have been developed [6]. The majority of them are based on searching the MPP by utilizing the sign of dP/dV as an indication of the search direction. Also digital implementations of MPPT have gained popularity because of the wide selection and technological advances of low-cost, microcontrollers and digital signal processors, which have enabled researchers the freedom to change the control algorithm, without extensively modifying the system hardware platform. All these advantages have encouraged research not only in digital controllers in general applications [7], but also in sustainable systems applications, such as solar power in [8] [9], wind power in [10] and a thermoelectric battery energy storage system [11]. All of these utilize a digital signal processor (DSP) to process sampled signals. But a thorough analysis of the previously discussed issues encountered when designing a DMPPT system where not provided. Thus, the analysis provided in this paper tackling these issues is relevant when designing and implementing a DMPPT system.

There exist many methods to realize MPPT [12] although many methods are either a slight modification or a variant of two methods [6] [12]-[13]. MPPT methods can be grouped into two major approaches. The first group of methods is based on voltage feedback [13]-[15]. In these methods a predetermined reference voltage is compared with the PV module voltage in a feedback loop shown in Fig. 1.3. Voltage feedback methods enable one to choose a desirable operating point for unknown or varying load conditions,

but they lead to energy inefficiencies because they are not able to adjust to changing environmental conditions

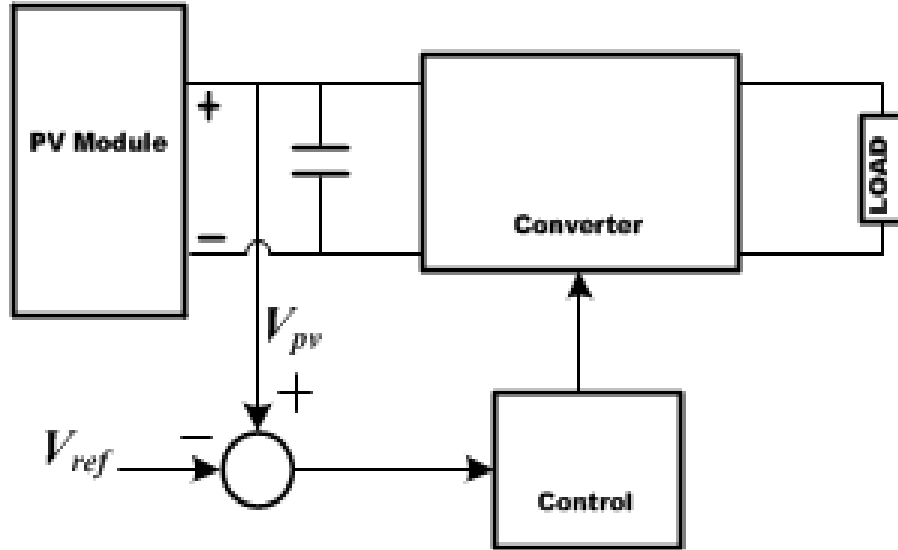


Figure 1.3 : Voltage Feedback System Configuration

A modification was done in [16] to change the reference voltage at periodic moments in time by momentarily interrupting the system operation and sampling the PV module open circuit voltage in order to update the reference voltage—usually around 70 to 80% of the PV module open circuit voltage (V_{OC}). A disadvantage of the method in [16] is that energy is wasted during system momentary interruptions. Another problem is that the method in [16] is sensitive to aging and dust accumulation, which leads to the issue that the reference voltage may no longer be taken as 70 – 80 % of V_{OC} .

The second group of methods is the power feedback methods, which are based on calculating the power by sensing the voltage and current generated from the PV module shown in Fig. 1.4.

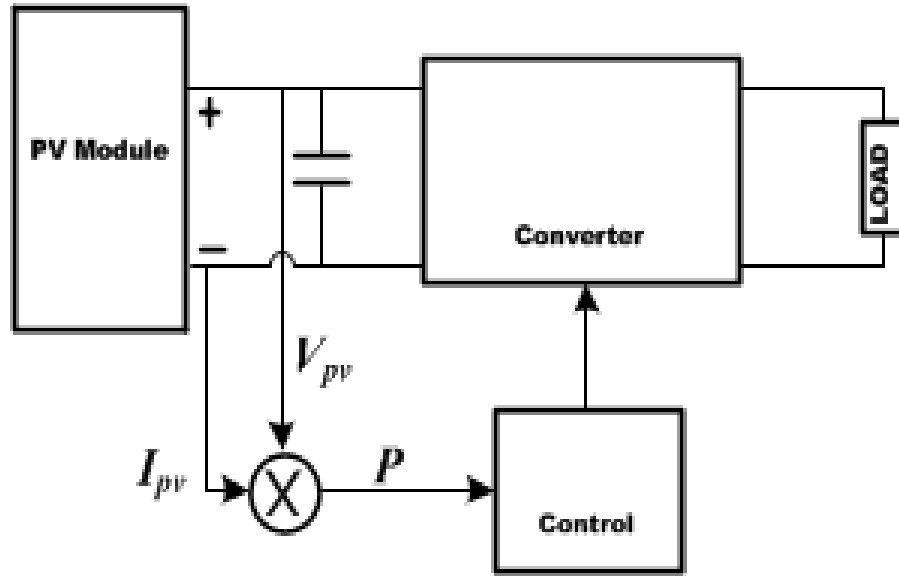


Figure 1.4 : Power Feedback System Configuration

Then, the majority of the algorithms attempt to keep the ratio dP/dV at zero. The Perturb and Observe method (P&O) [17]-[19] is a popular technique which is simple to implement digitally. But this method oscillates around the MPP causing energy losses. Also, at rapidly changing conditions, the operating point can move away from the MPP. An improved P&O method was presented in [18] to solve this problem but difficulties in choosing threshold values were left unaddressed. In [19] an optimization of the P&O method is presented in which the sampling frequency and the fix step size of the method are optimized to take into consideration the dc-dc converter interface and environmental effects. This optimization minimizes the oscillation around the MPP and prevents the system from failing in a rapidly changing environment. Hence, efficiency and stability of the P&O method are improved. However, this optimized strategy is a complex tuning process that eliminates the simple implementation merit of the P&O method and does not

fully eliminates the oscillation problem. The Incremental Inductance Method (INC) presented in [20] is another algorithm with the same objective of keeping $dP/dV=0$ but uses an incremental and instantaneous relation based on output current and voltage, I and V , respectively, equal to $dI/dV+I/V=0$. It still has the oscillation problem around the MPP and the step size is fixed. Oscillation around the MPP can be reduced with a small step size, but it leads to slow convergence to the MPP. Both the P&O and INC methods are considered as an elimination method or a trial and error process. Since both are fix step size methods, reaching the MPP or convergence is dependent on the initial point of the tracking process and the size of the step. In most cases if, in an attempt to reach the MPP faster, the step size is too large for both the P&O and INC methods, it will oscillate around the MPP. Classical root finding algorithms are considered iterative interpolation methods with variable step sizes. The use of variable step sizes in root finding algorithms indicate an inherent fundamental difference with the P&O and INC methods and prevent comparing their convergence speeds in a formal way on equal basis. However, it is possible to identify that owed to their variable step size one advantage of root finding based algorithms over the P&O and INC methods is that root finding techniques avoid issues with oscillations. Like the P&O and INC methods, there are many other MPPT algorithms built around the idea of using $dP/dV=0$, followed by evaluating $dP/dV<0$ or $dP/dV>0$ as the decision criterion for the next iteration step of an algorithm. The steepest descent method is widely used and presented in [21]. It is a variable step approach to MPPT that provides convergence speed to MPP close to that of the Newton method

approach. However, finding the step size factor is a difficult process and must be tuned for different PV modules.

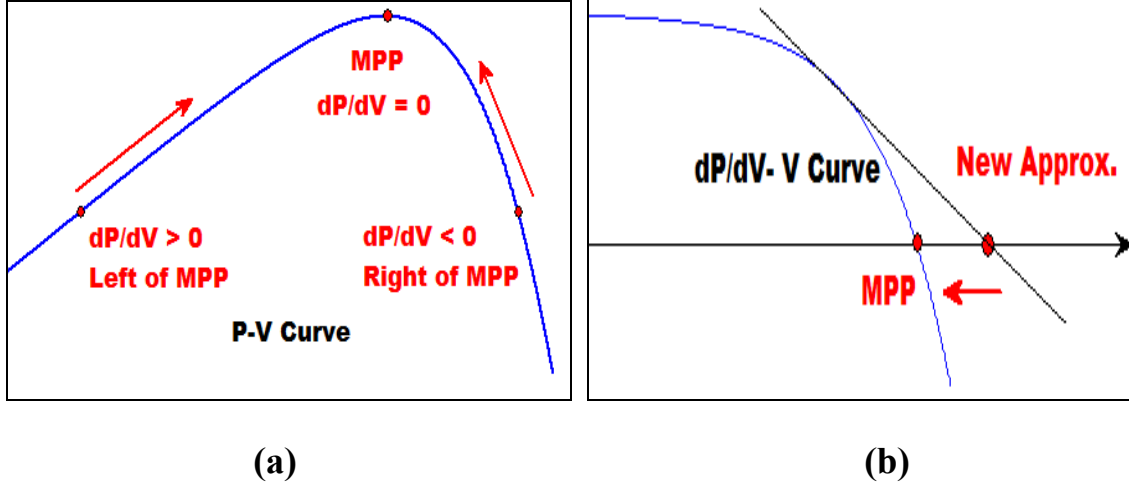


Figure 1.5 : Concept comparison between (a) conventional MPPT method and (b) Root finding Algorithm approach.

Of particular interest in this work is a newly proposed digital maximum power point tracking (DMPPT) based on a root finding MRFM. The MRFM is based on the same problem formulation than that specified in other power feedback algorithms: searching for $dP/dV=0$, yet the approach used in here considers the search for $dP/dV=0$ as a root finding mathematical problem. The proposed MRFM DMPPT method is well suited for MPPT because root convergence is guaranteed without observing oscillations around the MPP as observed in aforementioned methods. Unlike the optimized P&O [19], the proposed MRFM DMPPT method does not need a complex tuning process and is guaranteed to converge with no oscillation. In order to provide a complete approach to the discussion and to understand the advantages of the MRFM, this paper explores other

MPPT algorithms based on root finding methods. Thus, it is also relevant to consider applied research in practical optimization techniques to MPPT algorithms [21]-[24]. The method presented in [20] provides a fast convergence in cases where the initial search point is close to the MPP. Yet, it also has the possibility of diverging catastrophically. It also includes the need for calculating not only the first derivative but also the second derivative at any operating point which results in convergence error and accuracy compromises. The recent approach presented in [23] solves the diverging issue of [22] but convergence to the MPP is slow when compared to [21] and [22]. In contrast, the MRFM presented here and in [24] provides a faster convergence to MPP than in [23] which increases the efficiency of energy extraction from PV panels and achieves better performance under varying environmental conditions.

In [25] the effects due to partial shading of the PV panel with tree branches, leaves or clouds are presented. This causes a decrease in generated power from the PV and also multiple MPPs to occur. In order to present a common comparison approach with other root-finding algorithms, the work presented herein assumes that only a global MPP exists, with no other local MPP present. This approach can still address the aforementioned partial shading issues through hardware by dividing PV arrays and modules in sections, and making each of these sections the input of a multiple input converter, such as those proposed in [26]-[28]. Detailed evaluation of the implementation of such approach through multiple-input converters is covered along with the analysis of root finding MPP algorithms with local maxima.

1.2 SCOPE OF THIS RESEARCH

This dissertation discusses the application of classical mathematical root finding optimization methods for maximum power point tracking (MPPT) of photovoltaic (PV) systems. Since in this work these methods are implemented digitally, practical issues encountered when digitally implementing a method originally based on a continuous domain are also explored. In particular, this work discusses potential errors inherently caused by digital processes not substantially explored in previous MPPT papers, such as algorithm numerical stability, quantization error, and discretization error analysis. Other important issues found when power electronics systems are utilized as an interface for a sustainable energy application, such as choosing the specification for the digital pulse width modulation (DPWM) and converter parameters are also addressed and commented. Also a new MPPT strategy based on a Modified Regula Farsi Method (MFRM) is presented and studied according to the analysis mentioned above.

1.3 DISSERTATION ORGANIZATION

This paper is structured as follows: Chapter 2 introduces preliminary notions and tools that support and provide context for the analysis. In particular, it discusses PV modules model. Chapter 3 delves into the description of the mathematical basis for the root finding algorithms that are studied here for MPPT implementation. In particular, Chapter 4 describes the MRFM that is newly used in here for DMPPT. Chapter 5 discusses the application of classical root finding algorithms to DMPPT. Chapter 6

presents simulation and experimental results comparing each method and its merits are discussed. Preceding analysis is also validated in this Section. Chapter 7 presents the approach made to solve the shading effects problem in MPPT. Finally, Chapter 8 presents the conclusions of this work.

Chapter 2 : Photovoltaic Module Model

2.1 INTRODUCTION

PV is a device that converts sun energy to electric energy. It is constructed with numerous devices called solar cells, which are connected in series and parallel to obtain the voltage and current specifications that are needed. These clusters of solar cells are called modules or panels where in this dissertation we will refer to them as modules. PV modules are then connected in series and parallel to form a PV array. For purposes of simulating PVs with circuits and for research in MPPT algorithms a mathematical model of a PV is essential. The ideal and practical PV cell model and mathematical model are shown in Fig. 2.1-2.2 and (2.1)-(2.6)[29].

2.2 PHOTOVOLTAIC CELL MATHEMATICAL MODEL

Figure 2.1 shows an ideal model of a PV cell which consists of a current source and diode connected in series. But to appropriately model the characteristics of a PV cell for analysis purposes this model needs to be altered to meet our purposes. Figure 2.2 shows a conventional practical model of a PV cell used to provide context for the analysis. This model neglects dynamic effects of self capacitances. Still, the model is accurate enough as an additional tool to support the discussion but its knowledge is not

necessary to realize any of the root finding algorithms later discussed in this paper. From [27] the PV cell mathematical model as shown in Fig. 2.2.

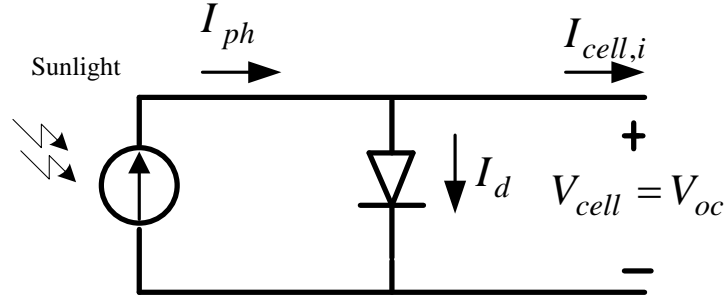


Figure 2.1: Ideal PV cell[29]

$$I_{cell,i} = I_{ph} - I_d \quad (2.1)$$

$$I_d = I_s \left(e^{\frac{qV_{oc}}{nkT}} - 1 \right) \quad (2.2)$$

I_{ph} : Photo Current	q : Electron Charge ($1.6 \times 10^{-19}\text{C}$)
I_d : Shockley Diode Equation	k : Boltzmann Constant ($1.38 \times 10^{-23}\text{J/K}$)
I_s : Diode Saturation Current	T : Temperature in Kelvin
$I_{cell,i}$: Ideal Cell Output Current	n : Diode Scaling Constant
V_{oc} :Open Circuit Cell Voltage	
V_{cell} : Cell Output Voltage	

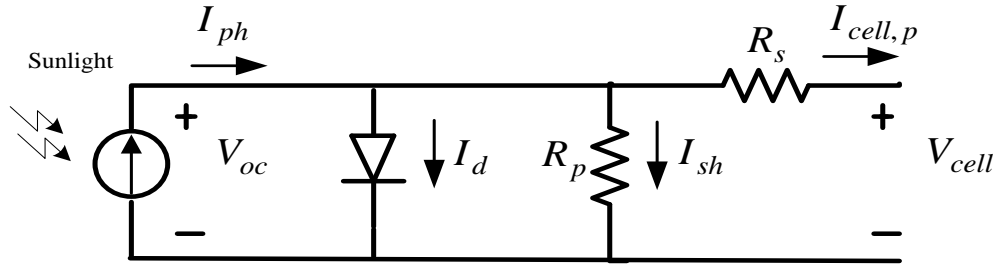


Figure 2.2 : Practical PV cell electrical model [29]

$$I_{cell,i} = I_{ph} - I_d \quad (2.3)$$

$$I_d = I_s \left(e^{\frac{qV_{oc}}{nkT}} - 1 \right) \quad (2.4)$$

$$I_{cell,p} = I_{ph} - I_d - I_{sh} \quad (2.5)$$

$$I_{cell,p} = I_{ph} - I_s \left(e^{\frac{qV_{cell}}{nkT}} - 1 \right) - \frac{V_{cell} + R_s \cdot I_{cell,p}}{R_p} \quad (2.6)$$

I_{ph} : Photo Current	R_p : Shunt Resistor
I_d : Shockley Diode Equation	R_s : Series Resistor
I_s : Diode Saturation Current	q : Electron Charge (1.6×10^{-19} C)
I_{sh} : Current through Shunt Resistor R_p	k : Boltzmann Constant (1.38×10^{-23} J/K)
$I_{cell,i}$: Ideal Cell Output Current	T : Temperature in Kelvin
$I_{cell,p}$: Practical Cell Output Current	n : Diode Scaling Constant
V_{oc} :Open Circuit Cell Voltage	V_{cell} : Cell Output Voltage

Equation (2.6) indicates two main factors affecting the PV cell output: temperature and the solar irradiance. The latter dependence is implicitly included in (2.6), in which I_{ph} is directly proportional to the solar radiation intensity.

2.3 PHOTOVOLTAIC CHARACTERISTIC

Since the amount of sunlight depends on the sun rays angle of incidence with respect to the panel, it is expected that a PV module's output will vary throughout the day and with weather conditions. As a result of these multiple factors affecting PV modules output, their power-voltage (P-V) and current-voltage (I-V) characteristics typically show potential for significant variations depending environmental conditions. Fig. 2.3 to 2.6 exemplify the wide range of possible outputs based on a PV module with the following nominal parameters at the Standard Testing Condition (S.T.C): V_{oc} , the open circuit voltage of the module is 43.2 V, I_{sc} , the short circuit current of the PV module is 5.47 A, P_{max} , the maximum power generated is 170 W and the corresponding voltage (V_{mp}) and current (I_{mp}) are 34.8 V and 4.9 A, respectively. As these figures show, the I-V characteristic is nonlinear and varies with different solar irradiance and temperature conditions.

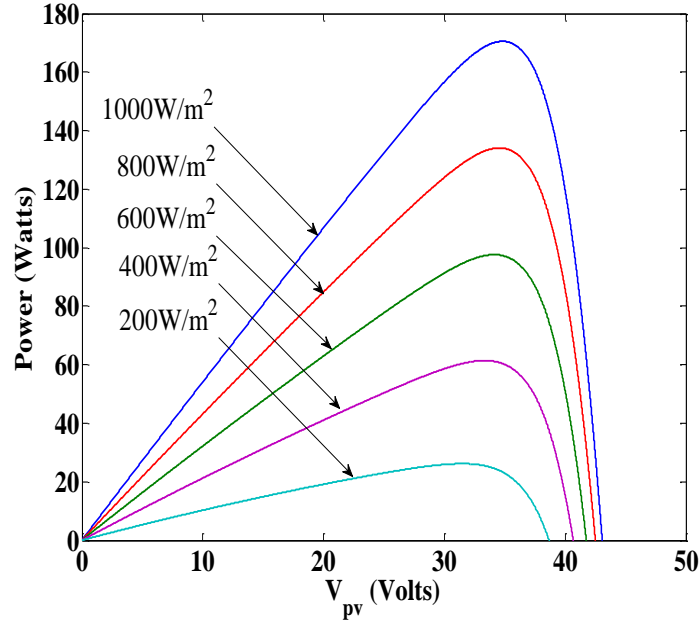


Figure 2.3: Irradiance effect on P-V Characteristic at Constant Temperature (25°C)

Figures 2.3 and 2.5 also indicate that for a given set of conditions (i.e. temperature and solar irradiance) there is a unique operating point for which the output power of the PV module is maximized. This point is called the Maximum Power Point (MPP) and it is achieved for the particular output voltage and current indicated by V_{mp} and I_{mp} , respectively.

Since it is expected that the MPP will vary, it is necessary to implement a control method applied to the power electronic converter interface in order to ensure efficient energy extraction from the PV module. This method is called a Maximum Power Point Tracker (MPPT). As Fig. 2.7 exemplifies, the objective is to track the PV module output to the point where $dP/dV = 0$. The MPPT methods discussed in this paper are classical optimization methods based on a root finding algorithm.

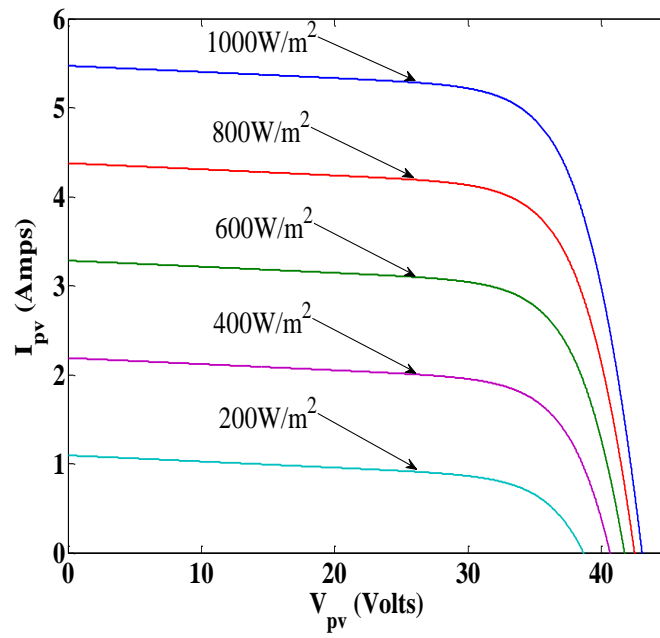


Figure 2.4: Irradiance effect on I-V Characteristic at Constant Temperature (25° C)

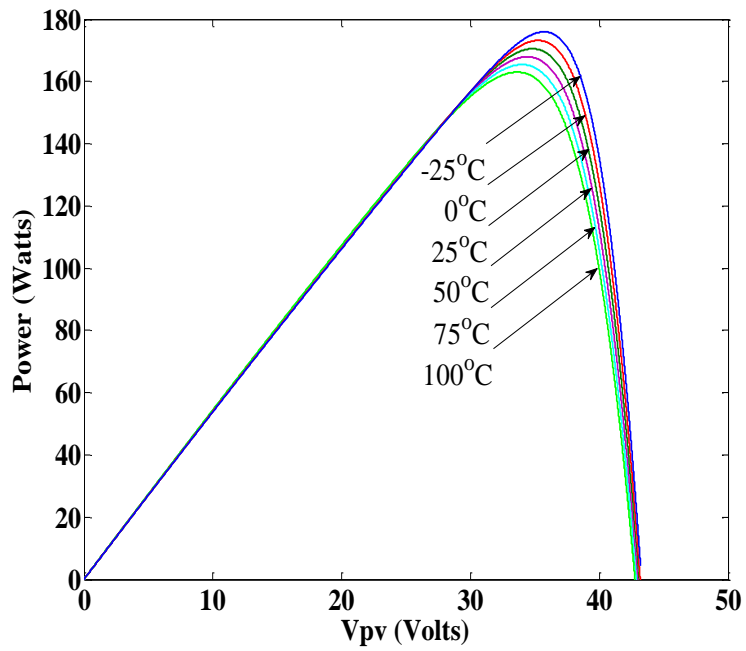


Figure 2.5: Temperature Effect on P-V Characteristic at constant irradiance (1000W/m2)

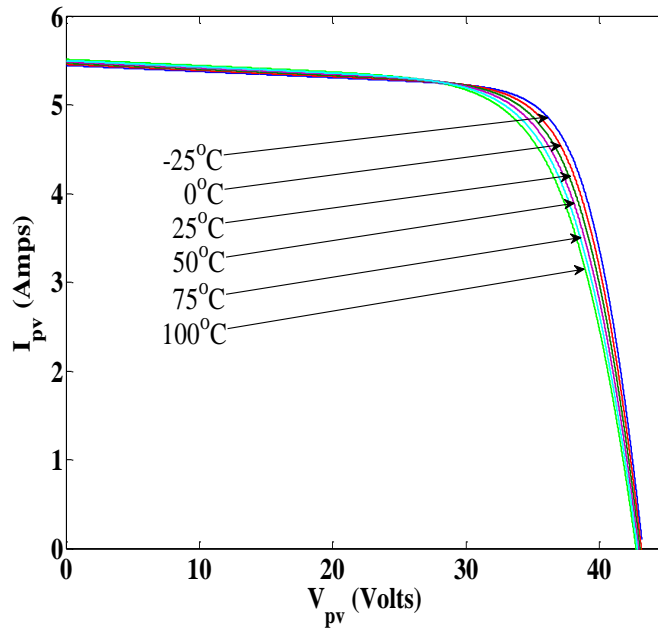


Figure 2.6: Temperature Effect on I-V Characteristic at constant irradiance (1000W/m²)

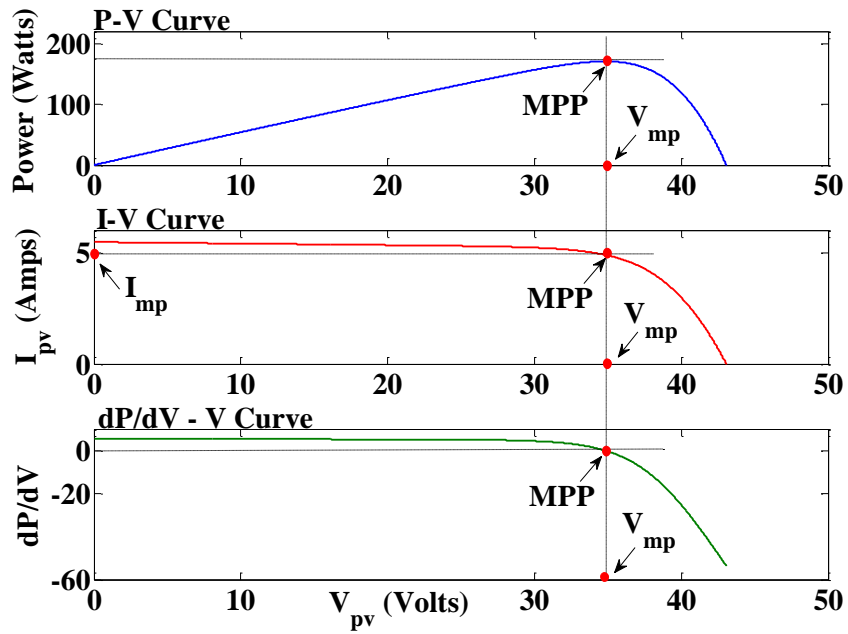


Figure 2.7: Maximum Power Point for different curves of a PV module.

As will be shown in the following sections these methods provide an alternative approach to variable step MPPT and achieve faster MPP tracking compared to fixed step algorithms. These methods, including a newly proposed MRFM, are explained in the next chapter and their main advantages and disadvantages are compared.

Chapter 3 : Root Finding Algorithms

3.1 INTRODUCTION

Since the problem definition specified in Chapter 2 involves finding the MPP—i.e., the point for which the derivative of the output power of a PV module with respect to its output voltage equals zero—it is natural to consider the implementation of conventional root finding algorithms to solve this problem. One advantage of root finding MPPT algorithms is that their iterative approach is not a model-based technique, such as [16], in which PV module parameters, such as R_p or R_s , need to be actually identified or implicitly estimated. On the contrary, root finding algorithms are a completely general approach that search for the zero crossing of a given function—any given function used as the input for the algorithm. Hence, although in this particular case these algorithms are used in a PV application, it is also possible to use the same algorithm in other applications with a physical realization different from the one discussed here, such as finding the MPP of fuel cells. Moreover, since root finding methods provide the theoretical mathematical basis for solving optimization problems (and finding the MPP is merely a particular optimization problem) these methods constitute the origin of many other MPPT methods [21]-[24]. Some of these algorithms [22] [23] have already been discussed in the past as a possible method to find the point where dP/dV equals zero. Others, such as the MRFM, are newly discussed approaches discussed here. Equally

important to understanding these methods, is to study their similarities and differences. Hence, this chapter explores these popular root finding algorithms and compare their performances. Since in these methods the solution is approached through an iterative process, they theoretically require an infinite number of steps to reach the solution with 100% accuracy. In practice, a tolerance condition will determine when the solution is reached. Hence, special attention is paid to evaluating the speed at which each algorithm reaches the tolerated approximation, also known as convergence rate.

3.2 OPEN METHODS

These methods are initiated with one or two initial approximations of the root. Two well known open methods will be introduced and also their application to MPPT will be shown.

3.2.1 Newton Raphson Method (NRM)

In order to find a value x^* that is a root of a function $f(x)$ —i.e., $f(x^*) = 0$ —the NRM is based on performing an iterative calculation given by

$$x_{n+1} = x_n - \frac{f(x_n)}{f'(x_n)} \quad n = 0, 1, 2, \dots \quad (3.1)$$

$$l_n(x) = f'(x_n) \cdot (x - x_n) + f(x_n) \quad n = 0, 1, 2, \dots \quad (3.2)$$

until $|f(x_n)| \leq \varepsilon$ (where ε is the tolerance). In the NRM, the point x_{n+1} is the root for the tangent line $l_n(x)$ to the function $f(x)$ at the point x_n . That is, $l_n(x_{n+1}) = 0$ where $l_n(x)$ is as shown in (3.2). This general process is represented in Fig. 3.1. The main advantage of the NRM is its fast convergence rate (order of convergence 2); the fastest among all the methods considered here. However, the NRM has important disadvantages. An important one of those is that this method requires derivative values of the function at each instance, which adds computational complexity and increase the error in the solution. Another even more important disadvantage, exemplified in Fig. 3.2, is that the algorithm will not converge for most initial value choices in the first iteration to the left of the MPP.

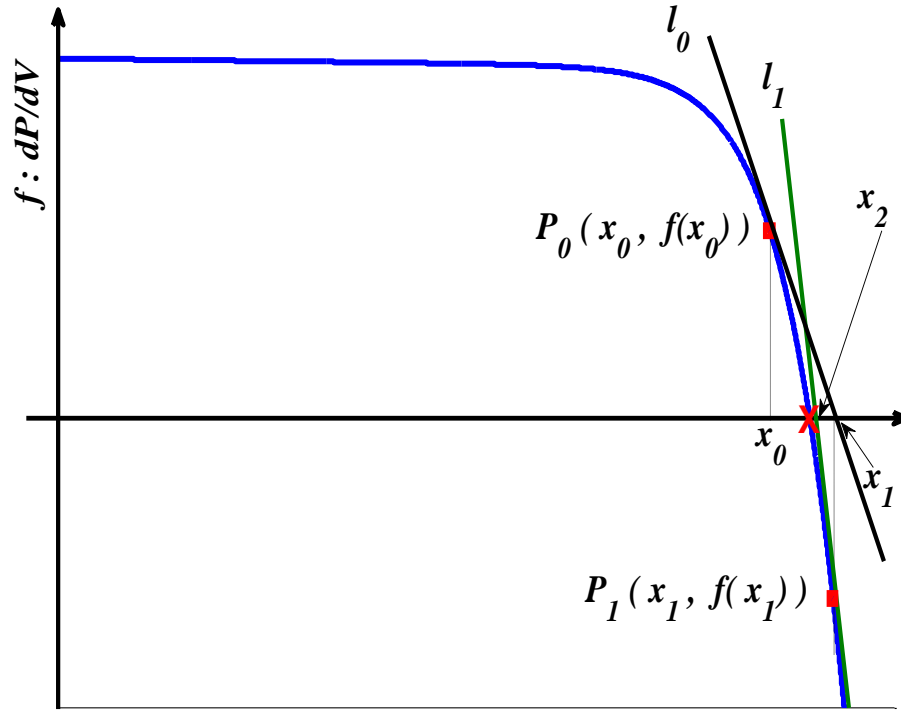


Figure 3.1: NRM x^* is represented by the cross.

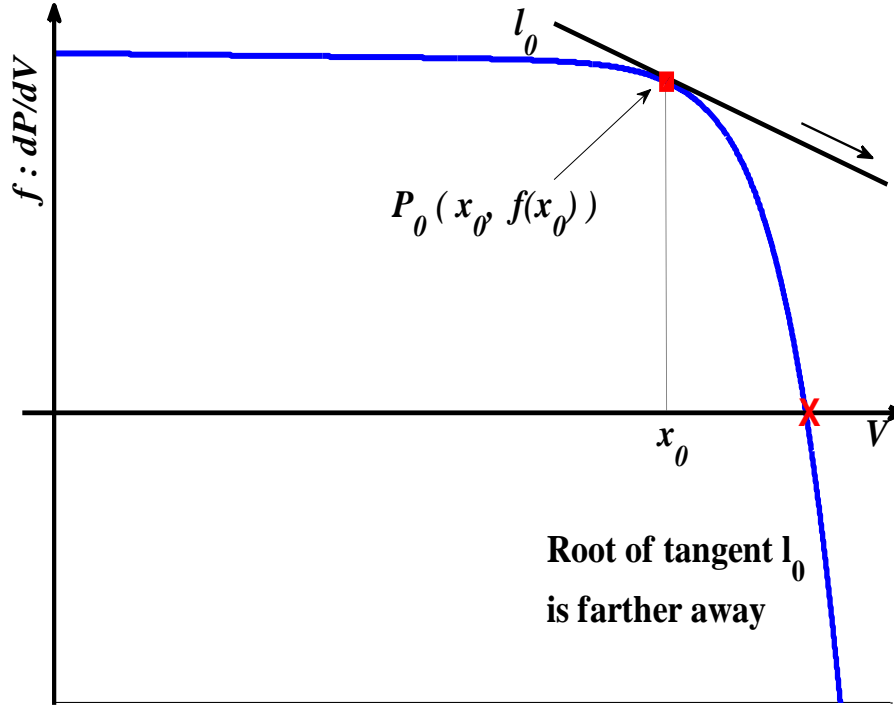


Figure 3.2: NRM (wrong initial value choice)

That is, only a very narrow interval of initial guesses will lead to a convergence to the MPP. Thus, in practical implementations, the NRM applied to MPPT is likely to diverge or to be numerically unstable.

3.2.2 Secant Method (SM)

The SM exemplified in Fig. 3.3 is in many ways similar to the NRM. The SM is another iterative algorithm, in which the fundamental equation is given by,

$$x_{n+1} = x_n - f(x_n) \cdot \frac{x_n - x_{n-1}}{f(x_n) - f(x_{n-1})} \quad n = 0, 1, 2, \dots \quad (3.3)$$

For the SM, x_{n+1} is the root for a secant line $h_n(x)$ to the function $f(x)$ at the point x_n such that $h_n(x_{n+1}) = 0$ with

$$h_n(x) = \frac{f(x_n) - f(x_{n-1})}{x_n - x_{n-1}} \cdot (x - x_n) + f(x_n) \quad n = 0, 1, 2, \dots \quad (3.4)$$

Like the NRM, convergence to a solution is not guaranteed with the SM. Also, the SM convergence rate has an order of 1.618, which is slightly slower than the NRM. Yet, in the SM there is no need to compute derivatives.

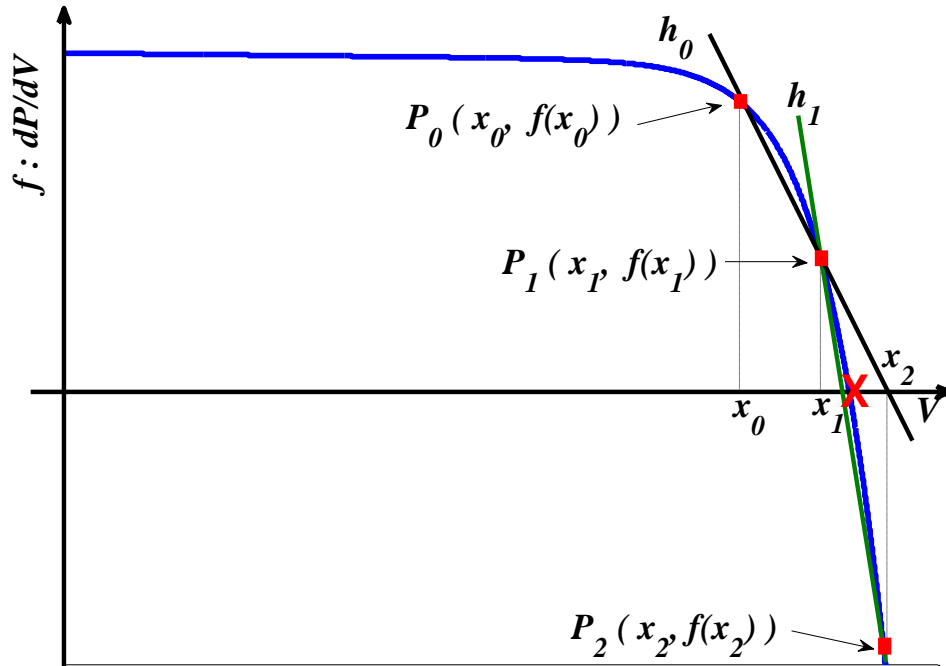


Figure 3.3: Secant Method (SM)

3.3 BRACKETING METHODS

Instead of relying on point estimates for the root like in the open methods, bracketing methods are based on an interval defined by two points. In the next immediate analysis, two of the most popular bracketing methods and a newly proposed algorithm are discussed.

3.3.1 Bisection Method (BSM)

The BSM algorithm, represented in Fig. 3.4, can be summarized in the following steps:

- (i) Given a well-defined function $f(x)$, choose a lower value x_l and an upper value x_u . These two points define an interval $[x_l, x_u]$ that must include the root x^* of $f(x)$. That is, $f(x)$ has opposing signs in x_l and x_u , e.g. $f(x_l)f(x_u) < 0$.
- (ii) Approximate the root to the midpoint x_m of the interval $[x_l, x_u]$. That is

$$x_m = \frac{x_u + x_l}{2} \quad (3.5)$$

- (iii) If $f(x_l)f(x_m) < 0$ then set $x_u = x_m$ and repeat the previous step. If $f(x_l)f(x_m) > 0$ then set $x_l = x_m$ and repeat the previous step. If $|f(x_m)| \leq \varepsilon$ (where ε is the tolerance) then take x_m as the root or approximation.

The BSM convergence rate is slower than the SM. Yet, with the BSM root convergence is guaranteed.

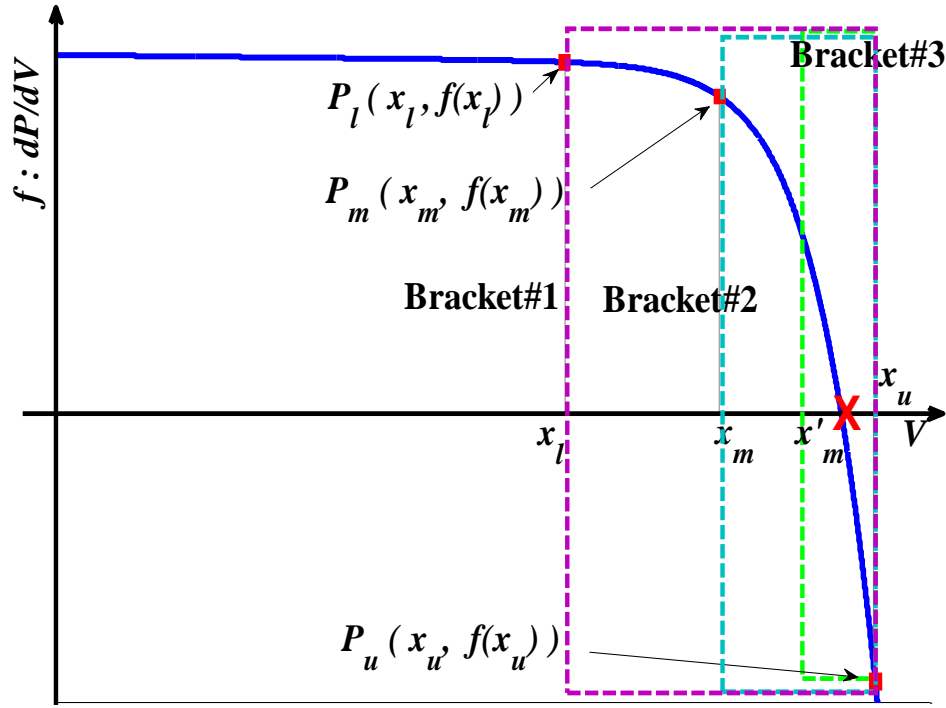


Figure 3.4 : Bisection Method(BSM)

3.3.2 Regula Falsi Method (RFM)

The RFM is a linearly convergent root finding algorithm for continuous functions with one independent variable. It is a hybrid of the bisection search theorem (BST) [15] and the secant method [14]. A value c_i , is derived from

$$c_i = \frac{x_l \cdot f(x_u) - x_u \cdot f(x_l)}{f(x_u) - f(x_l)}, \quad i = 0, 1, \dots \quad (3.6)$$

This found value c_i is then used to substitute the mid-point of each interval $[x_l, x_u]$ as the root approximation used in the BST method. This process is described in both the next algorithm and through Fig. 3.5.

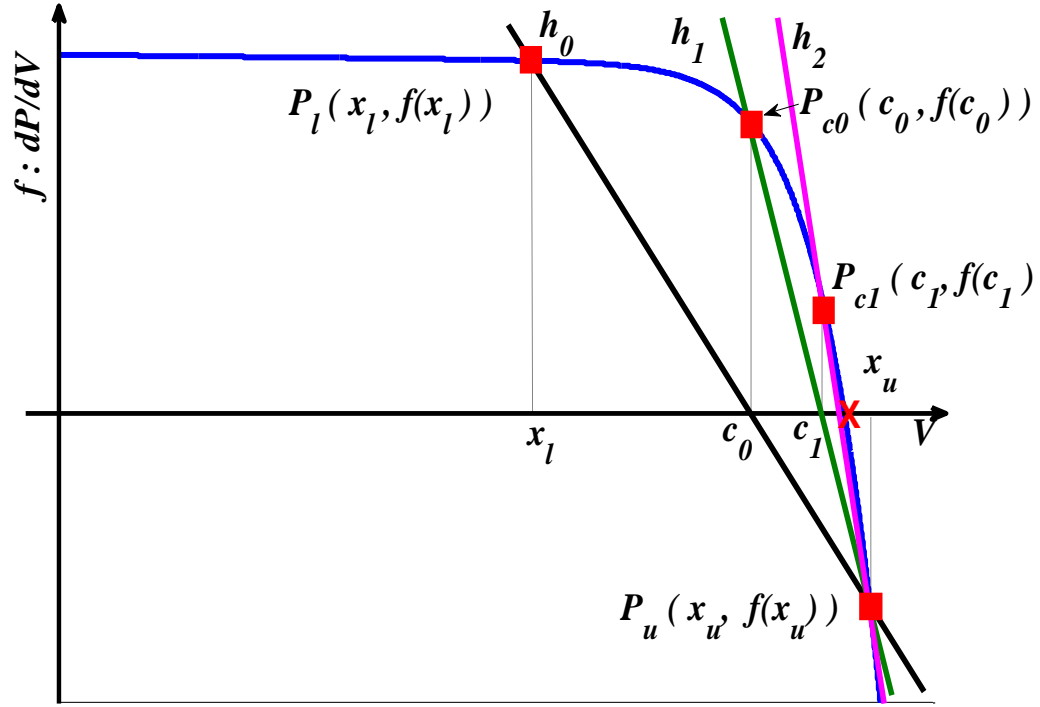


Figure 3.5: Regula Falsi (RFM)

- (i) Given a continuous function $f(x)$ find initial points x_l and x_u , such that $x_l \neq x_u$ and $f(x_l)f(x_u) < 0$. Hence, according to the intermediate value theorem the root of $f(x)$ is located inside the interval $[x_l, x_u]$.
- (ii) Calculate the approximate value for the root c_i with (3.6)

- (iii) If $|f(c_i)| \leq \varepsilon$ (where ε is the tolerance) then it is considered that the root have been reached and that c_i is the root. Else, if $f(c_i) \cdot f(x_u) < 0$ then let $x_l = c_i$, else if $f(c_i) \cdot f(x_l) < 0$ then let $x_u = c_i$. These changes yield a smaller interval.
- (iv) Iterate steps (ii) and (iii) until the root is reached

Although the RFM is only linearly convergent it is generally faster than the BST method because the RFM utilizes the magnitude data of $f(x)$ at each point, which is unique for every different function $f(x)$ depending on its curvature whereas the BST method only uses the sign information of $f(x)$. As Fig. 3.5 suggests, the RFM leaves always one endpoint of the interval fixed, which generates an opportunity for improvement. In the RFM root convergence is guaranteed as will be proved.

Proof of Convergence [30].

Theorem. Suppose for a continuous function $f \in C[a_0, b_0]$ there exists a number $z \in [a_0, b_0]$ such that $f(z)=0$. If for $a_0 < b_0$ with $f(b_0) < 0 < f(a_0)$, $f''(x) \leq 0$ and $c_n = \frac{a_n f(b_n) - b_n f(a_n)}{f(b_n) - f(a_n)}$ which is the sequence of points or approximation of the root generated by the Regula Falsi algorithm, for all $x \in [a_0, b_0]$ then the sequence $\{c_n\}$ converges to the zero $x=z$.

Proof. $h_k(x)$ is the secant or line that goes through the endpoints of a bracket interval $[a_k, b_k]$. A function is concave when $f''(x) \leq 0$ which is the condition of the function. So,

$$h_0(x) \leq f(x) \text{ for all } x \in [a_0, b_0]$$

Since $h_o(c_0)=0$ it follows that $f(c_0)\geq 0$ so that if $f(c_0)=0$ we have converged and $z=c_0$ otherwise, since $f''(x)\leq 0$ for the new bracket interval $[c_0, b_1]=[a_1, b_1]\subset[a_0, b_0]$ and $c_0=a_1<b_1=b_0$ with $f(b_0)=f(b_1)<0<f(a_1)=f(c_0)$ we repeat the above argument for a new bracket interval $[a_2, b_2]=[c_1, b_1]$ and conclude that in general $[a_{k+1}, b_{k+1}]=[c_k, b_k]$.

Since $c_k>a_k=c_{k-1}$ the sequence $\{c_k\}$ is monotonically increasing but since $c_k\leq b_k=b_0$ the sequence $\{c_k\}$ is bounded. Let's say c is the least upper bound of $\{c_k\}$, $c\geq c_n$ for all n . For any $\varepsilon>0$, $c-\varepsilon<c$ there is a positive integer N such that $c_N>c-\varepsilon$. If $n>N$ then,

$$c_n>c-\varepsilon$$

$$c-\varepsilon<c_n\leq c<c+\varepsilon$$

$$-\varepsilon<c_n-c<\varepsilon$$

$$|c-c_n|<\varepsilon$$

Which states that sequence $\{c_n\}$ converges to c , $\lim_{k\rightarrow\infty} c_k = c$ and $f(c)\geq 0$. So at $k=\infty$

the bracket interval will be $[c, b_0]$ and $c = \frac{cf(b_0)-b_0f(c)}{f(b_0)-f(c)}$ resulting in $(c-b_0)f(c)=0$. If $c=b_0$,

$f(c)=f(b_0)$ but $f(b_0)<0$ and $f(c)\geq 0$ so $c\neq b_0$ and $f(c)=0$. So we can now conclude that the sequence $\{c_k\}$ generated by Regula Falsi algorithm converges to c which is z or root of $f(x)$ \square

Chapter 4 : Modified Regula Falsi Method(MRFM)

4.1 INTRODUCTION

As Fig. 3.5 indicates, for a convex or concave function $f(x)$, the RFM converges to the root slowly because one of the end points of the root search interval is fixed, resulting in a constant magnitude for $f(x)$ at that particular point. This problem is improved by the MRFM (Fig. 4.2), introduced in a general theoretical context in [30]. The MRFM, is similar to the RFM except that the following process replaces the aforementioned step (ii) of the RFM:

(ii) If $f(x_l) \cdot f(x_u) < 0$ and $f(x_l) > 0$ then $f(x_u)$ is replaced in (3.6) by $f_p(x_u) = f(x_u)/2$ and

$$f_p(x_l) = f(x_l)$$

$$c_i = \frac{x_l \cdot f_p(x_u) - x_u \cdot f_p(x_l)}{f_p(x_u) - f_p(x_l)} = \frac{x_l \cdot f(x_u) \cdot 0.5 - x_u \cdot f(x_l)}{0.5 \cdot f(x_u) - f(x_l)}, \quad i=0,1,\dots \quad (4.1)$$

If $f(x_l) \cdot f(x_u) < 0$ and $f(x_u) < 0$ then $f(x_l)$ is replaced in (3.6) by $f_p(x_l) = f(x_l)/2$ and

$$f_p(x_u) = f(x_u)$$

$$c_i = \frac{x_l \cdot f_p(x_u) - x_u \cdot f_p(x_l)}{f_p(x_u) - f_p(x_l)} = \frac{x_l \cdot f(x_u) - x_u \cdot f(x_l) \cdot 0.5}{f(x_u) - 0.5 \cdot f(x_l)}, \quad i=0,1,\dots \quad (4.2)$$

That is, these changes effectively decrease the magnitude of $f(x)$ by 1/2 at one of the brackets ends in order to achieve faster convergence, as it is represented in Fig. 4.2.

Mathematicians have investigated many variation of the RFM, some by coming up with

different strategies on how much weight γ is put on the degrading factor or the retaining endpoint portion of the algorithm [31]-[39]. The MRFM ($\gamma=1/2$) is one of these variations and is known as the Illinois Method. These different options derived from the RFM ($\gamma=1$) are a potential area for additional research in order to increase the speed of convergence to the MPP. But to illustrate the choice of $\gamma=1/2$ as the best for the MRFM instead of any other unit fraction ($1/n$) a simple natural log function $f(x) = \ln x$ was chosen and analyzed. As shown in Fig. 4.1 a variant of the MRFM was done on $f(x) = \ln x$ choosing a different unit fraction weight value, such as $\gamma=1/2, 1/3, 1/4, 1/5$. From a rigorous and extensive iterative process the result shows in Fig. 4.1 that as n for $1/n$ increases from $n=3$, the number of iterative processes required to reach the root of $x=1$ increases significantly. This confirms that when choosing a unit fraction value weight for a MRFM, $\gamma=1/2$ is the best choice to reduce the amount of iterations needed or increase convergence speed.

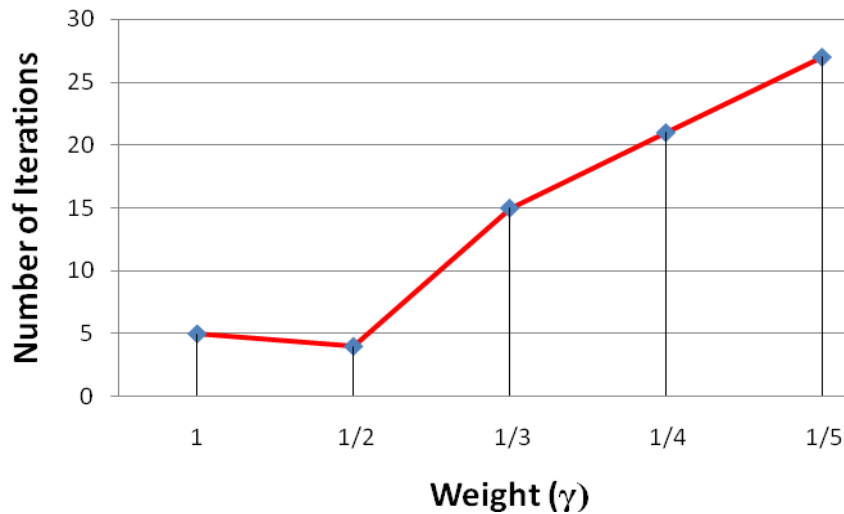


Figure 4.1 : Number of iterations required to reach 99.9% of the root of $f(x) = \ln(x)$ for different weight(γ) factors

As mentioned in [31]-[33],[38]-[39] many research, such as the Pegasus method, Modified Pegasus method, Anderson & Björck method, has been conducted in finding a weight factor other than a unit fraction to increase the speed of convergence but these weight factors require more complex computation and it's application to DMPPT is left for future work.

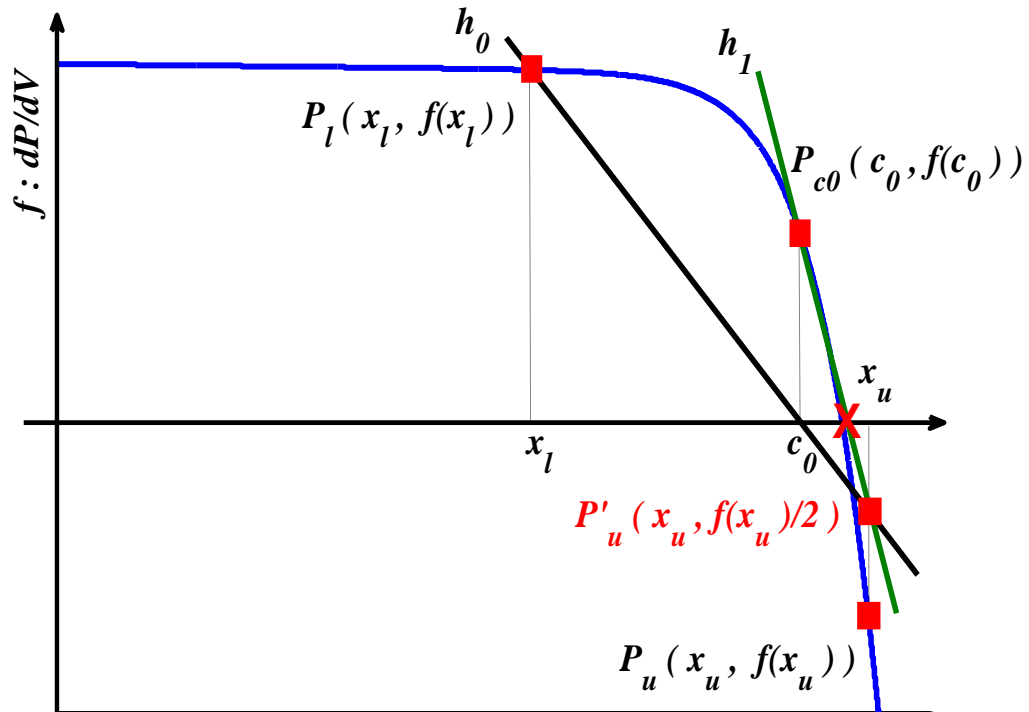


Figure 4.2 : Modified Regula Falsi (MRFM) DMPPT

Figure 4.3 shows the flow chart of the MRFM algorithm. The algorithm starts off with an initialization process followed by a sampling process. After the sampling process the data is analyzed to verify if an irradiation change had happened between data points. If so the data is sampled again and if it satisfies a predetermined criterion the MRFM

iterative process is done until it meets a termination condition. After that it enters idle mode where it periodically monitors for a change in irradiation.

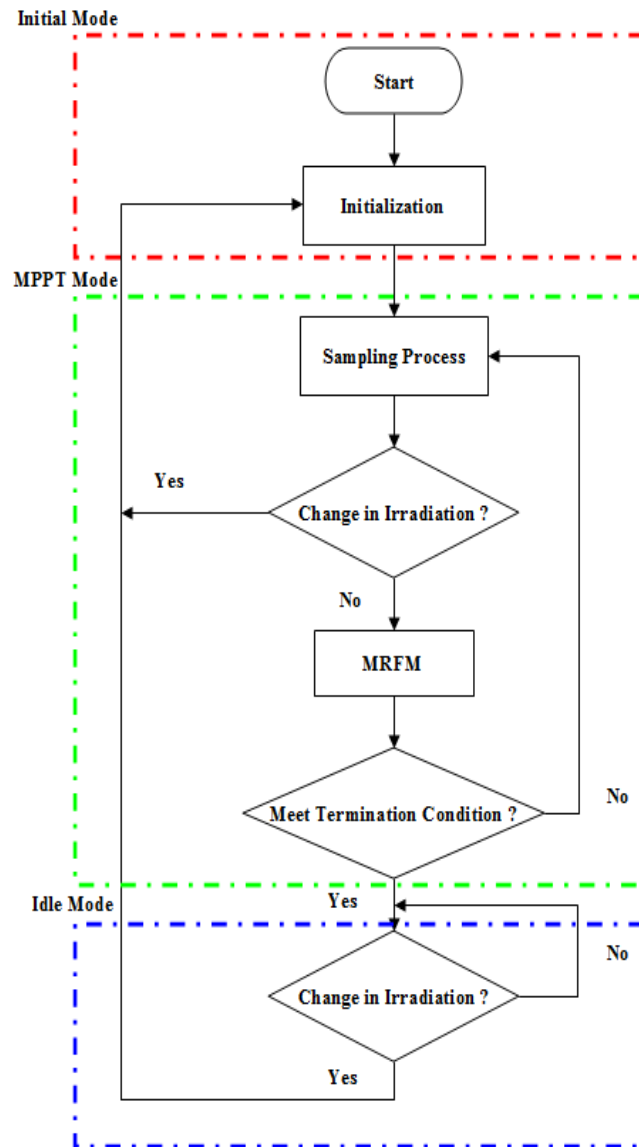


Figure 4.3 : MRFM Flow Chart

Chapter 5 : Analog Algorithms Application to Digital MPPT

5.1 INTRODUCTION

This chapter discusses implementation of the aforementioned algorithms into DMPPT methods. Since the dP/dV curve of a PV panel is a well defined concave function, a root that solves $dP/dV=0$ always exists. Hence, practical implementation of the aforementioned root finding algorithms in order to find the MPP imply that $f(x)$ needs to be replaced by dP/dV . Figures 3.1 to 4.1 exemplified the concepts and also represented how the methods mentioned above are applied to an analog MPPT. Since this work presents a new MPPT algorithm based on the MRFM, the focus of the analysis is on the MRFM. However, analogous conclusions can be simply drawn for the other methods, too.

5.2 NUMERICAL ANALYSIS

Since all the above methods are based on the assumption that the function $f(x)$ —which in MPPT is replaced by $f'(x)$, or dP/dV —for which the root is being sought is continuous, the analysis needs to examine what issues may arise when implementing those methods in a digital domain. These issues to consider when implementing DMPPT of root finding algorithms that are based on the assumption of continuity are: algorithm numerical stability, sampling-generated error of an analog signal—i.e., the quantization

error—and approximation of the value of a derivative in the digital domain—i.e., discretization error.

5.2.1 Numerical Stability

Each root finding optimization method is based on a repetitive process of finding a new approximation to the root. In the past, limitation in the computation resources, round-off errors and truncation errors critically affected the outcome of such an iterative process. However, technological advances in digital signal processing have made nowadays round-off and truncation errors to become negligible. When applying a root finding method in a digital system it is important for the algorithm to be numerically stable, i.e. it is proven to converge to a root. Proof of convergence of the root finding methods mentioned in this dissertation are well known and for that reason they are not discussed in detail here. Readers can find this detail analysis in textbooks, such as [30], in which proof of convergence is based on considering each new approximation as a monotonically increasing sequence, which is, then compared within an interval, from where it is identified that the sequence has an upper bound, which proofs that the sequence converges.

5.2.2 Quantization Error

In a digital implementation of a MPPT algorithm the voltage across the PV module (V_{pv}) and the current generated are sampled and processed by an Analog to Digital Converter (ADC) that discretizes the analog signal or measurement to be processed in the

digital domain. But a quantization error exists because of limited number of bits representing the measured or sampled value. The magnitude of the quantization error can range from 0 to half of the smallest resolution the ADC [7] which equals,

$$\text{Quantization Error Maximum Magnitude} = \frac{1}{2} \cdot \frac{V_{p-p}}{2^N} \quad (5.1)$$

where V_{p-p} is the peak to peak measurement range of the signal and N is the ADC resolution bits. From (5.1) it is shown that the higher the resolution (N) of the ADC the smaller the maximum error becomes. But the finer the resolution of an ADC is, the more expensive it becomes. Hence, there is a tradeoff between minimizing cost and quantization error. The quantization error can be minimized by decreasing the signal measurement range (V_{p-p}). This can be achieved by using a voltage divider circuit to decrease the signal range and sending that measured signal to a low voltage range ADC. The reduced signal value can then later be compensated through software programming to get the actual measured value before the voltage divider circuit. As it was mentioned for the round off and truncation errors, the quantization error issue can be ignored due to the continued decrease in the cost of high resolution ADC. Presently, a 12 or 16 bit resolution ADC are embedded as peripherals on many common inexpensive DSPs, such as the TI TMS320F28335 DSP chip. With such an ADC resolution, it is possible to obtain errors of about 0.1 mV to 2mV for a $\pm 10V$ range signal, which is sufficiently small to be ignored.

5.2.3 Discretization Error

Digital implementation of MPPT algorithms requires addressing issues with computing the dP/dV derivative in the digital domain. Since a digital processor can only process discrete data samples, a true derivative at an operating point cannot be achieved without some error called discretization error, $\mathcal{J}_{x_0}(h)$.

5.3 APPLICATION TO MRFM DMPPT

In this section the numerical analysis mentioned previous will be performed on the MRFM but the method done here may be taken and applied to any other analog MPPT method following similar steps that will be covered.

In the MRFM method a backward numerical differentiation quotient is used to approximate the derivative at an arbitrary operating point x_0 . When a derivative at an operating point (V_{x_0}) is needed the backward difference quotient is found by immediately sampling another value (V_{x_0}') separated from the operating point by a fixed small value ΔV . So the value of the finite difference quotient at point x_0 is

$$\left. \frac{dP}{dV} \right|_{V=x_0} \approx \frac{\Delta P}{\Delta V} = \frac{V_{x_0} \cdot I_{x_0} - V_{x_0}' \cdot I_{x_0}'}{V_{x_0} - V_{x_0}'} \quad (5.2)$$

where $V_{x_0}' = V_{x_0} - \Delta V$, and V_{x_0} , I_{x_0} , V_{x_0}' , and I_{x_0}' are sampled voltage and current values at point x_0 and x_0' , respectively.

From the Taylor series representation of the derivative of a function, $g(x)$ at point x_0 can be represented as,

$$\begin{aligned} g'(x_0) &= \frac{g(x_0) - g(x_0 - h)}{h} - \frac{g''(x_0) \cdot h^2}{2!} - \frac{g'''(x_0) \cdot h^3}{3!} - \dots \\ &= g_e'(x_0) - \frac{g''(x_0) \cdot h^2}{2!} - \frac{g'''(x_0) \cdot h^3}{3!} - \dots \end{aligned} \quad (5.3)$$

where h is the difference between x_0 and x_0' equivalent to ΔV in (5.2), and $g_e'(x_0)$ denotes the estimated derivative value equivalent to $\Delta P/\Delta V$ in (5.2). That is, $g(x)$ is analogous to the function $P(V)$. Then, the error between the true derivative and the estimated value is

$$\mathcal{G}_{x_0}(h) = g'(x_0) - g_e'(x_0) = -\frac{g''(x_0) \cdot h^2}{2!} - \frac{g'''(x_0) \cdot h^3}{3!} - \dots \quad (5.4)$$

From (5.4), it is shown that a sufficient value for h —analogous to ΔV in a practical MPPT implementation— between two sample points must be chosen to approximate a derivative value that has a small error $\mathcal{G}_{x_0}(h)$. Yet, h must also be large enough to provide a valid sample value in a noisy measurement environment. In doing so, the value of h and the corresponding discretization error $\mathcal{G}_{x_0}(h)$ generated by h must meet a specified tolerance range defined by the system designer.

As mentioned before, all root finding algorithms have a termination condition given by the tolerance for the searched root value. In the proposed MRFM, when implemented digitally, the tolerance was set to reach the MPP within 99.9% of its given value at the predetermined lowest irradiance condition. For the analysis, the lowest irradiance was chosen to be at 200W/m^2 . This irradiance condition was chosen for the MPPT algorithm design because for a fixed termination condition, as the irradiance

increases, the operating point range that meets the objective of falling within 99.9% of the MPP decreases (Fig. 5.1). Hence, if a high irradiance condition is chosen as the reference for specifying the tolerance, when the irradiance decreases from the reference level, it is possible to find termination conditions that are beyond the 99.9% of the MPP. In the particular examples used in this paper, another advantage of selecting 200W/m^2 as the reference irradiance level for the tolerance is that at this irradiance level $I_{sc} \approx 1\text{A}$. From the simulation data in Fig. 5.1 of the dP/dV vs. V curve, the termination condition is $|f'(x_n)| \leq 0.12$. This value corresponds to an interval of $\Delta V = 0.4\text{ V}$ around the MPP. This voltage difference is the error bound or accuracy tolerance considered in practical cases considered in this dissertation.

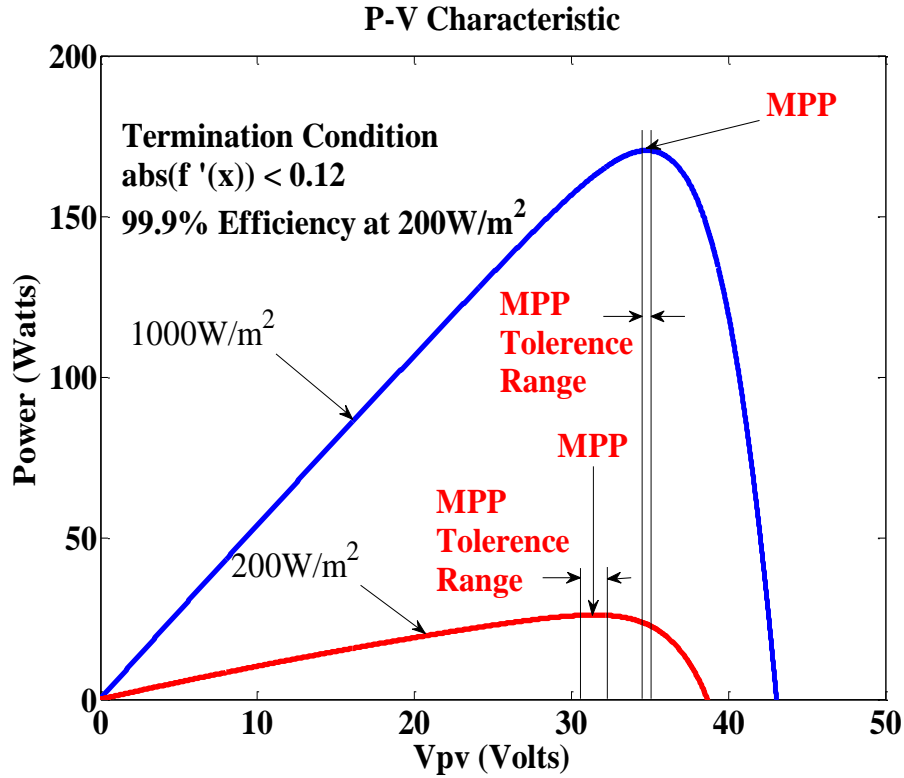


Figure 5.1: Termination condition comparison between two irradiance levels.

A low cost—less than a hundred dollars—digital MPP tracker can be realized with an inexpensive microcontroller that is still fast enough to run each step of the DMPPT algorithm within each sampling period (in the order of a msec.), and an ADC with a resolution that depends on the input signal range—yet, most DSP chips have this function already embedded. Evidently a power electronics converter with a DPWM controlled needs to be added. In this study a boost converter was chosen because it is simple and widely used for this application. However, the analysis can easily be extended to other dc-dc converters that can be used as power electronic interfaces for such systems. When the dc-dc converter is connected to a battery or a constant voltage load the output voltage of the converter is fixed. This is another assumption also considered in this work because batteries are often used in sustainable PV systems in order to power the load when there is not enough sunlight. The assumed constant output voltage is $V_{out} = 48V$. A microcontroller running the MPPT algorithm takes the discretized voltage and current values and generates a DPWM duty cycle D that regulates the converter input voltage (V_{pv}). V_{pv} is the voltage across the PV module. In the case of the boost converter used here if the duty cycles $D1$ and $D2$ correspond to input voltages V_{pv1} , V_{pv2} , respectively, and assuming $V_{pv1} < V_{pv2}$, $D1 > D2$, then $\Delta V = V_{pv2} - V_{pv1}$, and $\Delta D = D1 - D2$. Thus,

$$\Delta D = \frac{\Delta V}{V_{out}} \quad \text{or} \quad \Delta V = \Delta D \cdot V_{out} \quad . \quad (5.5)$$

From the definition of a derivative and from (5.3) and (5.4) the smaller the value of h is the closer the approximate value of a derivate is to its true value. Mathematically, with continuous variables and functions, there is no direct limitation in h (equivalent to

ΔV in (5.5)). However, in digital implementation of (5.2), ΔV in (5.5) is affected by the limited resolution of the DPWM. Hence, the resolution of the DPWM becomes the deciding factor when selecting ΔV . The smallest resolution of a DPWM is referred to as a tick or LSB and this will be the lower bound for ΔV . In the experimental setup here 1 tick is 25ns which is $\Delta D=0.00125$ for a 50 kHz switching frequency DPWM signal and from $V_{out} = 48$ V and (5.5) corresponds to $h = \Delta V = 0.06$ V.

In (5.4) $\mathcal{G}_{x_0}(h)$ depends on $g''(x_0)$, $g'''(x_0)$ and h —i.e., d^2P/dV^2 , d^3P/dV^3 and ΔV . The possible range of values for $g''(x_0)$ and $g'''(x_0)$ are shown in Figs. 5.2 and 5.3 for solar irradiances of 200W/m² and 1000W/m², respectively. Consider a worst case scenario when $g''(x_0)$ and $g'''(x_0)$ have their largest value—i.e., when the irradiance is 1000W/m². From Fig. 5.3, the range for $g''(x_0)$ and $g'''(x_0)$ are $-54 < g''(x_0) < 5.5$, $-10 < g'''(x_0) < -0.01$, $-1.37 < g'''(x_0) < 0$., respectively. Considering these values and the calculations indicated in Table I, the third order term of the discretization error ($\mathcal{G}_{x_0}(h)$) has a significantly small value ranging from 0.000054 to 0.00675. This range of values is less than 0.01, so the third order term in (5.4) can be ignored. Thus, the only significant term that needs to be considered is the second order term, so (5.4) becomes

$$\mathcal{G}_{x_0}(h) \approx -\frac{g''(x_0) \cdot h^2}{2!} \quad (5.6)$$

Table I. Parameter values for different tick values

Ticks	ΔD	$h = \Delta V$	$\frac{h^2}{2}$	$\max \left \frac{g'' h^2}{2} \right $	$\frac{h^3}{3!}$	$\max \left \frac{g''' h^3}{6} \right $
1 ticks	0.00125	0.06	0.0018	0.018	0.000036	0.000054
2 ticks	0.00250	0.12	0.0072	0.072	0.000288	0.000432
3 ticks	0.00375	0.18	0.0162	0.162	0.000972	0.001458
4 ticks	0.00500	0.24	0.0288	0.288	0.002304	0.003456
5 ticks	0.00625	0.30	0.0450	0.450	0.004500	0.006750

Once again, from (5.6), ideally the smaller h (or ΔV) is, the closer it is to its derivative true value at a given point. However, due to ambient EMI noise, switching noise of the dc-dc converter, and quantization errors mentioned before, a value of ΔV or h too small may cause errors to occur during data acquisition. This is illustrated in Fig. 5.4 which shows two sampling instances before and after a duty cycle change for two different cases. The first is for 1 tick ($\Delta V=0.06V$) and the second is for 3 ticks ($\Delta V=0.18V$). For the former case, it is shown that although the value for ΔV is small and decreases $\mathcal{G}_{xo}(h)$ the most, the step size is too small to overcome the effects of noise. Hence, an error occurs when sampling, whereas for the latter case the sampled values for the two instances are sufficient. Thus, an upper bound of h —i.e., ΔV — is also needed in order to complete the sampling portion of the controller design.. In short, h (or ΔV) must be a value small enough to keep $\mathcal{G}_{xo}(h)$ small but large enough so that the controller is robust against noise actions.

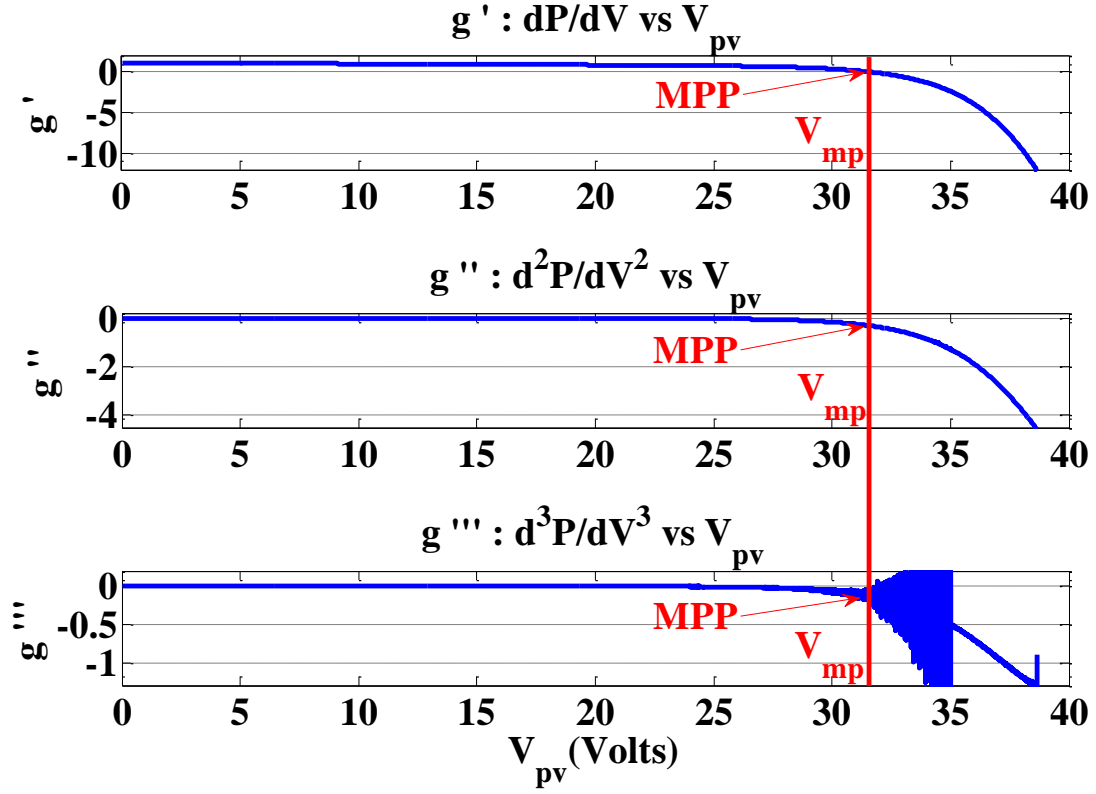


Figure 5.2: dP/dV , d^2P/dV^2 , and d^3P/dV^3 of PV module at 200W/m^2 , 25°C

Thus, in order to choose the interval h for the proposed method (e.g. the MRFM) one more criteria needs to be considered. From the MRFM algorithm, at each iteration the new approximation of the root is once again from (4.1) and (4.2),

$$c_n = \frac{a_n f_p(b_n) - b_n f_p(a_n)}{f_p(b_n) - f_p(a_n)} = \frac{a_n g'_p(b_n) - b_n g'_p(a_n)}{g'_p(b_n) - g'_p(a_n)} \quad (5.7)$$

where a_n and b_n are the lower and upper bound of an interval bracket $[a_n, b_n]$, also the subscript p indicates that the function $f(x)$ follows the condition mentioned in (4.1) and (4.2). The true value is denoted c_n^{true} and the estimation value affected by the approximation of the derivative or discretization error is c_n^{est} which is given by

$$c_n^{est} = \frac{a_n g'_{e,p}(b_n) - b_n g'_{e,p}(a_n)}{g'_{e,p}(b_n) - g'_{e,p}(a_n)} \quad (5.8)$$

Hence, from (5.4) and (5.7)

$$c_n^{true} = \frac{a_n g'_{p,b_n}(b_n) - b_n g'_{p,b_n}(a_n)}{g'_{p,b_n}(b_n) - g'_{p,b_n}(a_n)} = \frac{a_n g'_{e,p}(b_n) - b_n g'_{e,p}(a_n) + g_{p,b_n}(h) \cdot a_n - g_{p,a_n}(h) \cdot b_n}{g'_{e,p}(b_n) - g'_{e,p}(a_n) + g_{p,b_n}(h) - g_{p,a_n}(h)} \quad (5.9)$$

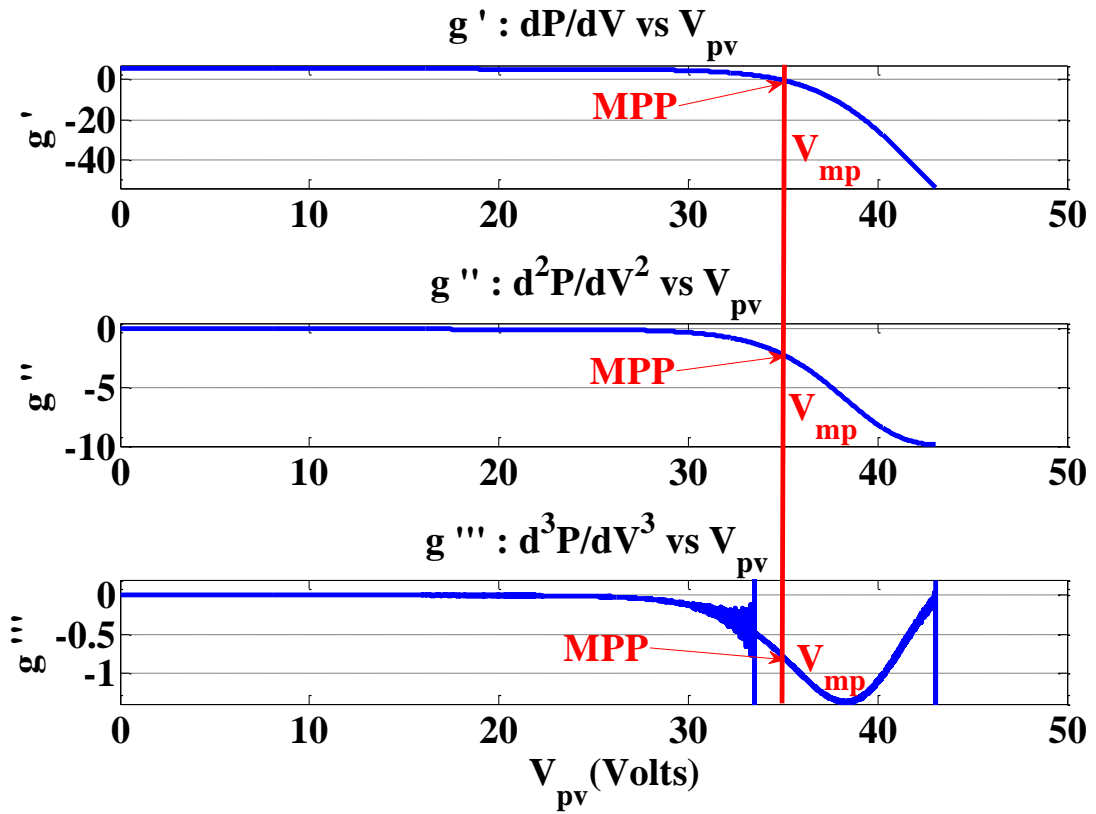


Figure 5.3: dP/dV , d^2P/dV^2 , and d^3P/dV^3 of PV module at $1000W/m^2$, $25^\circ C$ (STC)

Since from Fig. 5.3 the value of $g''(x)$ for the minimum voltage value is approximately 0 V and the value of $g''(x)$ for the maximum voltage value is approximately -10 V, then from (5.6) and assuming that b_n is the retaining point,

$$\begin{aligned} g_{p,b_n}(h) - g_{p,a_n}(h) &\approx -\frac{g''_p(b_n) \cdot h^2}{2!} + \frac{g''_p(a_n) \cdot h^2}{2!} = \frac{h^2}{2} (g''_p(a_n) - g''_p(b_n)) \\ &= \frac{h^2}{2} \left(g''_p(a_n) - \frac{g''_p(b_n)}{2} \right) < \left(0 - \frac{-10}{2} \right) \frac{h^2}{2} < 5 \frac{h^2}{2} \end{aligned} \quad (5.10)$$

Figure 5.3 also indicates that $-54 < g'(x_0) < 5$. Thus, from (5.10), $g'_{e,p}(b_n) - g'_{e,p}(a_n) \gg g_{bn}(h) - g_{an}(h)$. Therefore $g_{bn}(h) - g_{an}(h)$ can be ignored in the denominator of (5.9), so with the help of (5.8), (5.9) now becomes,

$$c_n^{true} = \frac{a_n g'_{e,p}(b_n) - b_n g'_{e,p}(a_n) + g_{p,b_n}(h) \cdot a_n - g_{p,a_n}(h) \cdot b_n}{g'_{e,p}(b_n) - g'_{e,p}(a_n)} = c_n^{est} + \varepsilon(h) \quad (5.11)$$

where $\varepsilon(h)$ is the error between c_n^{true} and c_n^{est} . Hence,

$$\begin{aligned} \varepsilon(h) &= \frac{g_{p,b_n}(h) \cdot a_n - g_{p,a_n}(h) \cdot b_n}{g'_{e,p}(b_n) - g'_{e,p}(a_n)} = \frac{h^2}{2} \left(g''_p(a_n) \cdot b_n - g''_p(b_n) \cdot a_n \right) \frac{1}{g'_{e,p}(b_n) - g'_{e,p}(a_n)} \\ &= \frac{h^2}{2} \left(g''_p(a_n) \cdot (a_n + \Delta V_n) - g''_p(a_n + \Delta V_n) \cdot a_n \right) \frac{1}{g'_{e,p}(a_n + \Delta V_n) - g'_{e,p}(a_n)} \end{aligned} \quad (5.12)$$

where ΔV_n is $b_n - a_n$. From (5.12) as $V_n \rightarrow 0$, $\varepsilon(h) \rightarrow 0$, which means as the iterative process of the MRFM continues, the bracket size decreases resulting in $c_n^{true} \approx c_n^{est}$. Thus, both the bracket size ΔV_n and the error $\varepsilon(h)$ are maximum for the initial bracket, For the MRFM [24] the initial bracket size ΔV_0 is 4V. This value for ΔV_0 is somewhat arbitrary as ΔV_0 could take any value up to V_{oc} . In this case it was considered about ten times the

tolerance and one tenth of V_{oc} . Next, an h that minimizes $\varepsilon(h)$ needs to be found.

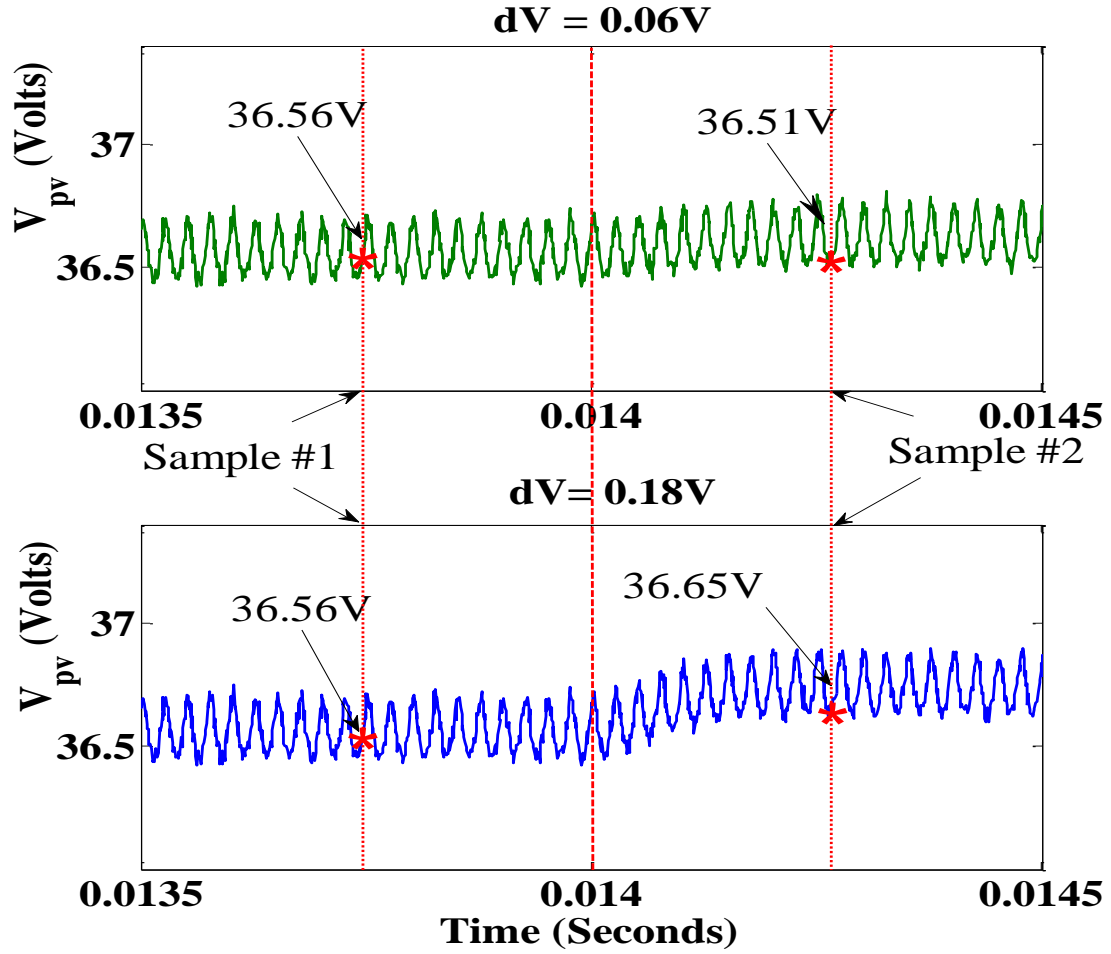


Figure 5.4: Error caused by a small ΔV value

Assuming that b_n is the retaining point (5.12) becomes,

$$\varepsilon(h) = \frac{h^2}{2} \left(g''(a_n) \cdot (a_n + \Delta_{v_n}) - \frac{g''(a_n + \Delta_{v_n})}{2} \cdot a_n \right) \frac{1}{\frac{g'_e(a_n + \Delta_{v_n})}{2} - g'_e(a_n)} < 5 \cdot \frac{h^2}{2} \quad (5.13)$$

To sum up, a value h needs to be chosen so that (5.6), (5.10), and (5.13) are small enough so they meet the tolerance condition of $\Delta V = 0.4$ V and so that $|g'(x_n)| \leq 0.12$. Yet,

h needs to be large enough to be robust against noise effects. In the experimental setup detailed in the next Section, the noise amplitude was measured to be 130 mV peak-to-peak so $h=0.18\text{V}$ was the smallest value large enough to overcome the effects of the noise. When $h = 0.18\text{ V}$ is used in (5.10), and (5.13) and considering from Fig. 5.4 that $g'(x)$ can take values between -54 and 5.5, it can be concluded that in order to approximate the derivative at a point $h = 0.18\text{ V}$ is a sufficiently good value representing the length of an interval given by two samples. Hence, in the practical application discussed next, when calculating derivatives from (5.2), ΔV is considered equal to 0.18 V.

The next section will illustrate simulated results of many different analog root finding methods implemented in a digital platform utilizing the parameters obtained in this section. A pair of samples will be obtained 0.18V apart for every sample value and for the bracketing methods (BSM, RFM, MRFM) an initial bracket size of 4V will be used. As for the open methods, for the purpose of showing that the method can be utilized in DMPPT for special cases, the simulation will begin at a starting point close to the MPP in order for the system to not diverge and evolve into an unstable state. This is done for the SM. And also a simulation is done to illustrate the system diverging when the initial point is far from the MPP. But due to the simulation only taking into consideration switching ripple noise and not the ambient EMI noise the merit for choosing a value as large as $h=0.18\text{V}$ is not clear. But from the experimental results shown in Chapter 6 the merit of choosing a value as large as $h=0.18\text{V}$ to find a pair for the sample value will be evident due to the ambient noise included from the experimental setup.

The values chosen in this section is model specific. In this research the SHARP NE-170U1 product data specifications [37] were used to do the analysis but the step by step method shown and described in this section can be applied to any PV module.

5.4 SIMULATION-BASED RESULT

A simulated comparison was initially explored in order to verify the root finding methods for DMPPT. The arguably two most popular DMPPT methods—the P&O and the INC methods—are also considered. The P&O method is widely used due to its implementation simplicity but the operating point constantly oscillates around the MPP resulting in loss of energy. This is illustrated in Fig. 5.5 – 5.6. Fig. 5.6 shows the system trying to track the MPP at dynamically changing environment and in this case it is simulated where the irradiation is changed from 1000W/m^2 to 200W/m^2 and 1000W/m^2 .

From the simulation results the unavoidable oscillation around the MPP can be seen in the voltage measurement and the corresponding power measurement. It is due to the control method relying on a fixed duty cycle step size where the duty cycle is increased when the operating point is on the right side of the MPP on the P-V curve and the duty cycle is decreased when the operating point is on the left side of the MPP on the P-V curve. This oscillation will continue infinitely even though it reaches the MPP because the next step is to perturb a fixed step and the process persists without end. In other words, the inherent issue in the P&O method is that it is a method intended to find the MPP, yet, when it finds it, it moves the system out of it. In this method a pair of sampled values 0.18V apart is not required for it does not require the computation of a

derivative value. The only aspect that the designer needs to take into consideration is the step size and make sure it is large enough so that the noise effect will not cause a faulty measurement in the sign of the power difference.

The other popular method is the INC method, which avoids the oscillation problem of the P&O method but as a fixed step method it involves a trade off associate with the step size choice: if the step-size is large the MPP is reached faster than when a small step size is chosen. But accuracy of large step-sizes is worse than for small step-sizes. Figs. 5.7 – 5.10 illustrates this tradeoff by showing the simulation results for two different cases. The first case chooses a large fixed step size ($\Delta D=0.01$) and when choosing a large step size as in Fig. 5.7 -5.8 MPPT arrives near the MPP faster. But also does not reach the MPP accurately. But when choosing a small step size as in Fig. 5.9-5.10 it reaches closer to the MPP but it takes longer to do so. Reaching the MPP accurately and quickly at a variable step size is important to increase the effectiveness and efficiency of the MPPT system.

Fig. 5.11 -5.13 shows the SM implemented as a DMPPT it is fast and accurate when the initial point is near the MPP but from Fig. 5.13 it can be seen that when the initial point is far from the MPP it diverges resulting in the system evolving into an unstable state. The NRM was not simulated due to the difficulty of the need to calculate the second derivative but similar results to those obtained by the SM will occur, when the initial value is near the MPP it will converge fast to the MPP but when the initial value is far from it, the NRM will diverge. Out of the 4 root finding algorithm considered, the NRM is the fastest method but due to the complication of calculating the second

derivative and the instability issues mentioned, without a safe-guarding method implemented with the algorithm, it is not a good choice as a MPPT algorithm. The next two bracketing methods and the proposed method solve the instability issue of the SM and the NRM which is seen in the following simulation results.

The BSM implemented as a DMPPT is shown in Fig. 5.14-5.15. It has been discussed in Chapter 3 that the MPP is guaranteed to be found. But it is slow compared to the RFM and MRFM in finding the MPP.

The RFM as discussed in Chapter 3 is faster than the BSM and also guarantees to reach the MPP. The simulation results of the RFM used as a DMPPT method is shown in Fig. 5.16-5.17 and the simulation results of the proposed method MRFM is shown in Fig. 5.18-5.19.

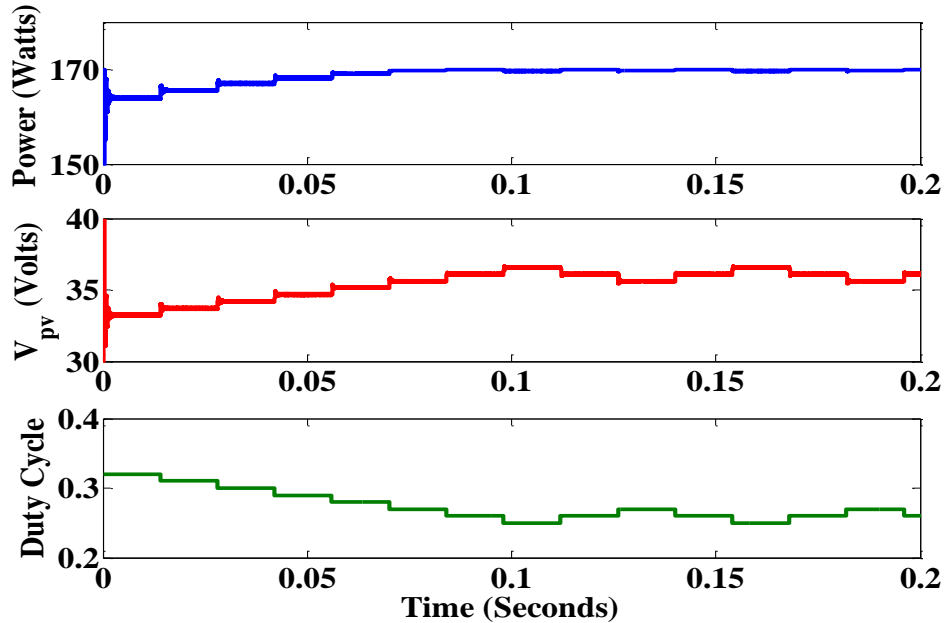


Figure 5.5 : Perturb & Observe Method MPPT @1000W/m²

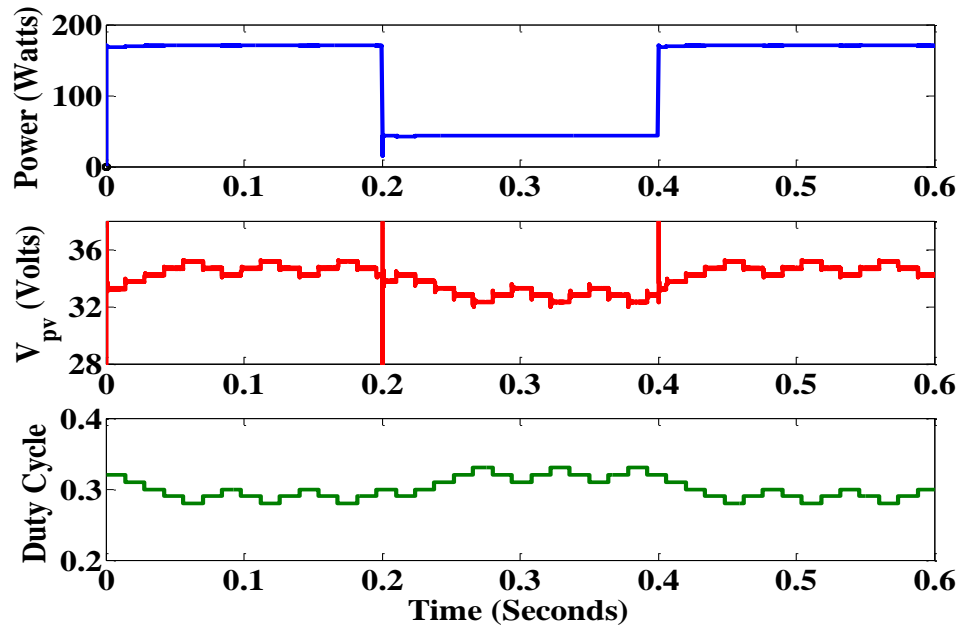


Figure 5.6 : Perturb & Observe Method MPPT in Dynamic Environment

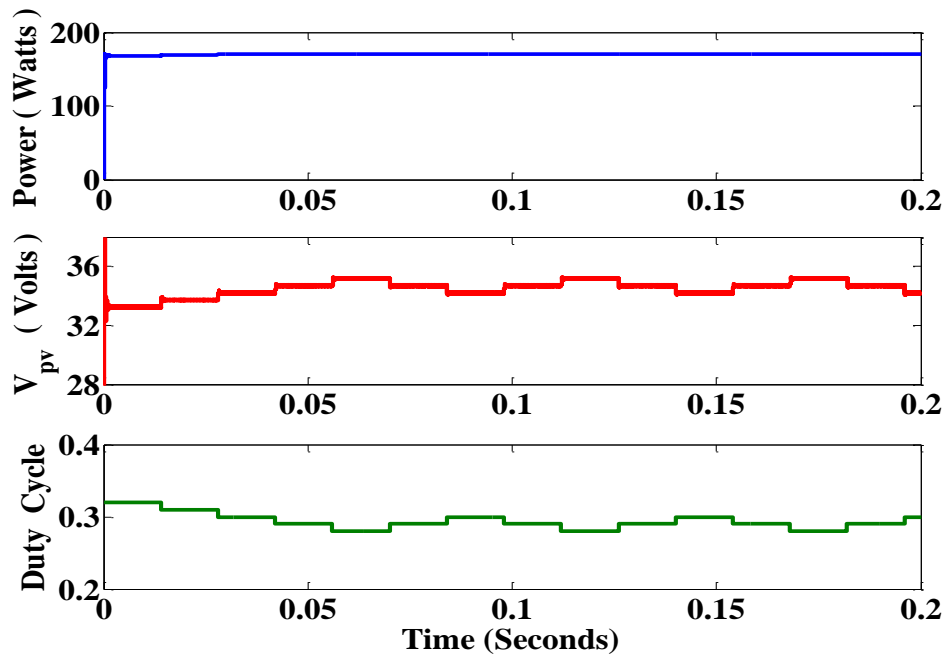


Figure 5.7 : INC MPPT @1000W/m² ($\Delta D=0.01$)

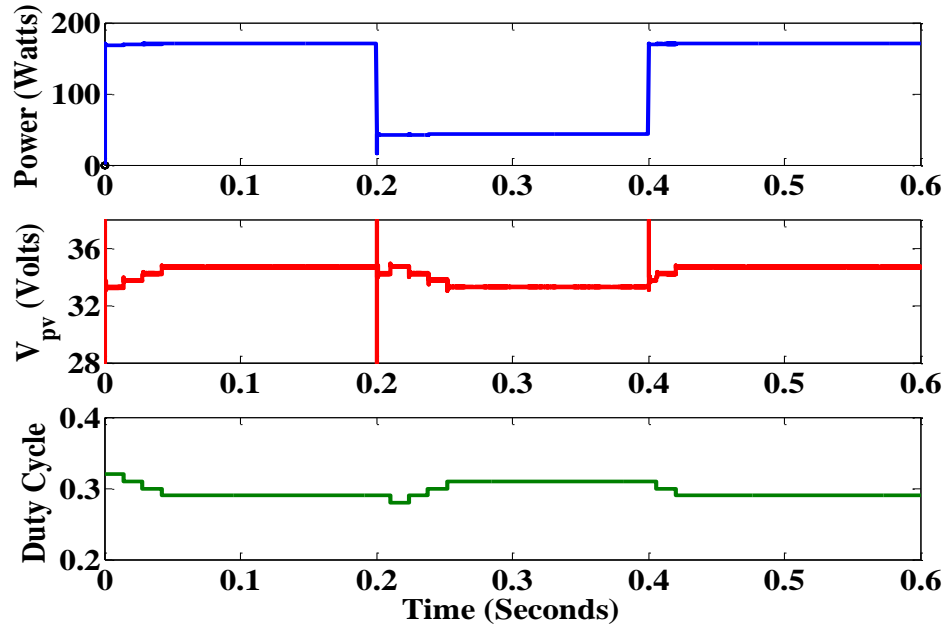


Figure 5.8 : INC MPPT in Dynamic Environment ($\Delta D=0.01$)

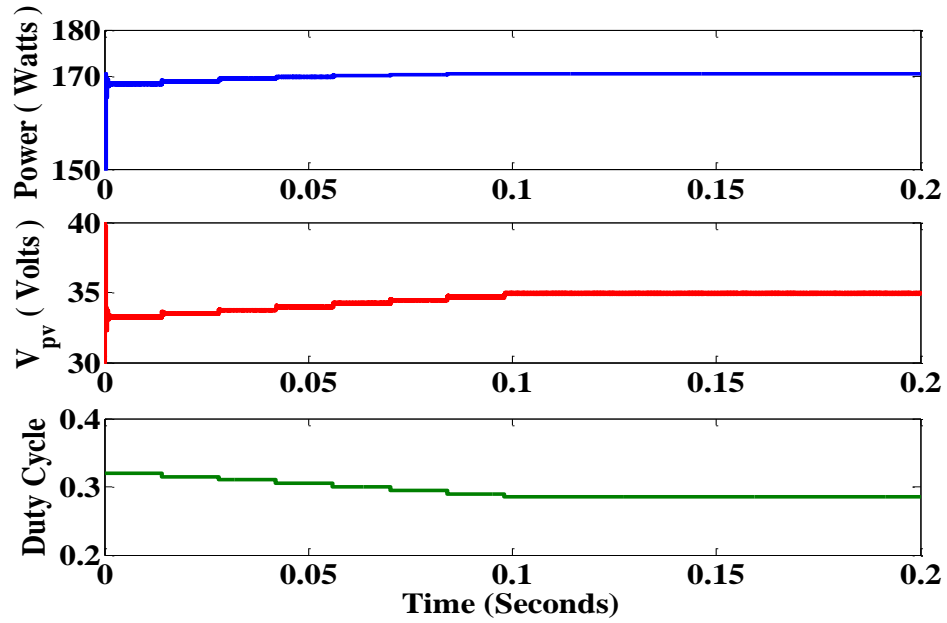


Figure 5.9 : INC MPPT @ 1000 W/m^2 ($\Delta D=0.005$)

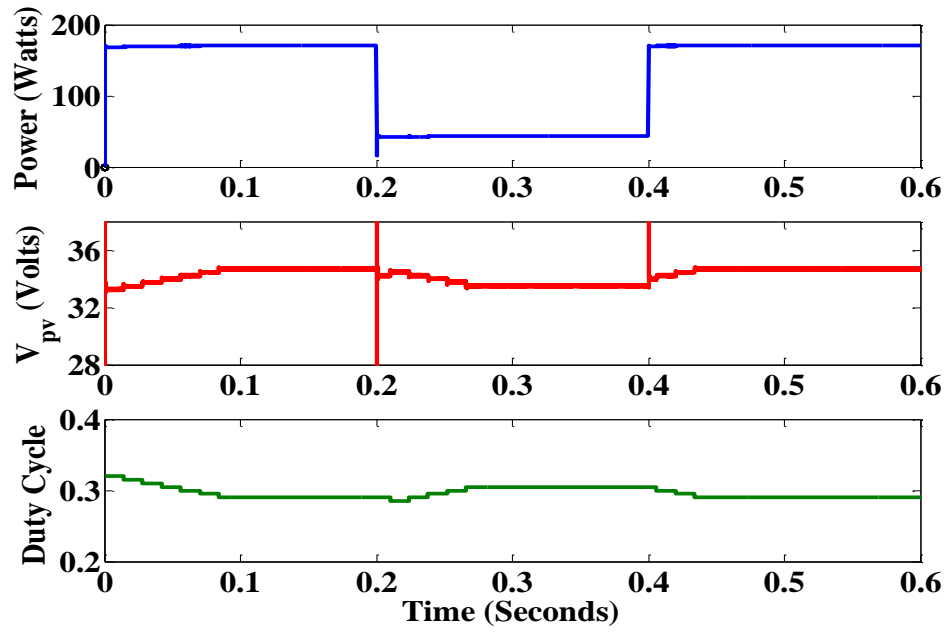


Figure 5.10 : INC MPPT in Dynamic Environment ($\Delta D=0.005$)

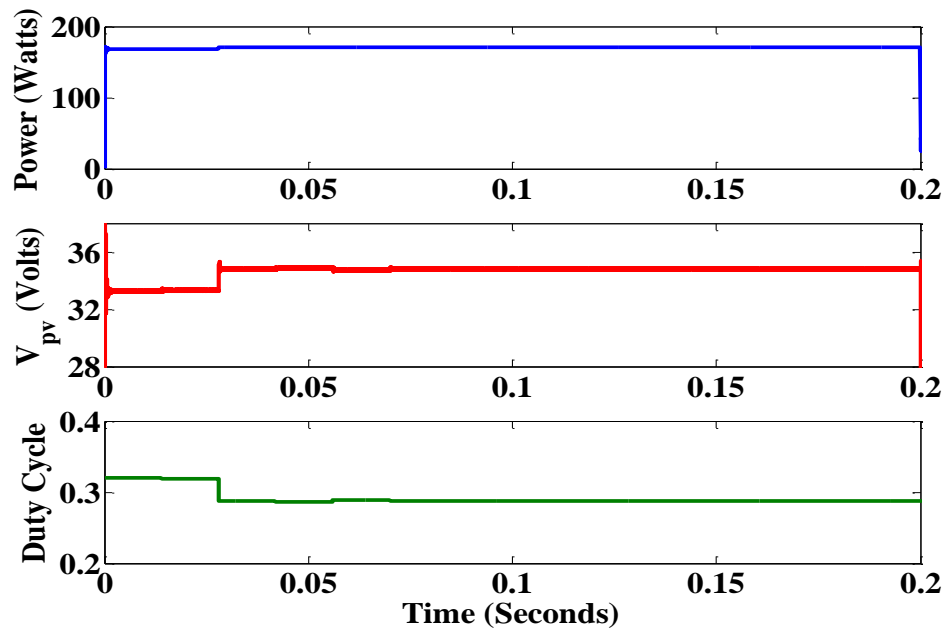


Figure 5.11 : Secant Method MPPT @1000W/m² (Initial Point near MPP)

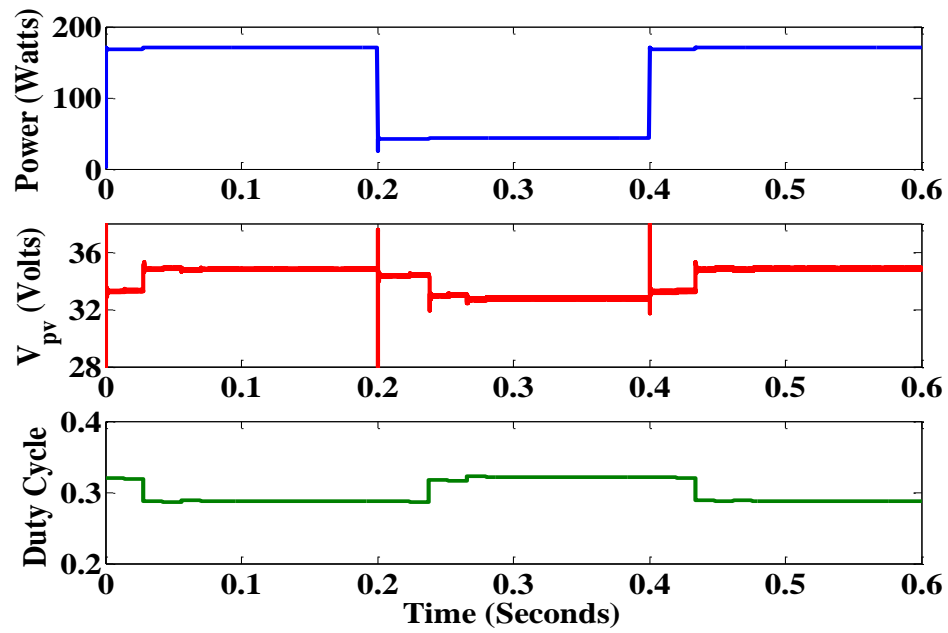


Figure 5.12 : Secant Method MPPT in Dynamic Environment (Initial Point near MPP)

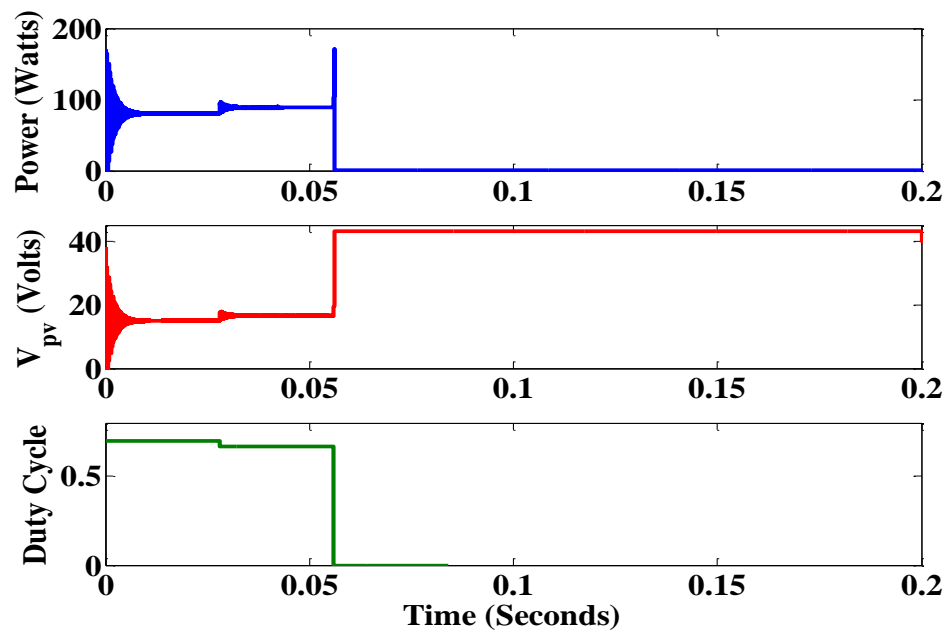


Figure 5.13 : Secant Method MPPT Initial Point far from MPP

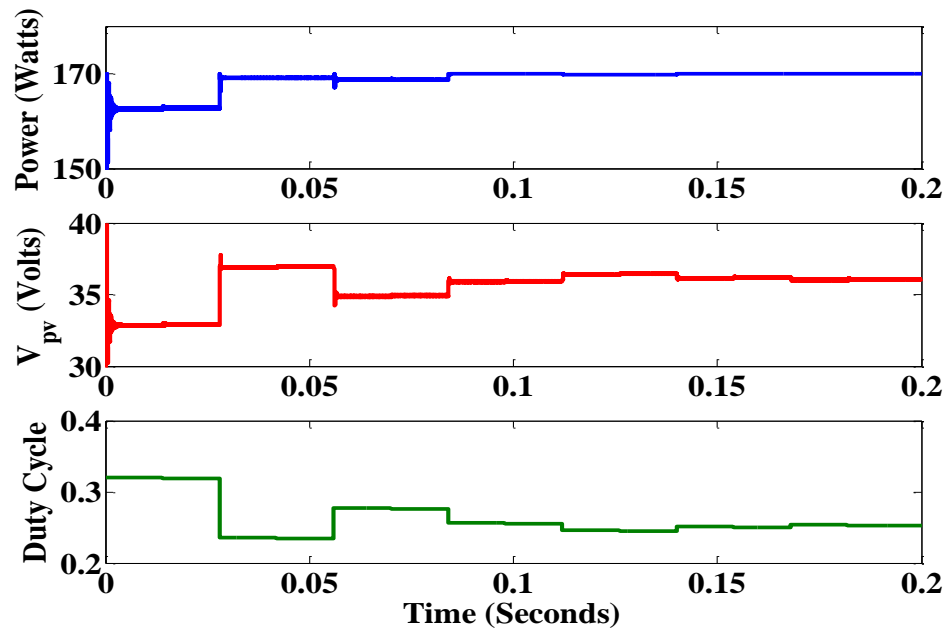


Figure 5.14 : Bisection Method MPPT @1000W/m²

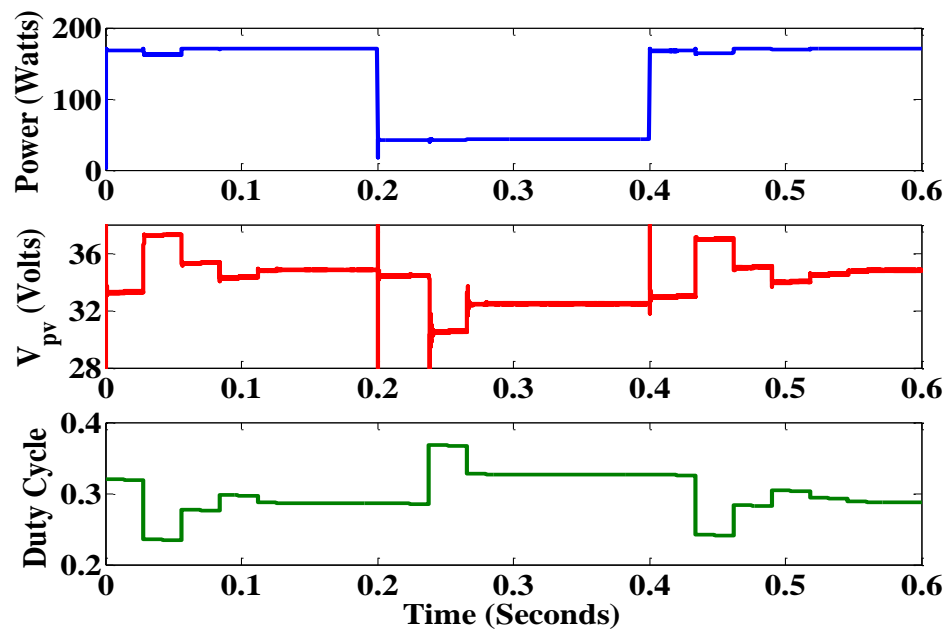


Figure 5.15 : Bisection Method MPPT in Dynamic Environment

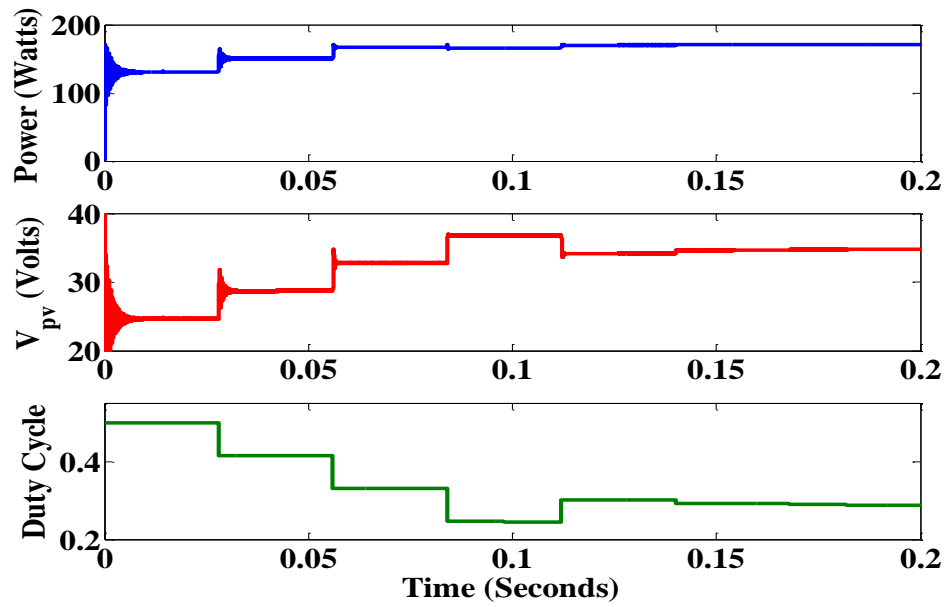


Figure 5.16 : Regula Falsi Method MPPT @1000W/m²

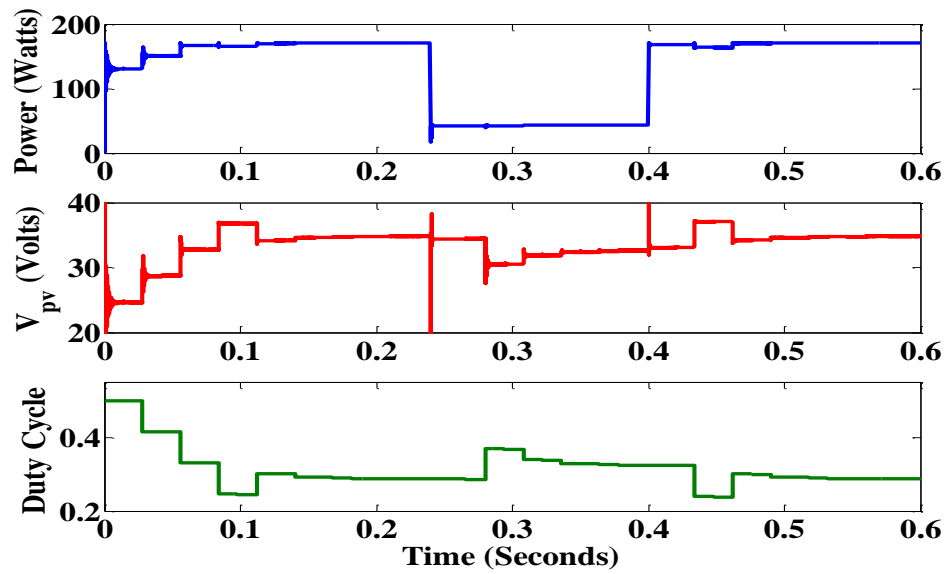


Figure 5.17 : Regula Falsi Method MPPT in Dynamic Environment

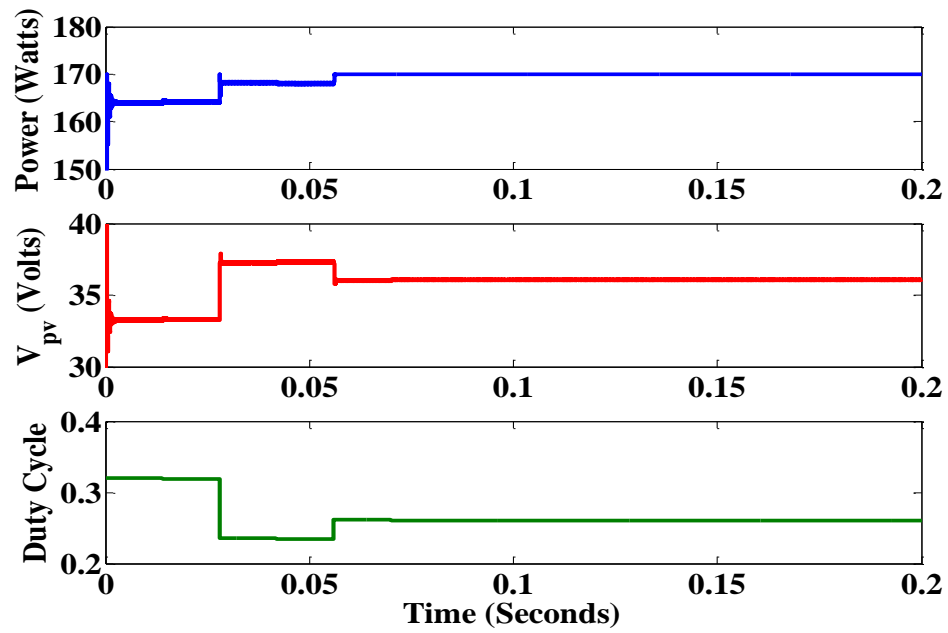


Figure 5.18 : Modified Regula Falsi Method MPPT @1000W/m²

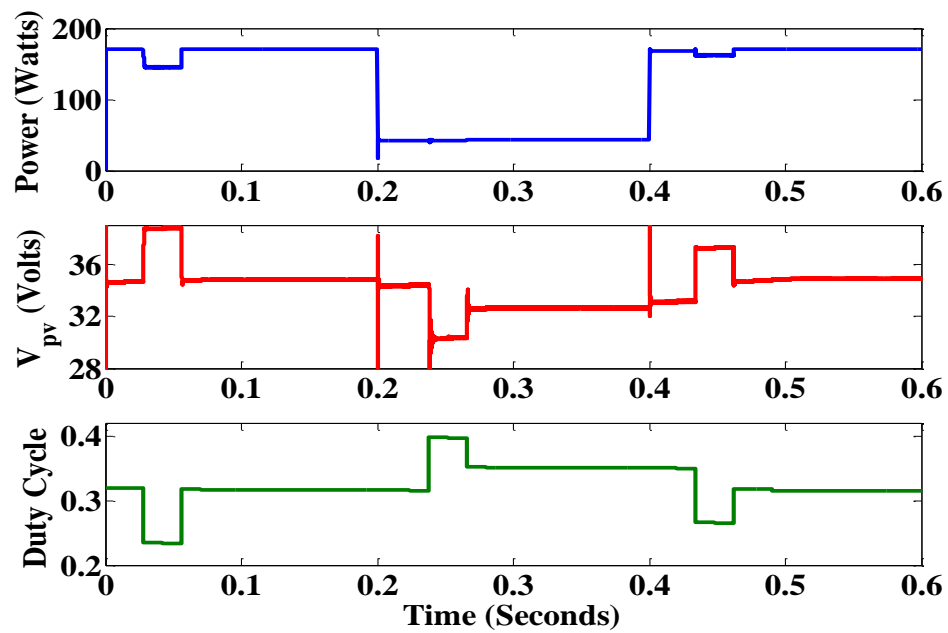


Figure 5.19 : Modified Regula Falsi Method MPPT in Dynamic Environment

5.4.1 Simulation-base comparison

Now to compare the different algorithms, simulation results were performed at S.T.C for different root finding algorithms and are shown in Fig. 5.20. Hence, the MPP is reached when V_{pv} equals $V_{mp} = 34.8$ V. The plots in Fig. 5.20 indicate that the SM takes 6 steps to reach the MPP, the BSM requires 14 steps, the RFM 10 steps, and the MRFM takes 6 steps to reach the MPP.

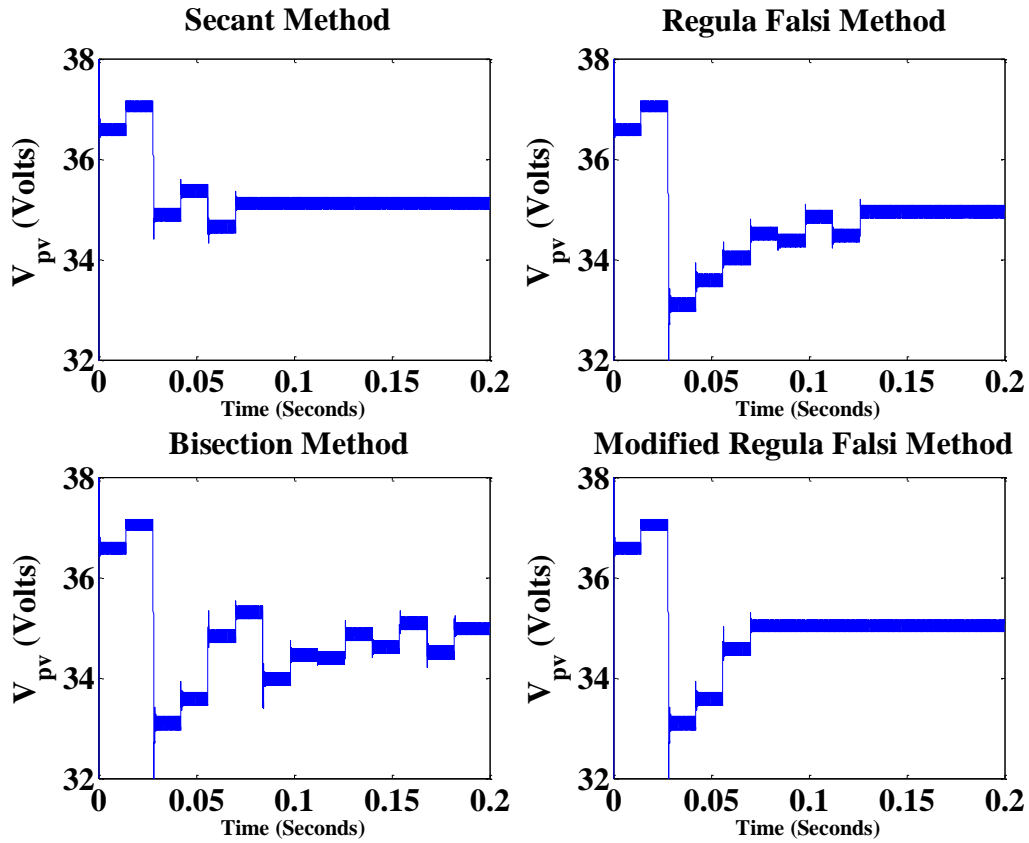


Figure 5.20 : Comparison of the Root Finding Methods DMPPT through simulations

Hence, these results confirm not only that the different root finding algorithms mentioned in this dissertation can be used as DMPPT algorithms (for the NRM, SM, when the initial conditions are good) but also that the MRFM is the fastest method in tracking the MPP. As Fig. 5.20 displays, digitally implemented SM DMPPT is fast and accurate but only when the initial point is near the MPP. However, when the initial point is far from the MPP, the SM diverges. Having the system work in an area close to the MPP is not possible due to the dynamically changing environment the PV model is in. The NRM was not simulated because it has similar behavior to the SM but it is more complex to implement due to the need to calculate the second derivative. Hence, although the NRM is the fastest method discussed earlier here, due to the complication of calculating the second derivative and the aforementioned instability issues, it is not a good choice as a MPPT algorithm. The next three aforementioned bracketing methods solve the instability issue of the SM and the NRM and are shown in Fig. 5.20. As it was discussed above and Fig. 5.20 shows, the DMPPT BSM implemented guarantees to find the MPP but it is slow compared to the RFM and MRFM in finding the MPP. After the initial bracketing procedure of finding a bracket that has the root or MPP inside, the bracket is continuously decreased in half while maintaining the MPP inside the bracket until a termination condition of a fixed tolerance value is met. This process is explicitly shown in Fig. 20. As Fig. 5.20 also displays, the RFM is faster than the BSM by 4 steps and, as it was discussed in the previous section, it also guarantees to reach the MPP. But also, since a retaining point exists, the RFM is slower than the MRFM. Figure 5.20 shows the MRFM as the fastest of all discussed methods that guarantees convergence to the

MPP. It reaches the MPP immediately after finding a bracketing interval. Moreover, compared with fixed step size algorithm (e.g. P&O and INC) the proposed MRFM is more accurate because in the MRFM the step size varies while approaching the MPP, whereas in fixed step cases, oscillation occurs around the true MPP. An example of a fixed step size DMPPT method is the P&O method and the INC method, which was shown in Fig. 5.5-5.10. The resulting oscillation effects of having a fixed step size method is illustrated in Fig. 5.5 -5.7 showing the operating point not being able to converge to the MPP and continuously oscillating around the MPP. Thus, having a variable step size method compared to a fixed step size method is a better choice. All the root finding methods mentioned in this chapter is a variable step size method and hence do not have the problem of infinite oscillation. But each root finding methods do have their pros and cons, such as the open methods (NRM, SM) being fast while having the possibility of evolving into an unstable state and the bracketing methods (BSM, RFM, MRFM) being slightly slower but guaranteed convergence. And through the analysis provided in this chapter it can be concluded that the best choice for a DMPPT utilizing the root finding algorithms is the MRFM.

Chapter 6 : Experimental Results

6.1 EXPERIMENT SYSTEM

A hardware prototype of the DMPPT system was built as shown in Fig. 6.1 -6.2. Tests were run for numerous different root finding based algorithms. The most popular P&O and INC methods were also included in the evaluation. To verify the true MPP at a certain experimental condition a voltage sweep was done for each experiment instance. This was done by running a program on the digital controller immediately after the MPP was reached where the controller started the duty cycle at $D=0.1$ and incrementally increase it until $D=0.7$. This process sweeps the voltage across the PV module where the voltage and the current measurements are sampled resulting in a power plot. From this plot the true MPP can be identified.

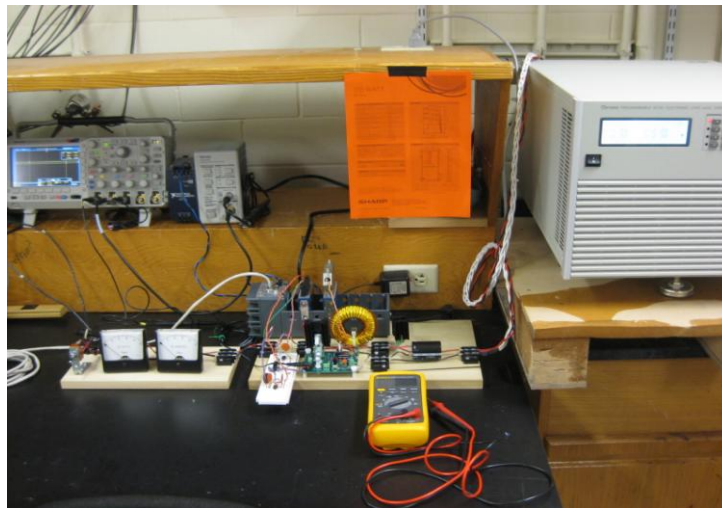


Figure 6.1 : Experiment system setup

The experimental setup consists of three major components, which is the PV module, the DC-DC converter and the Control System. These are explained in more detail in the next section.

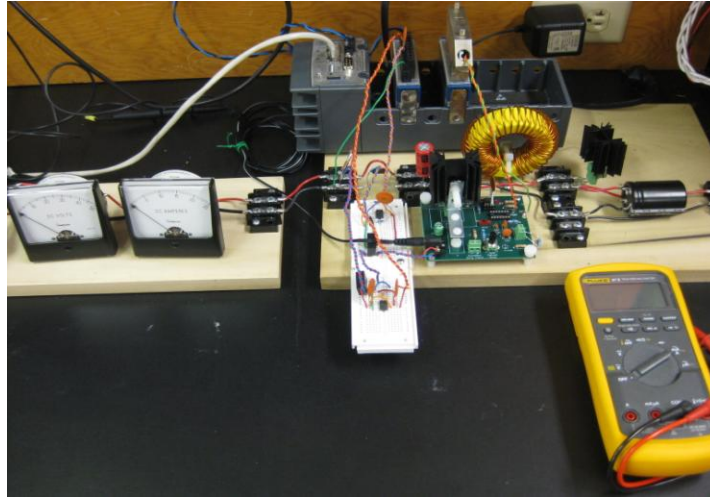


Figure 6.2 : Close up of experimental setup

6.1.1 Photovoltaic Module

Experiments were conducted with a Sharp NE-170U1 PV module under solar light in order to validate the analysis. The basic specification of this PV module at S.T.C. is: $V_{oc} = 43.2\text{V}$, $I_{sc} = 5.47\text{A}$, and $P_{max} = 170\text{W}$ at $V_{mp} = 34.8\text{V}$, $I_{mp} = 4.90\text{A}$.

6.1.2 DC-DC Converter

A boost converter was chosen to interface the PV module and to implement MPPT because of their simplicity and because boost-type of converters is a common choice to interface PV modules in practical applications. The boost converter is operated

in continuous conduction mode (CCM) and the circuit parameters corresponding to the circuit schematic in Fig. 6.3 are $L = 300 \mu\text{H}$, $C_2 = 1500 \mu\text{F}$, PV input Capacitor $C_1 = 10\mu\text{F}$, with a switching frequency of 50 kHz. The inductance value was chosen using (6.1) to keep the converter operating in the CCM even during low irradiance conditions when I_{in} is minimal. According to [39],

$$L > \frac{V_{in}}{2I_{in}f} \quad (6.1)$$

Equation (6.1) is derived from the boundary condition of continuous conduction which is when the minimum value of the inductor current ripple is zero. Hence, in order for the dc-dc converter to operate in continuous conduction mode the inductor value must meet the relation in (6.1).

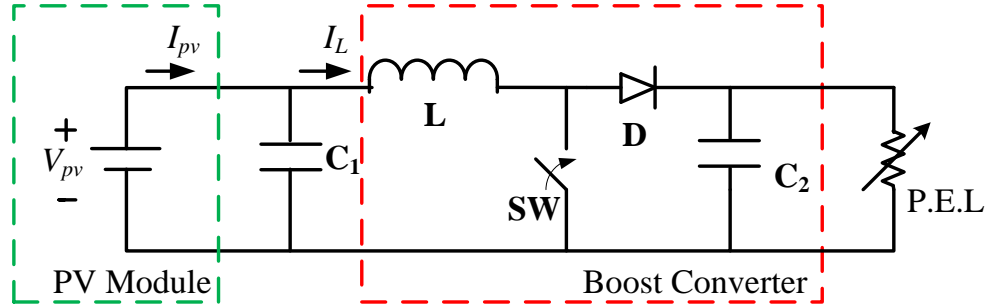


Figure 6.3 : Boost Converter Circuit with a PV module as a source

6.1.3 Control System

As mentioned in Chapter 5 a low cost digital MPP tracker can be commercially realized with an inexpensive microcontroller an ADC and a DPWM controlled boost converter. However, due to the prototyping nature of this project, a NI CompactRIO

system platform was used as shown in Fig. 6.4 because it provides more flexibility and implementation ease, particularly when control parameters need to be continuously changed. The voltage and current values were acquired through an NI 9215 Analog Input Output (AIO) Module into a standard computer from where they were captured. This AIO module has a 16 bit ADC with a signal range of $\pm 10V$. The control DPWM signal is generated by the Field Programmable Gate Array (FPGA) in the cRIO and it is output through a NI 9401 Digital Input Output (DIO) Module. The FPGA uses an internal clock of 40MHz to generate a tick every 25 ns and produces a DPWM signal as shown in Fig. 6.5. Thus, an 800 tick duration is required in order to generate a 50 kHz DPWM signal. This is derived by finding the period of the switching frequency which for 50 kHz is a 20000ns period signal. So $20000ns/25ns = 800$ ticks are required to generate a 50 kHz signal with a resolution of 25ns.

The 'On' or 'High' ticks are related to the duty cycle through (6.2).

$$k = \lceil 800D \rceil$$

$$(k : \text{Number of 'High' ticks for Duty Cycle } D) \quad (6.2)$$

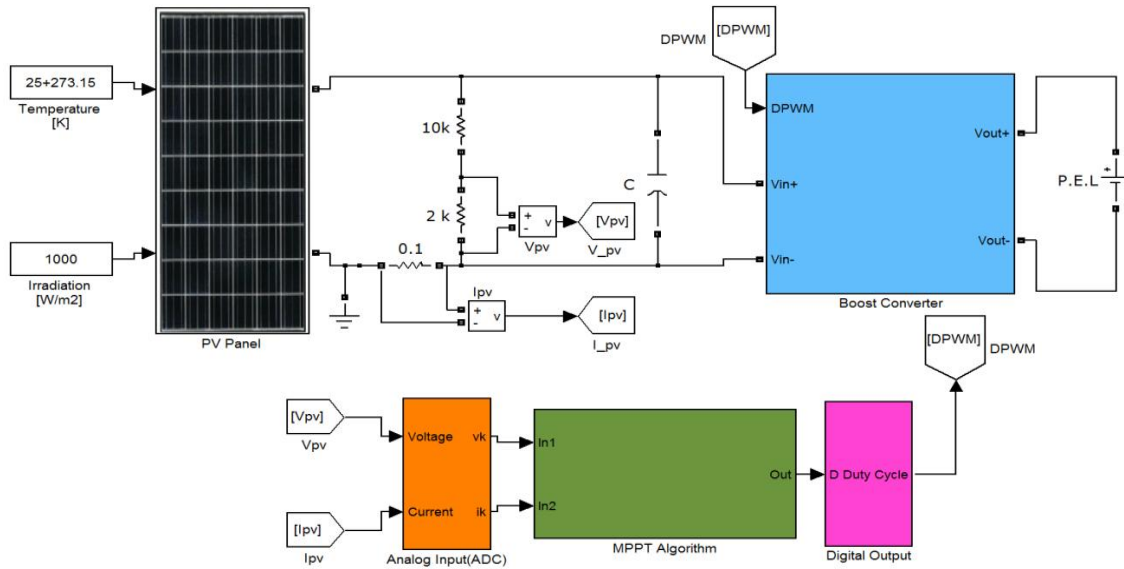


Figure 6.4: DMPPT Experimental Setup for DMPPT

6.2 EXPERIMENTAL RESULTS

Figures 6.6 to 6.12 shows the experimental results obtained for all of the root finding optimization methods mentioned in this paper. Each figure has two parts. The left side of each of these figures consists of the DMPPT algorithm tracking the MPP, i.e., it indicates real extracted power. On the right side, they show an I-V sweep done immediately after the tracking to verify the true MPP, i.e., it indicates real PV panel MPP. These experimental results follow the simulation outputs discussed in Chapter 5 very closely. Figures 6.6 to 6.8 are the experimental results of the P&O and INC methods. Figures 6.7 and 6.8 show the INC method at two different duty cycle step settings. Figure 6.7 is set at a large duty cycle step ($\Delta D=0.01$) in order to show that it

oscillates around the MPP, whereas Fig. 6.8 displays the case of a small duty cycle step ($\Delta D=0.005$) which takes longer to converge to the vicinity of the MPP. Figure 6.9 exemplifies the SM with a good initial condition choice. As shown, the SM reaches the MPP in 5 sets of samples. The first three sets of samples are the initial bracketing phase where the operating point is moved 4V at a time until it contains the root of MPP in the bracket before conducting the iterative process. One set consists of two samples to calculate the backward difference quotient. Figure 6.10 depicts the BSM. For this method, the MPP is reached in a total of 8 sets. As for the SM case the first three sets are the bracketing phase then the bracket is reduced in size by $\frac{1}{2}$ while containing the MPP within until a termination condition is met. Figure 6.11 exemplifies the RFM which requires a total of 5 sets to reach the MPP. After the initial bracketing phase the new approximation of the root is calculated and the operating point is moved to that point repetitively until a termination condition is met. Finally, Fig. 6.12 shows the MRFM. This newly proposed MPPT method is the fastest of all of those tested here, reaching the MPP in a total of 4 sets. Therefore, experiments validate the analysis showing not only convergence to the MPP for the discussed root-finding methods, but also that the newly proposed method based on the MRFM converges to the MPP faster than all other methods with ensured convergence to the MPP.

The controller used in this experiment is the NI CompactRIO which provides a wide range of input and output modules that can be chosen by the engineer and configured to do numerous different data acquisition tasks. In the DMPPT setup an analog input module and a digital output module is needed to control the dc-dc converter

to track the MPP of the PV module. In choosing the analog module not only is the input voltage range important to be checked but the ADC resolution is also important to reduce quantization noise mentioned in Chapter 5. Also the sampling rate is an important factor that needs to be considered when choosing an analog input module. When choosing the sampling rate it depends on the system dynamic response whether it is a fast changing system and also whether or not monitoring the transient is important. In the case of the setup for this research, samples that were used in the calculation were the sampled value obtained after the system had reached a predetermined steady state so the need for a high speed sampling rate module was not critical. An NI 9215 AIO module was used which has a 16 bit ADC with a signal range of $\pm 10\text{V}$ and sampling rate of 100k Samples/s and 4 channels. As for choosing the digital output module the possible output resolution of the output signal is important especially when the DMPPT algorithm like the root finding algorithms evaluated in this research requires a computation of a derivative a fine resolution is required from the digital output module. This is governed by the clock speed that drives the digital output module. In the NI CompactRIO a FPGA is embedded that is capable of generating a 40MHz clock which triggers the NI 9401 DIO Module used in this research giving a resolution of 25ns and comes with 8 channels.

The NI CompactRIO was also used in the solar car project done at the University of Texas at Austin supervised by Professor Gary Hallock. Because of the many capabilities of the device it was used to control the motors, monitor battery charge and health and communication functions. In the previous solar car models, an independent MPPT system was purchased and used to track the MPP on the solar arrays. In the new

solar car model the possibility of doing the MPPT of the solar arrays utilizing the NI CompactRIO and the MRFM DMPPT method were brought up and initial research and tests proved promising results.

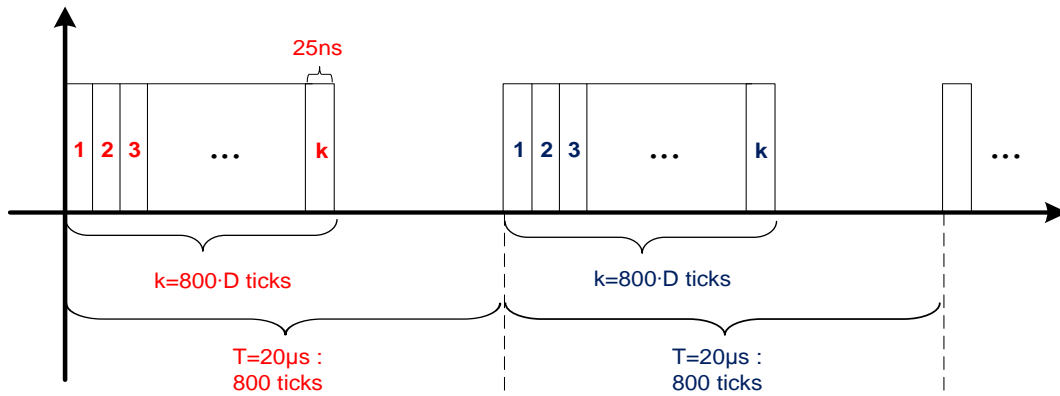


Figure 6.5 : DPWM signal from the FPGA

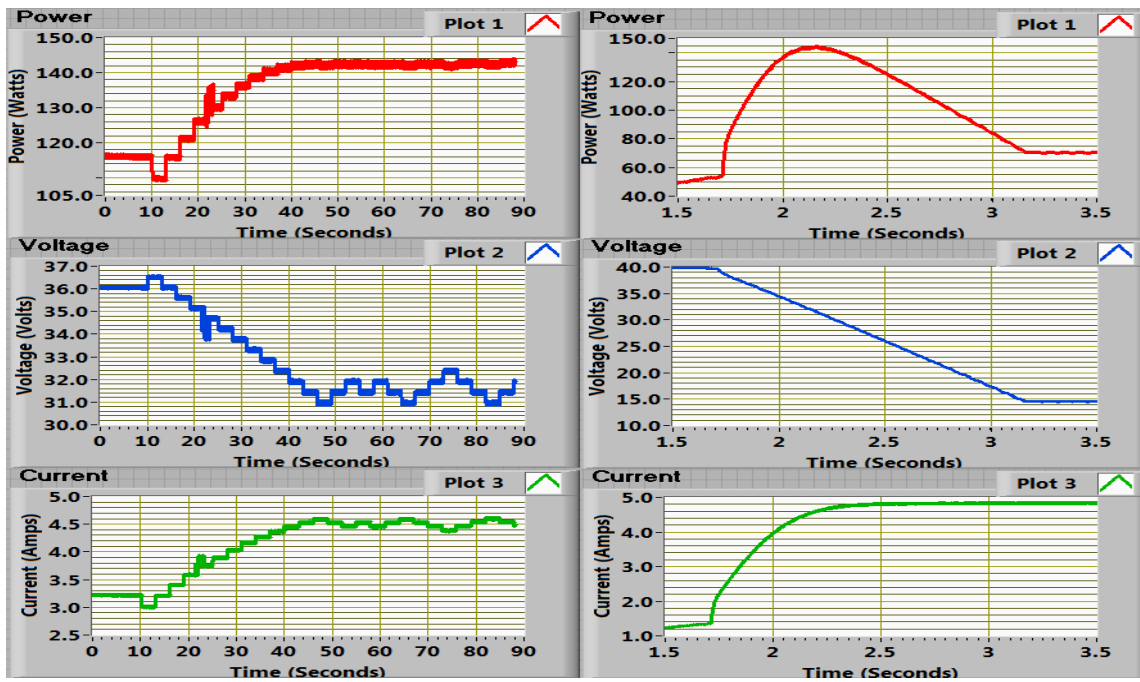


Figure 6.6 : Experimentally generated results for the P&O DMPPT

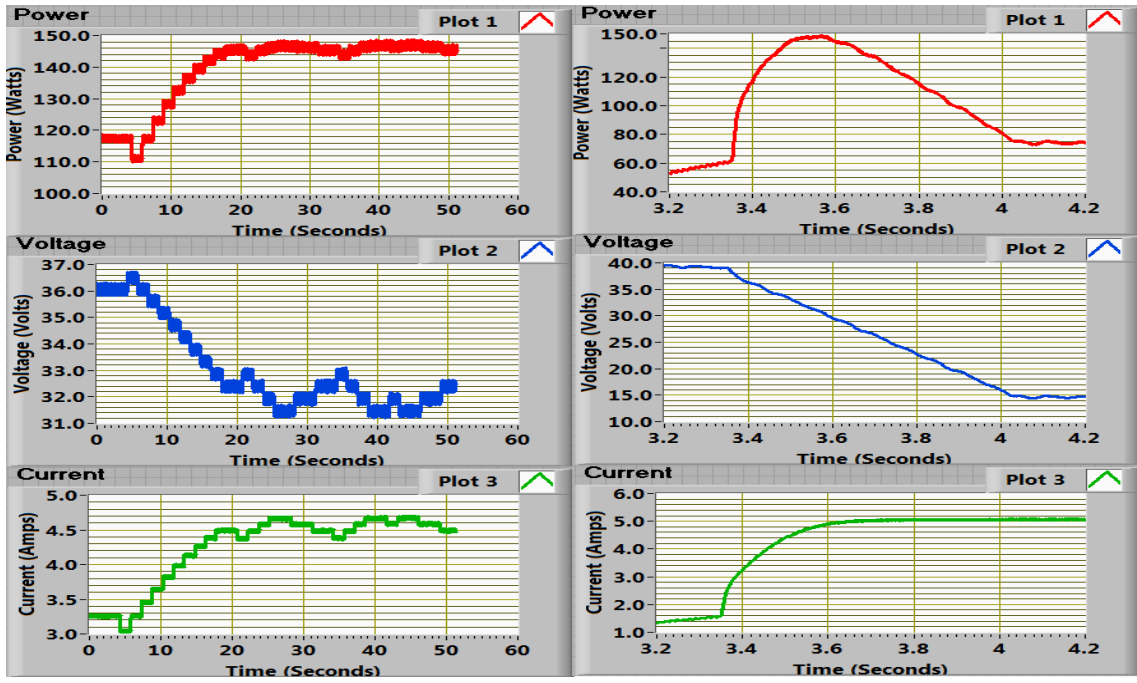


Figure 6.7 : Experimentally generated results for the INC DMPPT, $\Delta D=0.01$

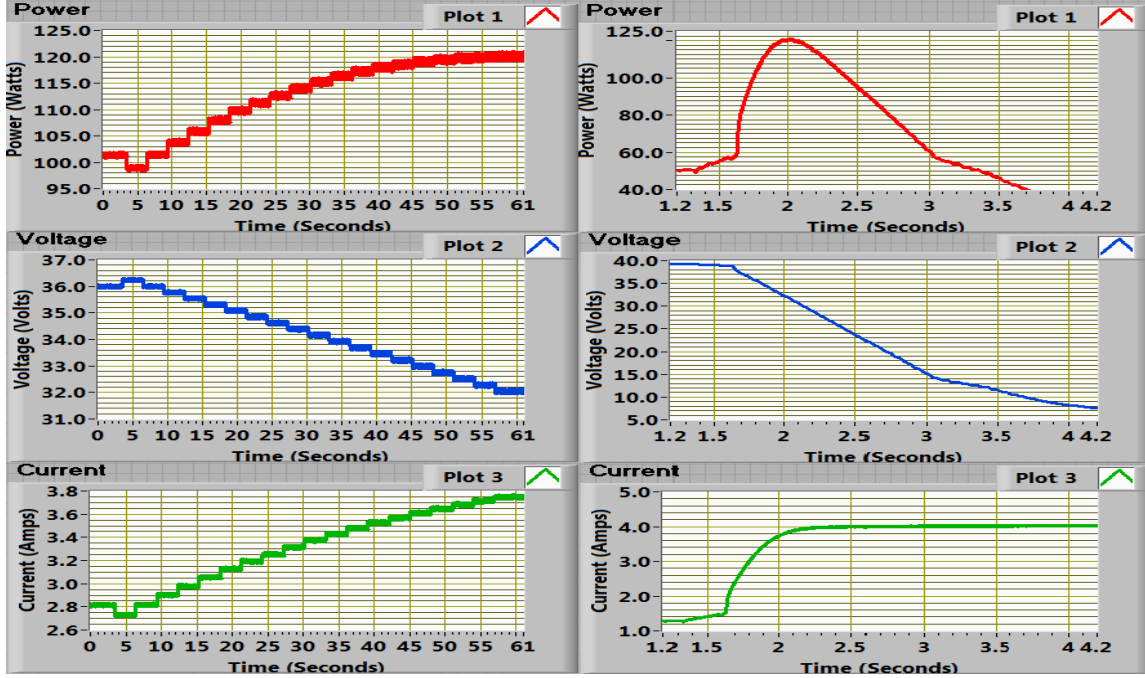


Figure 6.8 : Experimentally generated results for the INC DMPPT, $\Delta D=0.005$

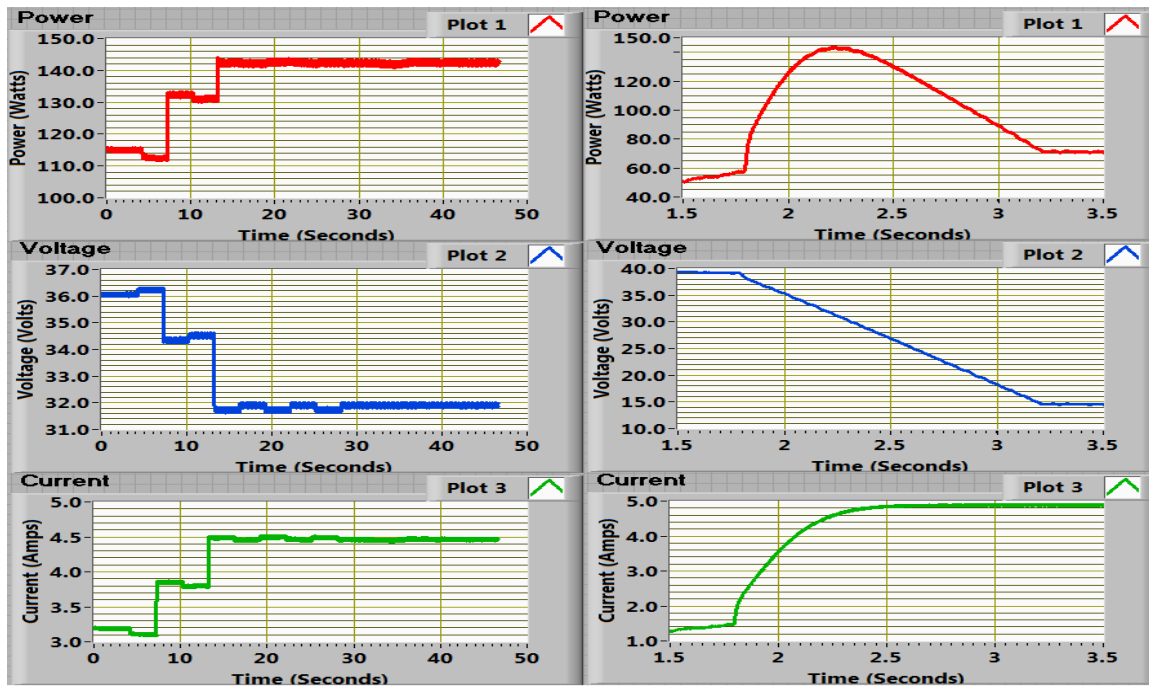


Figure 6.9 : Experimentally generated results for the SM DMPPT

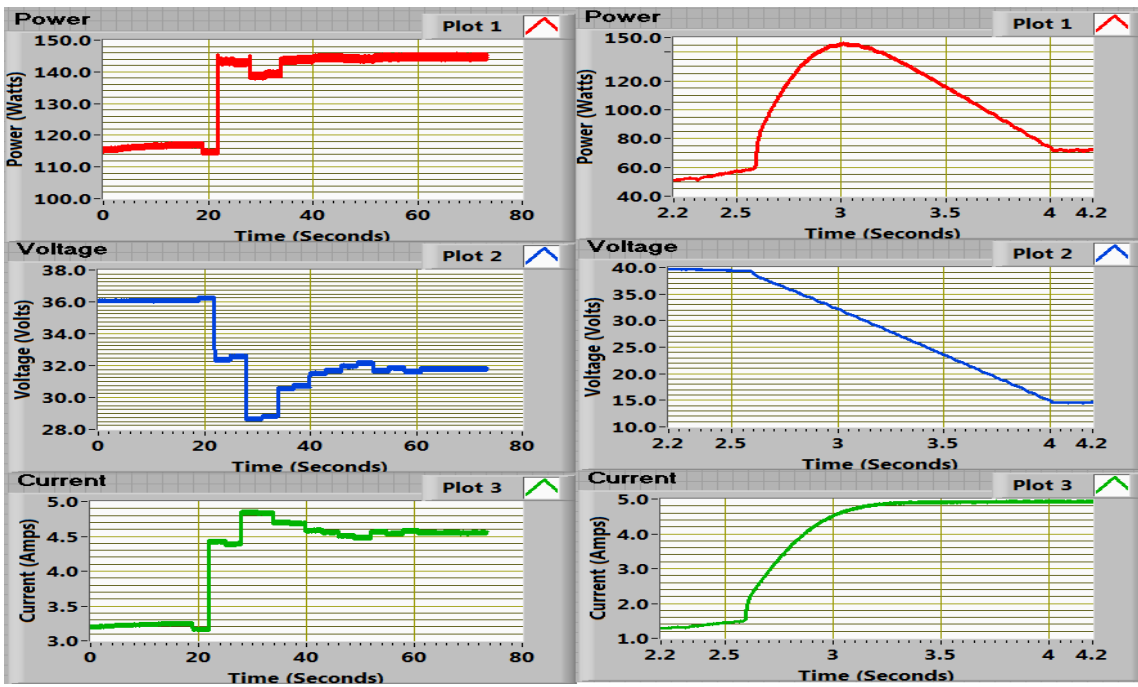


Figure 6.10 : Experimentally generated results for the BSM DMPPT

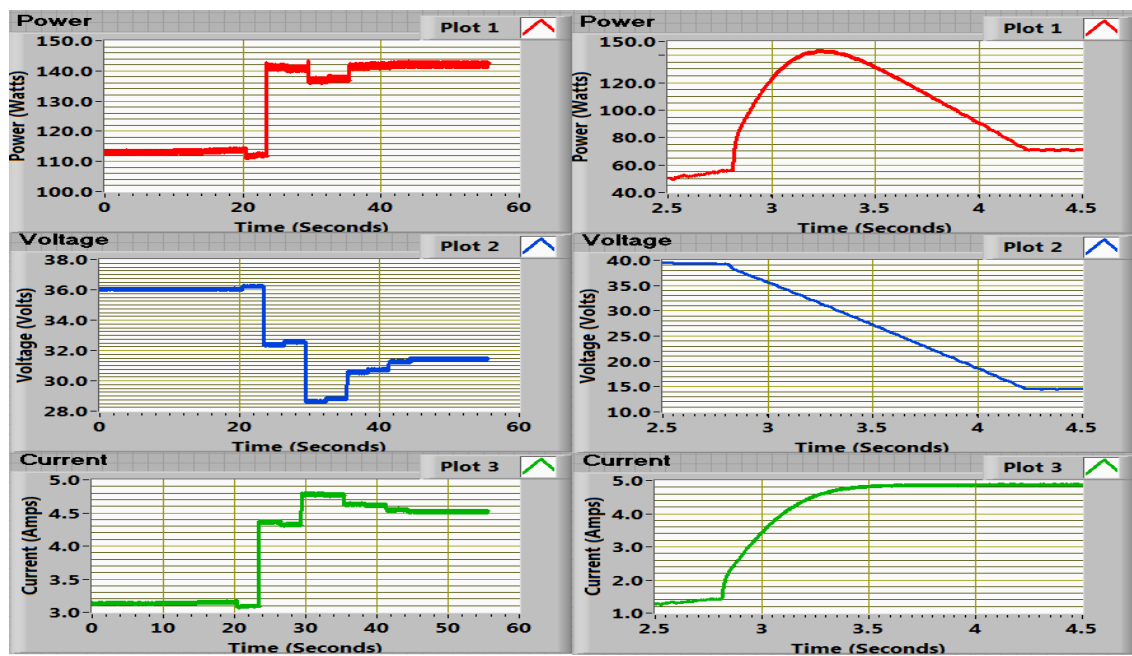


Figure 6.11 : Experimentally generated results for the RFM DMPPT

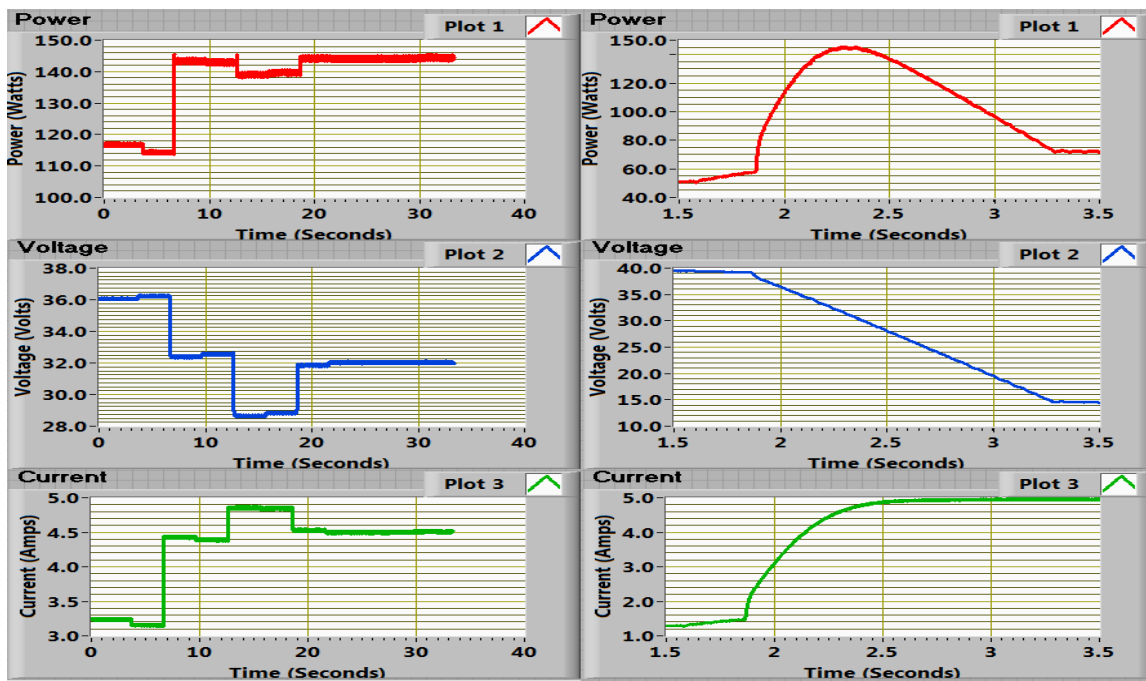


Figure 6.12 : Experimentally generated results for the MRFM DMPPT

Chapter 7 : Shading Effects

7.1 INTRODUCTION

The performance of a photovoltaic module is not only affected by the temperature and irradiance as mentioned in Chapter 2 but also shading [40]. Due to partial shading on the PV module shown in Fig. 7.1 the partially shaded area will generate less current than the unshaded area or cells. A PV module divided into four subsections is shown in Fig. 7.1.

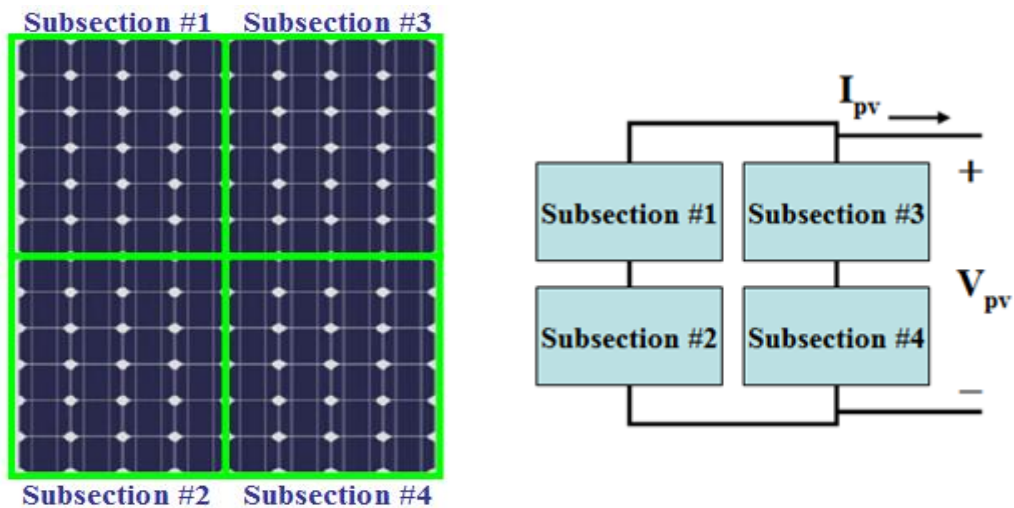


Figure 7.1 : PV module divided into 4 subsections

For each subsection (Subsection #1 – Subsection #4) shown in Fig. 7.2 all cells are connected in series which requires the same amount of current to flow in all cells. Since the unshaded cells generate a larger current than the shaded cell it will force the shaded cell to operate at higher current value than it can produce and to do it would have

to operate in the reverse bias region causing the cell to act as load rather than a generator [41]. This results in the shaded cell to dissipate power as heat and causes “hot spots” which can harm the PV module by degrading the cell and in cases the whole system by affecting its performance. So in order to minimize the effect of partial shading a diode is connected in parallel to the cell to allow the current to bypass the shaded cell. By connecting the bypass diode it will decrease the amount of dissipated power resulting on the shaded cell. But it will also result in multiple peaks in the P-V plot.

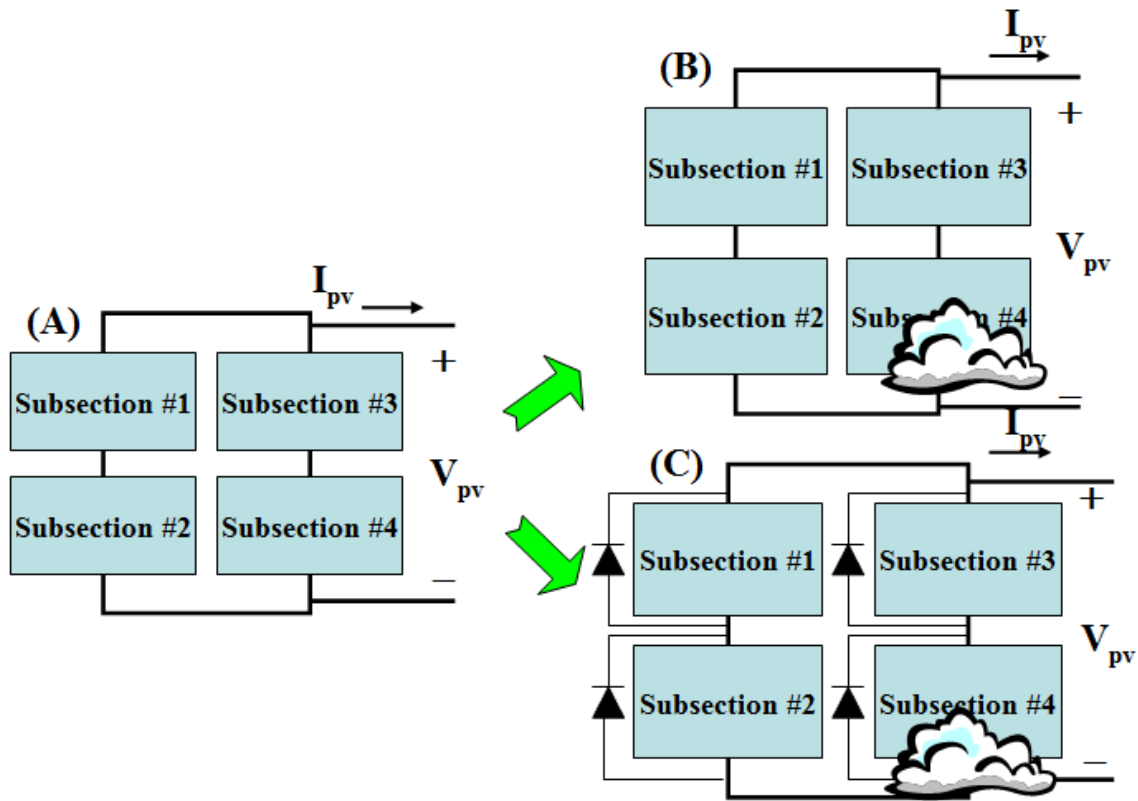


Figure 7.2 : (A) PV Module Divided into Subsections (B) Partially shaded PV Module w/o Bypass Diode (C) Partially shaded PV Module w/ Bypass Diode

Fig. 7.3 shows the I-V plot of case (B) in Fig. 7.2 which shows a decrease in the maximum current being generated from the PV module and Fig. 7.4 shows the resulting

decrease in maximum power that is able to be extracted. Fig. 7.5 shows the I-V plot of case (C) in Fig. 7.2 where the multiple threshold breakdown happens across the diode in the mathematical model in chapter 2. This is the reason for the multiple peaks shown in Fig. 7.6.

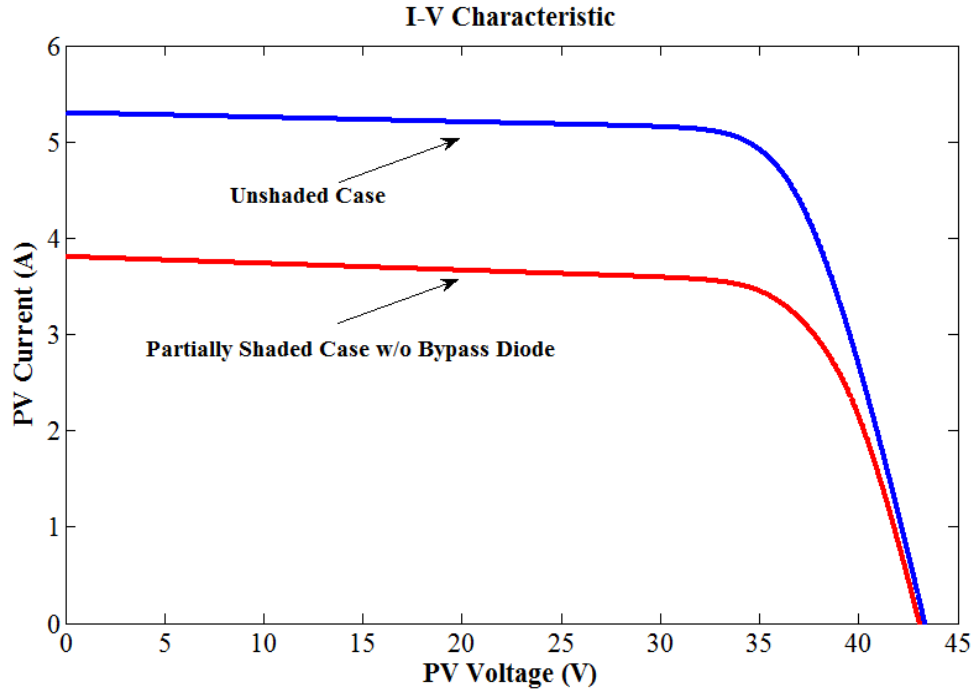


Figure 7.3 : I-V Plot for Unshaded & Partially Shaded Case w/o Bypass Diode

Due to the multiple peaks shown in Fig. 7.6 the possibility of tracking the wrong MPP increases and the effectiveness of utilizing the existing MPPT methods are reduced resulting in a decrease in power extraction efficiency of the PV module [40]. This erroneous tracking of the MPP due to multiple peaks also applies to the root finding methods mentioned in this research.

Many research [40]-[52] has been done in the past to solve this problem and in this research the method done in [45] which is to divide a PV module into subsections and to use a multiple input converter (MIC) as the power electronic interface for each subsection and individually track the MPP for each one was chosen and shown to increase the efficiency of power extraction. This hardware solution was applied to the MRFM DMPPT method to show that the MRFM is feasible in a partial shading condition.

Besides what was proposed in [45] the majority of the approach to solving the problem of the multiple local maximum due to partial shading are algorithm based [42]-[44],[47]-[48], [50]-[52]. For instance in [42], Fibonacci sequence is used to track the global MPP under partially shaded conditions. In [43] is a variant of the P&O method that utilizes pilot or monitoring cells. And in [44] a state space-based approach is presented to search the global MPP which is fast, accurate but is system specific, complex, and requires numerous sensors. In [47] they have proposed a two-stage method to track the global MPP. In the first stage, the operating point moves into a close area of the global MPP then in the second stage it converges to the actual global MPP. In [48] the proposed method is based on the critical observation that the peaks follow a specific trend that is 80% of the V_{oc} . In [50] the method proposed is based on INC method with step-size variation. In [51] Particle Swarm Optimization (PSO) algorithm has been employed in the proposed method to track the global MPP. In [52] a variant of the Particle Swarm Optimization algorithm known as the Adaptive Perceptive Particle Swarm Optimization is used to trace the global MPP.

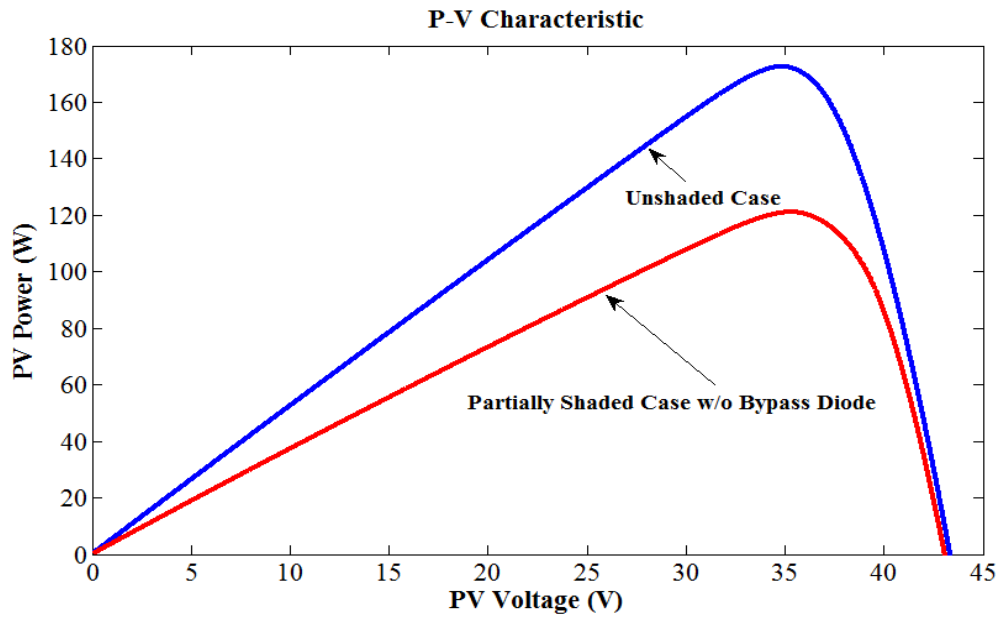


Figure 7.4 : P-V Plot for Unshaded & Partially Shaded Case w/o Bypass Diode

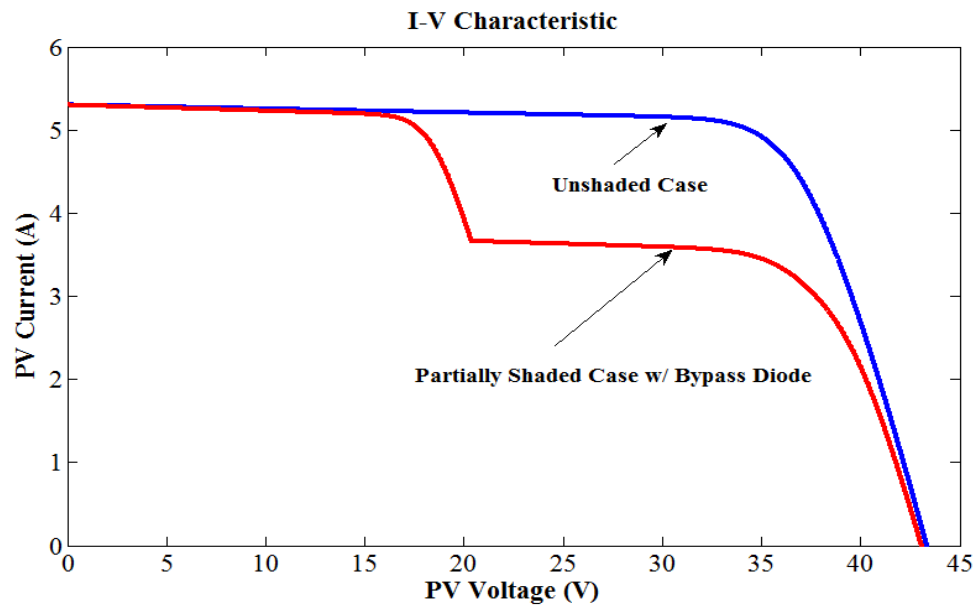


Figure 7.5 : I-V Plot for Unshaded & Partially Shaded Case w/ Bypass Diode

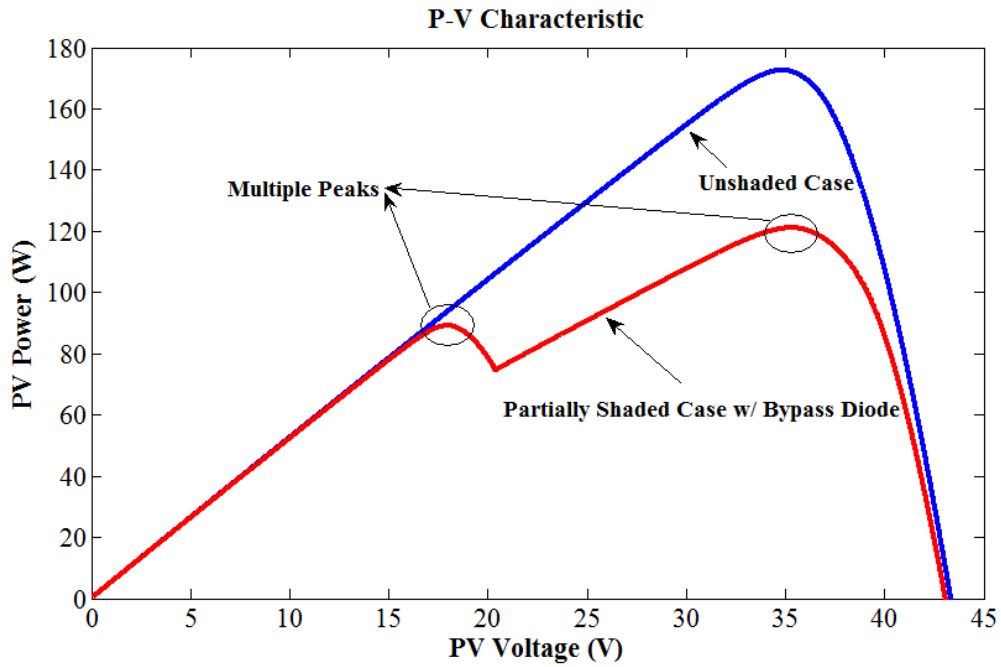


Figure 7.6 : P-V Plot for Unshaded & Partially Shaded Case w/ Bypass Diode

7.2 MULTIPLE INPUT CONVERTER

A Multiple Input Converter (MIC) is a promising topology for diversification of multiple energy source where in this case multiple subsections of a PV module are the multiple sources[53]- [59]. It is a circuit that if compared to a combination of several single input topology converters is more cost effective, compact in size, requires fewer components, and is easier for future expansion.

In this research a PV module is divided into subsections and each subsection is connected as an energy source to each leg of a multiple input boost converter.

7.3 DMPPT USING MIC

By utilizing a multiple input boost converter and having each subsection of a PV module as the input for each leg as shown in Fig. 7.7 it is possible to do the DMPPT on each leg of the converter individually. By doing the DMPPT on each subsection separately rather than on the whole entire PV module increases the efficiency of power extraction significantly. A simulation was done for two different cases where the first case was a PV module with partial shading on subsection #4 and the MRFM DMPPT was done on the entire PV module. The simulated system is shown in Fig. 7.8. On the other case MRFM DMPPT was done on each subsection of a PV module individually where the partial shading and the temperature and irradiation conditions were exactly the same as the previous case and the simulated system is shown in Fig. 7.9.

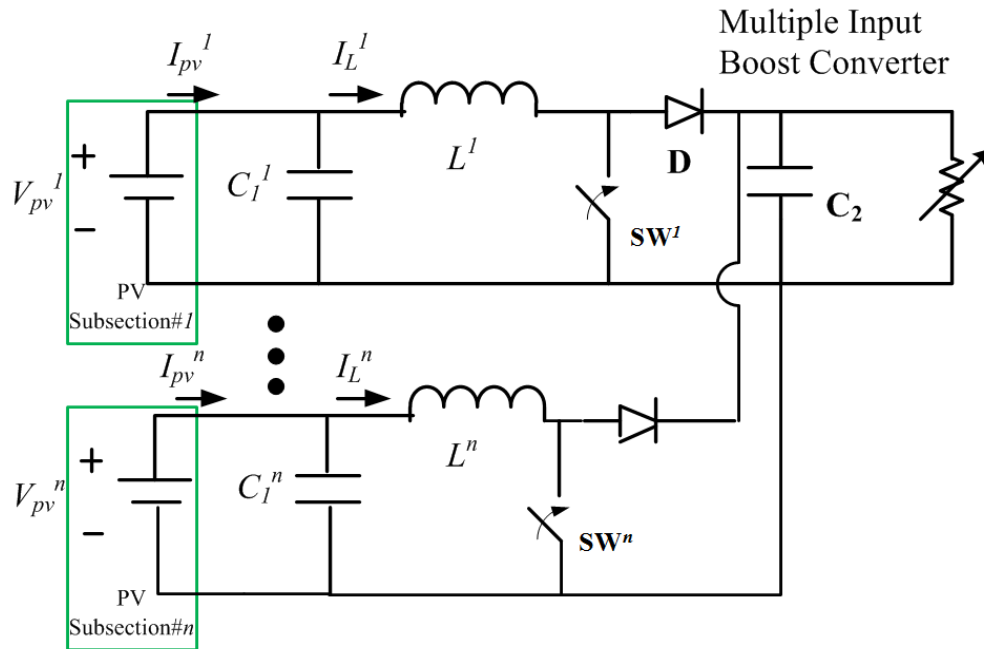


Figure 7.7 : Multiple Input Boost Converter connected to subsections of a PV Module

Each subsection of the PV module was simulated to generate 43.2W at 25°C, 1000W/m² and 17.1W at 25°C, 400W/m². So this results in 172.8W being generated by the PV module at no shading condition.

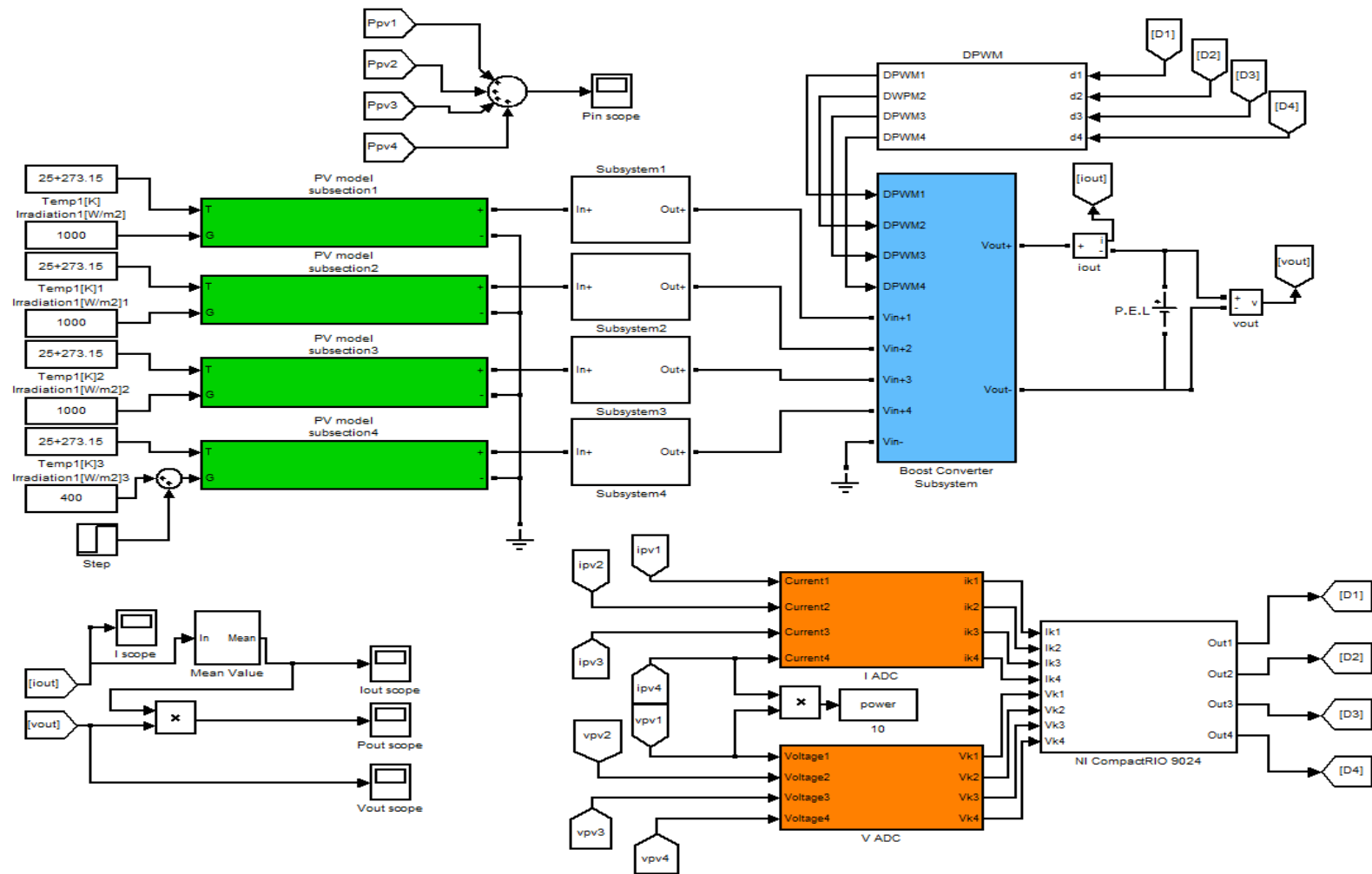


Figure 7.9 : DMPPT System with Partial Shading utilizing Multiple Input Boost Converter

7.3.1 Simulation Results

Figure 7.10 shows the multiple peaks in the P-V plot for the partial shading condition of the simulated P-V panel. From the simulation result in Fig. 7.11 it is shown that the MRFM DMMT process from the system of Fig. 7.8 has tracked the false local maxima in the partial shading condition and the system is generating 89.1W. The latter part shows the system generating the maximum power of the PV module of 172.8W after the shading has cleared away. As for Fig. 7.12 it shows the simulation result of the system in Fig. 7.9 generating 146.7W during the same partial shading as was done in the system shown in Fig. 7.8 which is close to 1.5 times the power generated in Fig. 7.11.

So in conclusion by dividing up the PV module into subsections and utilizing a MIC as the power electronic interface to do the DMPPT on each subsection of the PV module proved to increase the power extraction efficiency of the system.

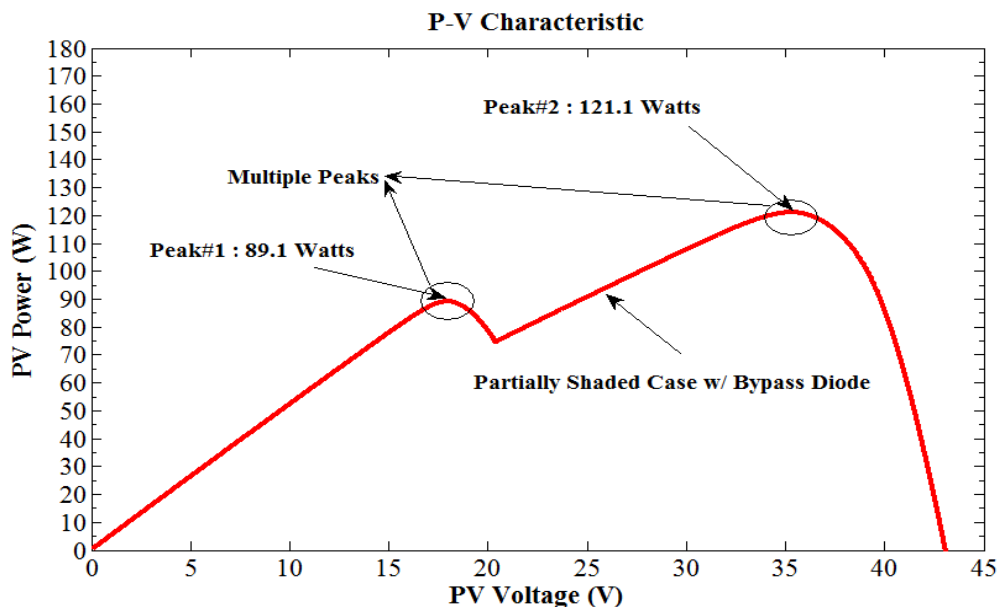


Figure 7.10 : P-V plot of simulated PV module with partial shading

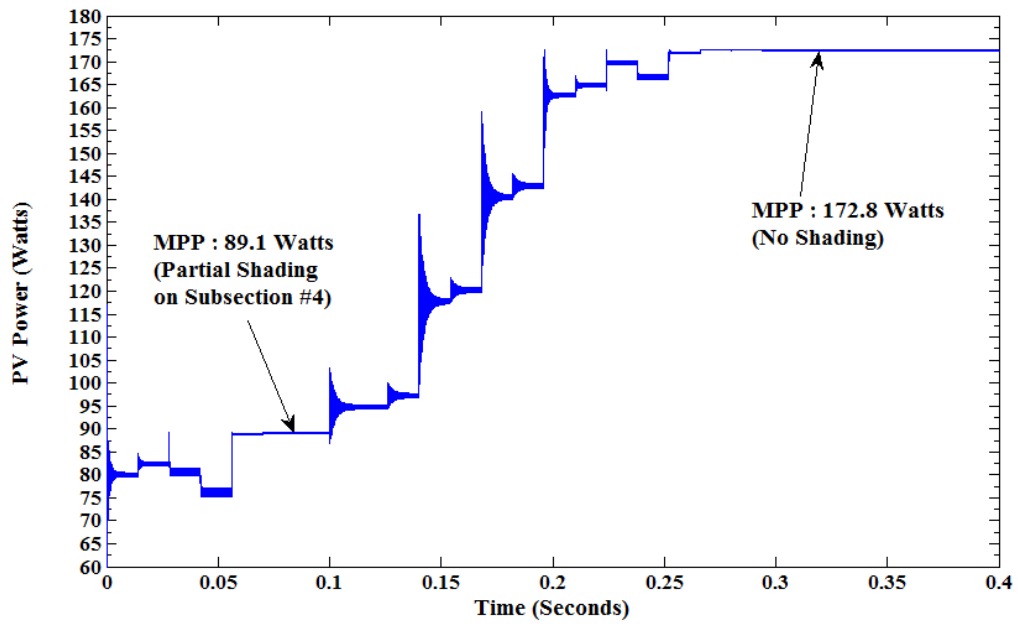


Figure 7.11 : Simulation result of MRFM DMPPT for the system in Fig. 7.8

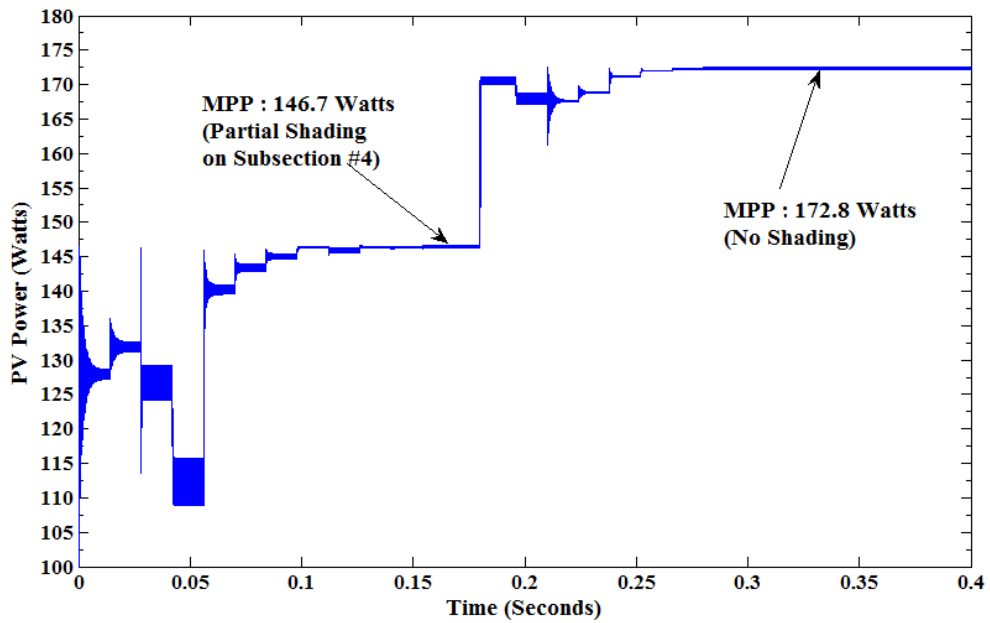


Figure 7.12 : Simulation result of MRFM DMPPT for the system in Fig. 7.9(MICs)

Chapter 8 : Conclusion

8.1 SUMMARY

Photovoltaic systems are one of the leading technologies envisioned in order to achieve carbon footprint reduction and more sustainable energy generation means. In these systems, power electronic interfaces are essential components because they allow the necessary energy efficiency conversion to harness this renewable energy source. Hence, MPPT methods are key enablers of a more energy sustainable society. Due to their implementation ease, low cost and flexible operation, in the past few years more and more controllers for such sustainable systems are being implemented on a digital platform. This dissertation has discussed an alternative perspective to the classical approach to MPPT. A numerical analysis approach for finding a root for the dP/dV function was performed. In particular, this paper comprehensively discussed classical root finding algorithms and their use for MPPT was verified. Since these methods had been originally developed in a continuous variable domain, this work included thorough mathematical analysis that validates their implementation in a digital domain. This mathematical analysis discussed the impact of digitalizing such control strategies in terms of convergence to the MPP by exploring numerical stability characteristics of the root finding methods in the digital domain and the effect of quantization and discretization errors. Based on the analysis a new variable step DMPPT method called the MRFM was presented and its implementation was discussed. The analysis was validated both with

simulations and with a hardware-based experimental test bed. All of the experiments were performed with the same test bed. No hardware alteration was needed in order to implement each method which in addition of highlighting a merit of digital implementation it also ensures uniformity and unbiased testing for all discussed methods. These evaluations confirm the analysis by demonstrating that digitally implemented classical root finding MPPT operate as expected. Bracketed methods are identified to be better options than open interval methods because in the latter convergence to the MPP is not ensured. Simulations and experiments also confirm that the proposed MRFM is the fastest of the discussed algorithm to reach the MPP.

Since the effects of partial shading are an important issue in solar energy extraction and MPPT, a hardware solution to this problem has been investigated and verified through simulation. The hardware solution was to utilize MICs and partition the PV module into subsections to do the MPPT on each subsection separately. In this research, to verify the validity of this approach of utilizing a MIC to solve the partial shading effects a multiple input boost converter was used to connect the partitioned subsections of the PV module as inputs to each leg of the MIC. Without the MIC the DMPPT system was shown through simulations, to track the wrong MPP resulting in an inefficient energy extraction of the PV module. However, when using the MIC it was verified through simulation not only that the proposed MRFM can also be implemented in a multiple input converter, but also that the power extraction for the entire system under partially shading conditions increased significantly.

8.2 FUTURE WORK

This analysis was focused on solar applications but can also be extended to applications in the wind power generation and fuel cell power generation applications. It is also possible to extend the system to where the sources connected to the multiple input converter is not only just the subsections of the PV module but other renewable energy sources and also incorporating a battery as another source and utilizing a multiple input bidirectional converter to be able to not only store energy but also provide energy in cases where the solar or wind energy isn't available. This is a favorable system for the power system of a plug in hybrid electric vehicle (PHEV) which is an important technology that will help to address issues that may conduct to an energy crisis or may aggravate an existing one.

Appendix A

A.1 MATLAB CODE

This appendix includes the MATLAB code used to simulate the plots in Chapter 5 and 7.

[Perturb & Observe Algorithm]

```
function [D, out] = MPPT(ik, vk)

persistent vk_store
persistent ik_store
persistent index
persistent stage
persistent Dref

if isempty(vk_store)
    vk_store = zeros(2,1);
    ik_store = zeros(2,1);
    index = 1;
    stage = 0;
    Dref = 0.5;

end

deltaD = 0.01;

switch stage

    case 0
        Dref=0.5;
        stage = stage +1;
    case 1
        vk_store(index) = vk;
        ik_store(index) = ik;

        index = index+1;
        stage = stage+1;

        Dref = Dref - deltaD;

    case 2
        vk_store(index) = vk;
        ik_store(index) = ik;
```

```

P2 = vk_store(2)*ik_store(2);
P1 = vk_store(1)*ik_store(1);

dP = P2 - P1;
dV = vk_store(2)-vk_store(1);

if(dP==0)
    Dref=Dref;
else
    if(dP>0)
        if(dV>0)
            Dref=Dref-deltaD; %coming in from the left side of
                               MPP
        else
            Dref=Dref+deltaD; %coming in from the right side of
                               MPP
        end
    else
        if(dV>0)
            Dref=Dref+deltaD; %pulling back towards mpp on LHS
        else
            Dref=Dref-deltaD; %pulling back towards mpp on RHS
        end
    end
end

vk_store(1) = vk_store(2);
ik_store(1) = ik_store(2);

index = 2;
stage = 2;

end

D = Dref;
out = vk_store;

```

[Incremental Conductance Algorithm]

```

function [D, out] = MPPT(ik, vk)

persistent vk_store
persistent ik_store
persistent index
persistent stage
persistent Dref

```

```

if isempty(vk_store)
    vk_store = zeros(2,1);
    ik_store = zeros(2,1);
    index = 1;
    stage = 0;
    Dref = 0.5;

end

deltaD = 0.01;

switch stage

    case 0
        Dref=0.5;
        stage = stage +1;
    case 1
        vk_store(index) = vk;
        ik_store(index) = ik;

        index = index+1;
        stage = stage+1;

        Dref = Dref - deltaD;

    case 2
        vk_store(index) = vk;
        ik_store(index) = ik;

        dV = vk_store(2)-vk_store(1);
        dI = ik_store(2)-ik_store(1);

        if(dV==0)

            if(dI>0.02)
                Dref=Dref-deltaD;
            elseif(dI<-0.02)
                Dref=Dref+deltaD;
            else
                Dref = Dref;
            end
        end

        if(dV~=0)
            INC = ik_store(2)/vk_store(2)+dI/dV;
            if(INC>0.02)
                Dref=Dref-deltaD;
            elseif(INC<-0.02)

```



```

                                Dref=Dref+deltaD;
                        else
                                Dref = Dref;
                        end
                end
                vk_store(1) = vk_store(2);
                ik_store(1) = ik_store(2);

                index = 2;
                stage = 2;

end

D = Dref;
out = vk_store;

```

[Secant Method Algorithm]

```

function D = MPPT(ik, vk, V_L)

persistent vk_store
persistent ik_store
persistent index
persistent stage
persistent Dref
persistent P

if isempty(vk_store)
    vk_store = zeros(6,1);
    ik_store = zeros(6,1);
    index = 1;
    stage = 0;
    Dref = 0.7;
    P=0;
end

switch stage

    case 0
        Dref=0.25;
        stage = stage +1;

    case 1
        vk_store(index) = vk;
        ik_store(index) = ik;

```

```

        Dref = Dref - 0.48/V_L; %currently NI9401 1LSB is 0.005
        index = index +1;
        stage = stage +1;

case 2
    vk_store(index) = vk;
    ik_store(index) = ik;

    P1 = vk_store(1)*ik_store(1);
    P2 = vk_store(2)*ik_store(2);
    P3 = vk_store(3)*ik_store(3);
    P4 = vk_store(4)*ik_store(4);

    if(vk_store(3)==0)
        Dref = Dref +sign(P1-P2)*2.2/V_L;

        index = index + 1;
        stage = stage - 1;
    else

        fda = (P2-P1)./(vk_store(2)-vk_store(1));
        fdb = (P4-P3)./(vk_store(4)-vk_store(3));
        ck = vk_store(4)-(fdb*(vk_store(4)-vk_store(2))/(fdb-fda));

        Dref = Dref+((vk_store(4)-ck)/V_L) + 0.48/V_L;

        index = index+1;
        stage = stage +1;
    end

case 3
    vk_store(index) = vk;
    ik_store(index) = ik;

    Dref = Dref - 0.48/V_L; %currently NI9401 1LSB is 0.005
    index = index+1;
    stage = stage +1;

case 4
    vk_store(index) = vk;
    ik_store(index) = ik;
    P1 = vk_store(1)*ik_store(1);
    P2 = vk_store(2)*ik_store(2);
    P3 = vk_store(3)*ik_store(3);
    P4 = vk_store(4)*ik_store(4);
    P5 = vk_store(5)*ik_store(5);
    P6 = vk_store(6)*ik_store(6);

```

```

fda = (P2-P1) ./ (vk_store(2)-vk_store(1));
fdb = (P4-P3) ./ (vk_store(4)-vk_store(3));
fdc = (P6-P5) ./ (vk_store(6)-vk_store(5));

vk_store(1) = vk_store(3);
ik_store(1) = ik_store(3);
vk_store(2) = vk_store(4);
ik_store(2) = ik_store(4);
vk_store(3) = vk_store(5);
ik_store(3) = ik_store(5);
vk_store(4) = vk_store(6);
ik_store(4) = ik_store(6);

ck = vk_store(4)-1*(fdc*(vk_store(4)-vk_store(2)) ./ (fdc-fdb));

tol = ck-vk_store(6);
if (abs(tol)<0.12)
    stage = 5;
    P= vk_store(4)*ik_store(4);
    Dref = Dref;
else
    Dref = Dref+((vk_store(4)-ck)/V_L) + 0.48/V_L;
    stage = 3;
    index = 5;
end

otherwise
    if(P-vk*ik<1 && P-vk*ik>-1)

        Dref = Dref;
        vk_store = zeros(6,1);
        ik_store = zeros(6,1);
        stage = 5;
        else
            if(stage<6)
                Dref=Dref;
                stage = stage +1;
            else
                vk_store(1)=vk;
                ik_store(1)=ik;
                Dref = Dref - 0.48/V_L;
                vk_store(2:6)=zeros(5,1);
                ik_store(2:6)=zeros(5,1);
                index = 2;
                stage =2;
            end
        end

    end

end
D = Dref;

```

[Bisection Method Algorithm]

```
function [D, out] = MPPT(ik, vk, V_L)

persistent vk_store
persistent ik_store
persistent index
persistent stage
persistent Dref
persistent P

if isempty(vk_store)
    vk_store = zeros(6,1);
    ik_store = zeros(6,1);
    index = 1;
    stage = 0;
    Dref = 0.8;
    P=0;
end

switch stage

    case 0
        Dref=0.8;
        stage = stage +1;

    case 1
        vk_store(index) = vk;
        ik_store(index) = ik;

        Dref = Dref - 0.001; %currently NI9401 1LSB is 0.005
        index = index+1;
        stage = stage +1;

    case 2
        vk_store(index) = vk;
        ik_store(index) = ik;

        P1 = vk_store(1)*ik_store(1);
        P2 = vk_store(2)*ik_store(2);
        P3 = vk_store(3)*ik_store(3);
        P4 = vk_store(4)*ik_store(4);

        if(vk_store(3)==0)
            Dref = Dref +sign(P1-P2)*3/V_L;

            index = index+1;
```

```

        stage = stage -1;

elseif(sign(P2-P1)==sign(P4-P3))
    Dref = Dref +sign(P1-P2)*3/V_L;

    vk_store(1) = vk_store(3);
    ik_store(1) = ik_store(3);
    vk_store(2) = vk_store(4);
    ik_store(2) = ik_store(4);
    index = 3;
    stage = 1;
else

    ck = (vk_store(2)+vk_store(4))./2;

    Dref = Dref+((vk_store(4)-ck)/V_L) + 0.001;

    index = index+1;
    stage = stage +1;
end

case 3
    vk_store(index) = vk;
    ik_store(index) = ik;

    Dref = Dref - 0.001; %currently NI9401 1LSB is 0.005
    index = index+1;
    stage = stage +1;

case 4
    vk_store(index) = vk;
    ik_store(index) = ik;
    P1 = vk_store(1)*ik_store(1);
    P2 = vk_store(2)*ik_store(2);
    P3 = vk_store(3)*ik_store(3);
    P4 = vk_store(4)*ik_store(4);
    P5 = vk_store(5)*ik_store(5);
    P6 = vk_store(6)*ik_store(6);

    if(sign(P6-P5)==sign(P2-P1))

        fdc = (P6-P5)./(vk_store(6)-vk_store(5));

        ck = (vk_store(6)+ vk_store(4))./2;

    else

        fdc = (P6-P5)./(vk_store(6)-vk_store(5));

```

```

        ck = (vk_store(2)+vk_store(6))./2;

    end

    stage = 3;
    index = 5;

    if (fdc<0.15 && fdc>-0.15)
        stage = 5;
        P= vk_store(6)*ik_store(6);
        Dref = Dref;
    else

        Dref = Dref-((ck-vk_store(6))/V_L)+0.001;
    end
    otherwise
        if(P-vk*ik<1 && P-vk*ik>-1)

            Dref = Dref;
            vk_store = zeros(6,1);
            ik_store = zeros(6,1);
            stage = 5;
        else
            if(stage==5)
                Dref=Dref;
                stage = stage +1;
            else
                vk_store(1)=vk;
                ik_store(1)=ik;
                Dref = Dref - 0.001;
                vk_store(2:6)=zeros(5,1);
                ik_store(2:6)=zeros(5,1);
                index = 2;
                stage =2;
            end
        end
    end

end

D = Dref;
out = vk_store;

```

[Regula Falsi Method Algorithm]

```
function [D, outv, outi] = MPPT(ik, vk, V_L)

persistent vk_store
persistent ik_store
persistent index
persistent stage
persistent Dref
persistent P

if isempty(vk_store) % Initialize
    vk_store = zeros(6,1);
    ik_store = zeros(6,1);
    index = 1;
    stage = 0;
    Dref = 0.7;
    P=0;
end

switch stage

    case 0 % Initial Duty Cycle
        Dref=0.25;
        stage = stage +1;

    case 1 % Acuire First Sample
        vk_store(index) = vk;
        ik_store(index) = ik;

        Dref = Dref - 0.48/V_L; % Currently NI9401 1LSB is 0.005
        index = index +1;
        stage = stage +1;

    case 2 % Acuire First Sample Pair
        vk_store(index) = vk;
        ik_store(index) = ik;

        % if(vk_store(2)-vk_store(1)>2 || vk_store(2)-vk_store(1)<0.5)
        % % Check for irradiatin change
        % vk_store(1) = vk_store(2); % Acquire again starting from
here
        % ik_store(1) = ik_store(2);
        %
        % Dref = Dref - 0.48/V_L;
        % index = 2;
        % stage = 2;
        %
```

```

% else

P1 = vk_store(1)*ik_store(1); % Calculate power at each
                               sample
P2 = vk_store(2)*ik_store(2);
P3 = vk_store(3)*ik_store(3);
P4 = vk_store(4)*ik_store(4);

if(vk_store(3)==0) % Check for second sample pair

    Dref = Dref +sign(P1-P2)*4/V_L; % 4 V

    index = index +1;
    stage = stage -1;

elseif(sign(P2-P1)==sign(P4-P3)) % Check if second sample
                                   pair
                                   % is on the same side
    Dref = Dref +sign(P1-P2)*4/V_L;

    vk_store(1) = vk_store(3); % Choose second sample pair
    ik_store(1) = ik_store(3); % as first pair
    vk_store(2) = vk_store(4);
    ik_store(2) = ik_store(4);
    index = 3;
    stage = 1;

else
    fda = (P2-P1)./(vk_store(2)-vk_store(1));
    fdb = (P4-P3)./(vk_store(4)-vk_store(3));
    % Calculate next FP position
    if(P1<P2)
        fpda=fda;
        fpdb=fdb;
    else
        fpda=fda;
        fpdb=fdb;
    end

    ck = (vk_store(2)*fpdb-vk_store(4)*fpda)./(fpdb-fpda);

    Dref = Dref+((vk_store(4)-ck)/V_L) +0.48/V_L;
    % 0.001 is to place first sample at 0.05V before the calculated
    value
    index = index +1;
    stage = stage +1;

% end
end

```



```

case 3
    vk_store(index) = vk; % Acquire new position
    ik_store(index) = ik;

    Dref = Dref - 0.48/V_L; %currently NI9401 1LSB is 0.005
    index = index +1;
    stage = stage +1;

case 4 % Acquire new position pair
    vk_store(index) = vk;
    ik_store(index) = ik;

%     if(vk_store(6)-vk_store(5)>2|| vk_store(6)-vk_store(5)<0.5)
%         % Check for irradiatin change
%         vk_store(1) = vk_store(6); % Acquire again starting from
here
%         ik_store(1) = ik_store(6);
%         Dref = Dref - 0.48/V_L;
%         vk_store(2:6)=zeros(5,1);
%         ik_store(2:6)=zeros(5,1);
%         index = 2;
%         stage = 2;
%     else

    P1 = vk_store(1)*ik_store(1); % Calculate power at each
sample
    P2 = vk_store(2)*ik_store(2);
    P3 = vk_store(3)*ik_store(3);
    P4 = vk_store(4)*ik_store(4);
    P5 = vk_store(5)*ik_store(5);
    P6 = vk_store(6)*ik_store(6);

    if(sign(P6-P5)==sign(P2-P1))% Check if new position sample
pair
        % is on the same side
        fdb = (P4-P3)./(vk_store(4)-vk_store(3));
        fdc = (P6-P5)./(vk_store(6)-vk_store(5));

        if(P1<P2)
            fpdb=fdb;
            fpdc=fdc;
        else
            fpdb=fdb;
            fpdc=fdc;
        end

        ck = (vk_store(6)*fpdb-vk_store(4)*fpdc)./(fpdb-fpdc);

        vk_store(1) = vk_store(5); %New A

```

```

        ik_store(1) = ik_store(5);
        vk_store(2) = vk_store(6);
        ik_store(2) = ik_store(6);

    else
        fda = (P2-P1)./(vk_store(2)-vk_store(1));
        fdc = (P6-P5)./(vk_store(6)-vk_store(5));

        if(P1<P2)
            fpda=fda;
            fpdc=fdc;
        else
            fpda=fda;
            fpdc=fdc;
        end

        ck = (vk_store(2)*fpdc-vk_store(6)*fpda)./(fpdc-fpda);

        vk_store(3) = vk_store(5); % New B
        ik_store(3) = ik_store(5);
        vk_store(4) = vk_store(6);
        ik_store(4) = ik_store(6);

    end

    stage = 3;
    index = 5;
    tol = ck- vk_store(6);

    if (abs(tol)<0.1) % Check tolerance
        stage = 5;
        P= vk_store(6)*ik_store(6); % Store value
        Dref = Dref;
    else
        Dref = Dref-((ck-vk_store(6))/V_L)+0.48/V_L;
    % end
    end

otherwise
    if(abs(P-vk*ik)<100)% Monitor irradiation change after reaching
MPP

        Dref = Dref; % Keep at MPP
        vk_store = zeros(6,1);
        ik_store = zeros(6,1);
        stage = 5;

    else
        if(stage<6)
            Dref=Dref;
            stage = stage +1;

```

```

        else
            vk_store(1)=vk;
            ik_store(1)=ik;
            Dref = Dref - 0.48/V_L;
            vk_store(2:6)=zeros(5,1);
            ik_store(2:6)=zeros(5,1);
            index = 2;
            stage = 2;
        end
    end
end

D = Dref;
outv = vk_store;
outi = ik_store;

```

[Modified Regula Falsi Method Algorithm]

```

function [D, outv, outi] = MPPT(ik, vk, V_L)

persistent vk_store
persistent ik_store
persistent index
persistent stage
persistent Dref
persistent P

if isempty(vk_store) % Initialize
    vk_store = zeros(6,1);
    ik_store = zeros(6,1);
    index = 1;
    stage = 0;
    Dref = 0.7;
    P=0;
end

switch stage

    case 0 % Initial Duty Cycle
        Dref=0.25;
        stage = stage +1;

    case 1 % Acuire First Sample
        vk_store(index) = vk;
        ik_store(index) = ik;

        Dref = Dref - 0.48/V_L; % Currently NI9401 1LSB is 0.005
        index = index +1;
        stage = stage +1;

```

```

case 2                                % Acuire First Sample Pair
    vk_store(index) = vk;
    ik_store(index) = ik;

%     if(vk_store(2)-vk_store(1)>2 || vk_store(2)-vk_store(1)<0.5)
%                                     % Check for irradiatin change
%     vk_store(1) = vk_store(2); % Acquire again starting from
here
%     ik_store(1) = ik_store(2);
%
%     Dref = Dref - 0.48/V_L;
%     index = 2;
%     stage = 2;
%
% else

    P1 = vk_store(1)*ik_store(1); % Calculate power at each
                                sample
    P2 = vk_store(2)*ik_store(2);
    P3 = vk_store(3)*ik_store(3);
    P4 = vk_store(4)*ik_store(4);

    if(vk_store(3)==0) % Check for second sample pair

        Dref = Dref +sign(P1-P2)*4/V_L; % 4 V

        index = index +1;
        stage = stage -1;

    elseif(sign(P2-P1)==sign(P4-P3)) % Check if second sample
                                    pair
                                    % is on the same side
        Dref = Dref +sign(P1-P2)*4/V_L;

        vk_store(1) = vk_store(3); % Choose second sample pair
        ik_store(1) = ik_store(3); % as first pair
        vk_store(2) = vk_store(4);
        ik_store(2) = ik_store(4);
        index = 3;
        stage = 1;

    else
        fda = (P2-P1)./(vk_store(2)-vk_store(1));
        fdb = (P4-P3)./(vk_store(4)-vk_store(3));
                                % Calculate next FP position
        if(P1<P2)

```

```

        fpda=fda;
        fpdb=fdb/2;
    else
        fpda=fda/2;
        fpdb=fdb;
    end

    ck = (vk_store(2)*fpdb-vk_store(4)*fpda)./(fpdb-fpda);

    Dref = Dref+((vk_store(4)-ck)/V_L) +0.48/V_L;
    % 0.001 is to place first sample at 0.05V before the calculated
value
    index = index +1;
    stage = stage +1;
    % end
end

case 3
    vk_store(index) = vk; % Acquire new position
    ik_store(index) = ik;

    Dref = Dref - 0.48/V_L; %currently NI9401 1LSB is 0.005
    index = index +1;
    stage = stage +1;

case 4 % Acquire new position pair
    vk_store(index) = vk;
    ik_store(index) = ik;

%     if(vk_store(6)-vk_store(5)>2|| vk_store(6)-vk_store(5)<0.5)
%         % Check for irradiatin change
%         vk_store(1) = vk_store(6); % Acquire again starting from
here
%         ik_store(1) = ik_store(6);
%         Dref = Dref - 0.48/V_L;
%         vk_store(2:6)=zeros(5,1);
%         ik_store(2:6)=zeros(5,1);
%         index = 2;
%         stage = 2;
%     else

    P1 = vk_store(1)*ik_store(1); % Calculate power at each
sample
    P2 = vk_store(2)*ik_store(2);
    P3 = vk_store(3)*ik_store(3);
    P4 = vk_store(4)*ik_store(4);
    P5 = vk_store(5)*ik_store(5);
    P6 = vk_store(6)*ik_store(6);

    if(sign(P6-P5)==sign(P2-P1)) % Check if new position sample

```

pair

```
                                % is on the same side
fdb = (P4-P3)./(vk_store(4)-vk_store(3));
fdc = (P6-P5)./(vk_store(6)-vk_store(5));

    if(P1<P2)
        fpdb=fdb/2;
        fpdc=fdc;
    else
        fpdb=fdb;
        fpdc=fdc/2;
    end

    ck = (vk_store(6)*fpdb-vk_store(4)*fpdc)./(fpdb-fpdc);

    vk_store(1) = vk_store(5); %New A
    ik_store(1) = ik_store(5);
    vk_store(2) = vk_store(6);
    ik_store(2) = ik_store(6);

else
    fda = (P2-P1)./(vk_store(2)-vk_store(1));
    fdc = (P6-P5)./(vk_store(6)-vk_store(5));

    if(P1<P2)
        fpda=fda;
        fpdc=fdc/2;
    else
        fpda=fda/2;
        fpdc=fdc;
    end

    ck = (vk_store(2)*fpdc-vk_store(6)*fpda)./(fpdc-fpda);

    vk_store(3) = vk_store(5); % New B
    ik_store(3) = ik_store(5);
    vk_store(4) = vk_store(6);
    ik_store(4) = ik_store(6);

end

stage = 3;
index = 5;
tol = ck- vk_store(6);

    if (abs(tol)<0.1) % Check tolerance
        stage = 5;
        P= vk_store(6)*ik_store(6); % Store value
        Dref = Dref;
    else
        Dref = Dref-((ck-vk_store(6))/V_L)+0.48/V_L;
```

```

%     end
end

otherwise
    if(abs(P-vk*ik)<1)% Monitor irradiation change after reaching MPP

        Dref = Dref; % Keep at MPP
        vk_store = zeros(6,1);
        ik_store = zeros(6,1);
        stage = 5;

    else
        if(stage<6)
            Dref=Dref;
            stage = stage +1;
        else
            vk_store(1)=vk;
            ik_store(1)=ik;
            Dref = Dref - 0.48/V_L;
            vk_store(2:6)=zeros(5,1);
            ik_store(2:6)=zeros(5,1);
            index = 2;
            stage = 2;
        end
    end
end

D = Dref;
outv = vk_store;
outi = ik_store;

```

A.2 LABVIEW VI'S

This appendix includes the LabVIEW vi's used to get the experimental results in Chapter 6.

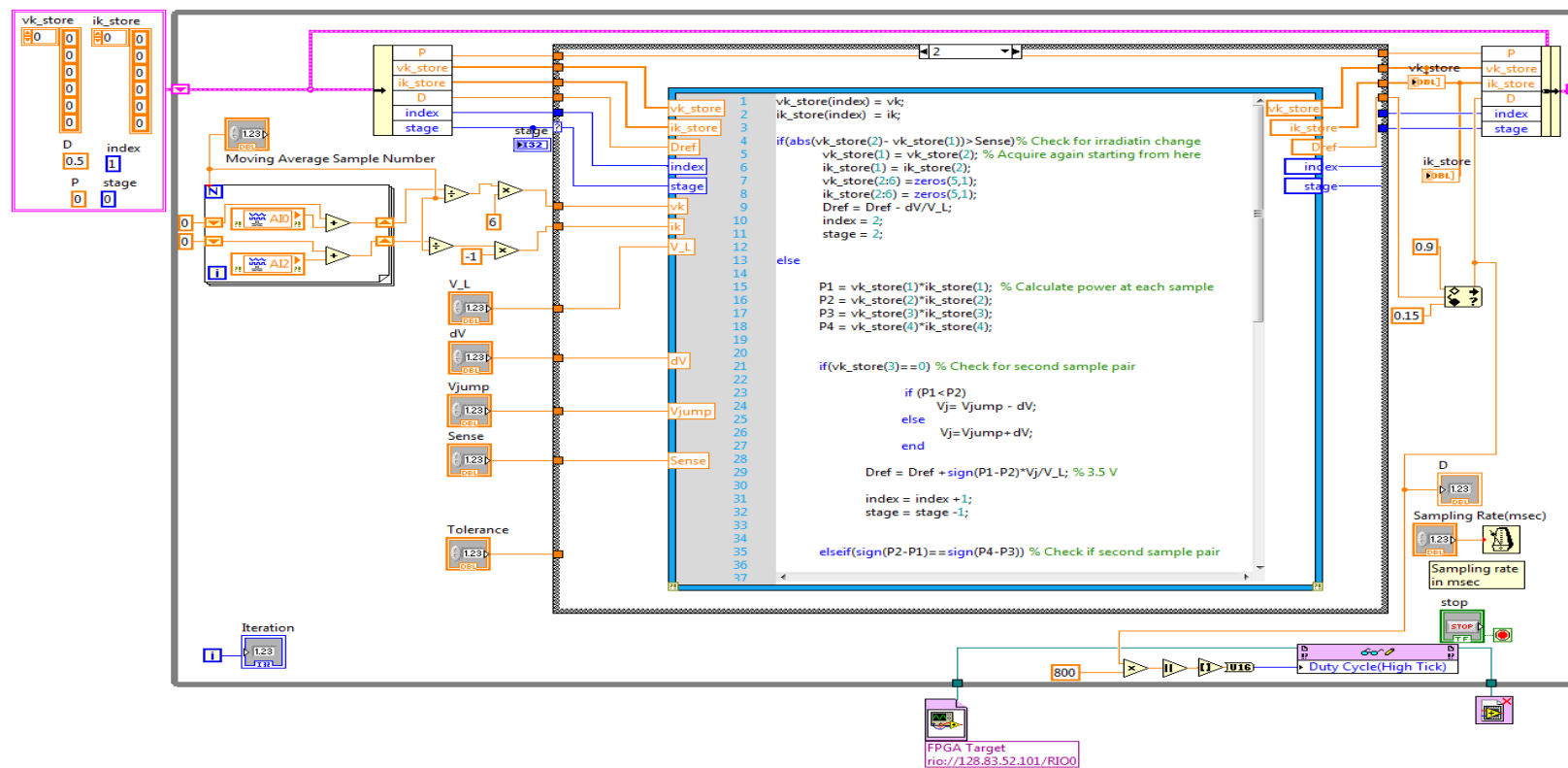


Figure A2.1 : VI of MRFM DMPPT

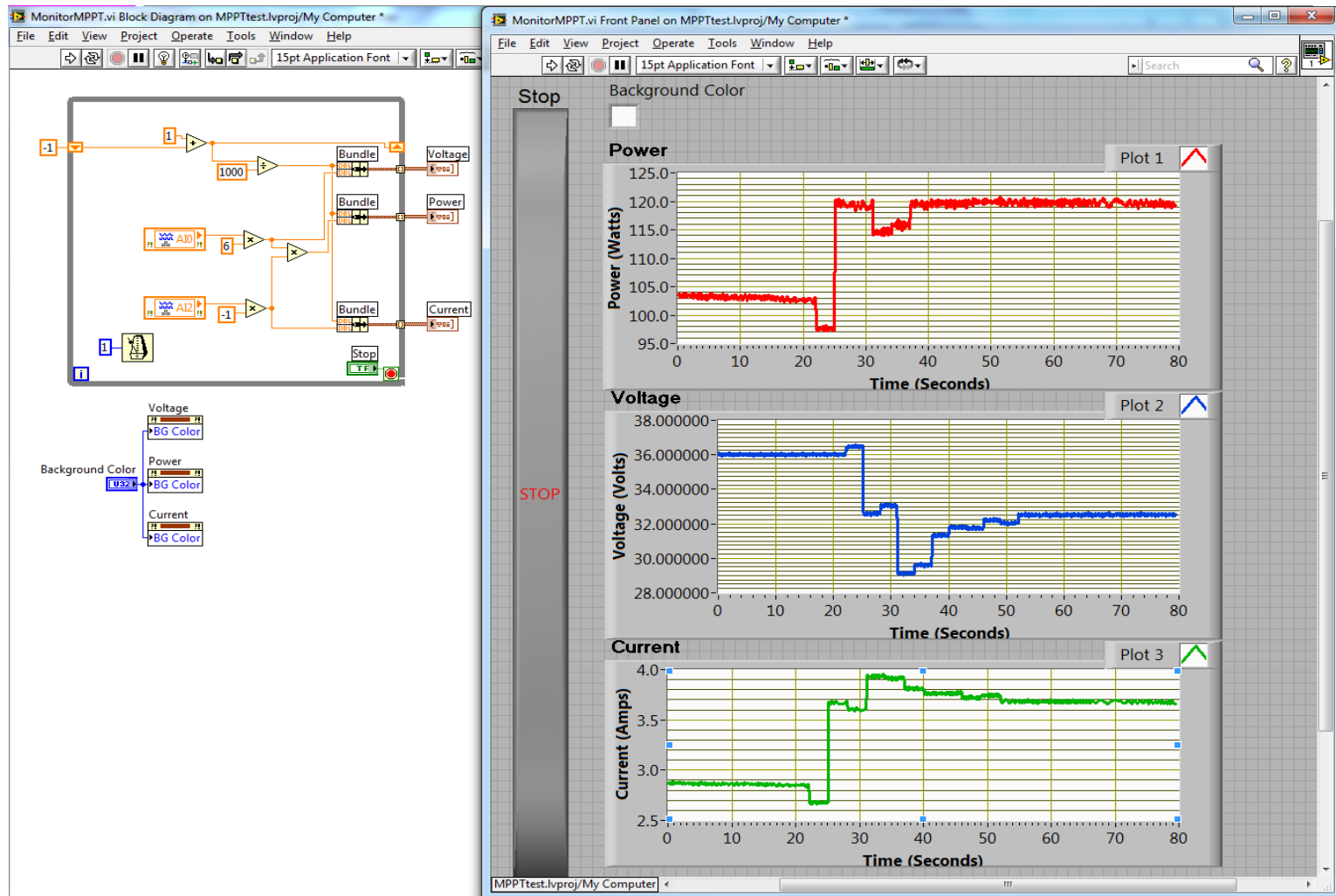


Figure A2.2 : VI of Monitoring the Generated Power, Panel Voltage and Panel Current

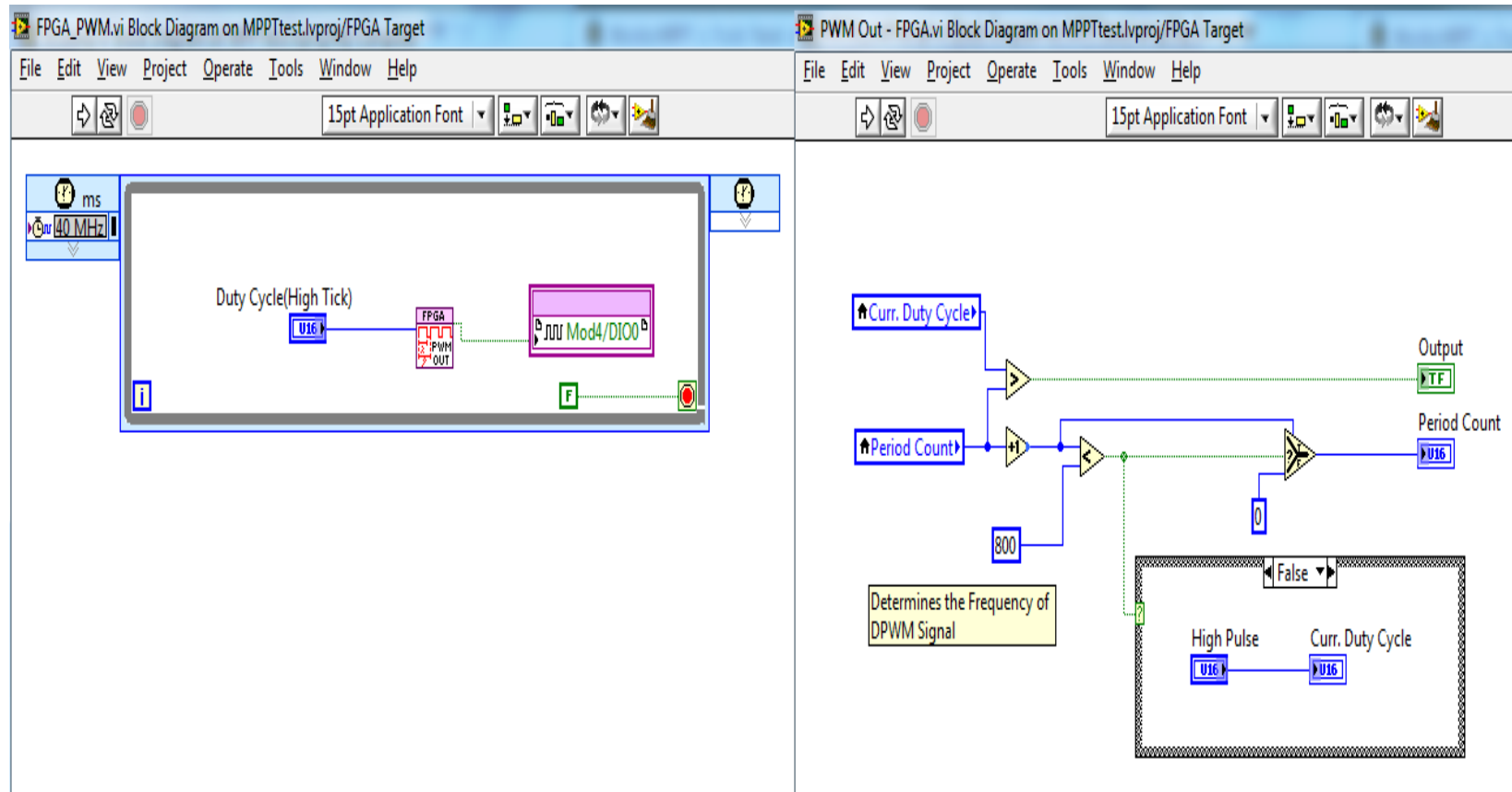


Figure A2.4 : VI of DPWM generating code that is embedded in FPGA of NI CompactRIO

References

- [1] World Energy Outlook 2009 Published Nov 10 2009 by International Energy Agency.
- [2] American Energy: "The Renewable Path to Energy Security," Worldwatch Institute. September 2006. [Online]. Available:
<http://www.worldwatch.org/files/pdf/AmericanEnergy.pdf>.
- [3] NREL, "Best Research Cell Efficiencies," [Online]. Available :
http://www.nrel.gov/pv/thin_film/docs/kaz_best_research_cells.ppt.
- [4] Ryan Wiser, et al., "Letting the Sun Shine on Solar Costs: An Empirical Investigation of Photovoltaic Cost Trends in California," [Online]. Available:
<http://eetd.lbl.gov/ea/ems/reports/59282.pdf>.
- [5] U.S. Department of Energy, "Guide to Tribal Energy Development," [Online]. Available:
http://www1.eere.energy.gov/tribalenergy/guide/costs_solar_photovoltaics.html.
- [6] T. Esum and P. Chapman, "Comparison of Photovoltaic Array Maximum Power Point Tracking Techniques," IEEE Transaction on Energy Conversion, vol. 22, no. 2, pp. 439–449, June 2007.
- [7] S. Busso and P. Mattavelli, "Digital Control in Power Electronics," Morgan & Claypool Publishers, San Rafael, CA , 2006.
- [8] J. W. Kimball, and P. T. Krein, "Discrete-time ripple correlation control for maximum power point tracking," IEEE Transactions on Power Electronics, vol. 23, no. 5, pp. 2353–2362, September 2008.

- [9] F. Liu , S. Duan , F. Liu , B. Liu and Y. Kang "A variable step size INC MPPT method for PV systems", IEEE Transactions on Industrial Electronics, vol. 55, no. 7, pp. 2622- 2008, July 2008.
- [10] B. Shen , B Mwinyiwiwa , Y. Zhang and B.-T. Ooi "Sensorless maximum power point tracking of wind by DFIG using rotor position phase lock loop (PLL)", IEEE Transactions on Power Electronics, vol. 24, no. 4, pp. 942 2009, April 2009.
- [11] Rae-Young Kim, Jih-Sheng Lai, York, B., Koran, A. "Analysis and Design of Maximum Power Point Tracking Scheme for Thermoelectric Battery Energy Storage System", IEEE Transactions on Industrial Electronics, vol. 56, no. 9, pp. 3709, September 2009.
- [12] E. Koutroulis, K. Kalaitzakis, and N. C. Voulgaris, "Development of a Microcontroller-based, Photovoltaic Maximum Power Point Tracking control system,"IEEE Trans. Power Electron., vol. 16, no. 1, pp. 46–54, Jan. 2001.
- [13] C. Hua, J. Lin, and C. Shen, "Implementation of a DSP-controlled Photovoltaic System with Peak Power Tracking," IEEE Trans. Ind. Electron., vol. 45, pp. 99–107, Feb. 1998.
- [14] C. R. Sullivan and M. J. Powers, "A High-efficiency Maximum Power Point Tracker for Photovoltaic Arrays in a Solar-powered Race Vehicle," Proc. IEEE Power Electron. Spec. Conf., pp. 574 - 580, Jun. 1993.

- [15] Maheshappa et al., 1998 H.D. Maheshappa, J. Nagaraju and M.V. Krishna Murthy, "An Improved Maximum Power Point Tracker Using a Step-up Converter with Current Locked Loop," *Renewable Energy* vol. 13, no. 2, pp. 195–201, Feb. 1998.
- [16] M. A. S. Masoum, H. Dehbonei, and E. F. Fuchs, "Theoretical and Experimental Analyses of Photovoltaic Systems with Voltage and Current Based Maximum Power-point Tracking," *IEEE Trans. Energy Conversion*, vol. 17, pp. 514–522, Dec. 2002.
- [17] Salameh Z, Dagher F, Lynch W. "Step-down Maximum Power Point Tracker for Photovoltaic Systems," *Solar Energy*, vol. 46, no. 5, pp. 279–282, 1991.
- [18] N. Femia, G. Petrone, G. Spagnuolo, et al, "Perturb and Observe MPPT Technique Robustness Improved," in *Proceedings of IEEE International Symposium on Industrial Electronics*, vol. 2, pp. 845-852, May 2004.
- [19] N. Femia , G. Petrone , G. Spagnuolo and M. Vitelli "Optimization of perturb and observe maximum power point tracking method", *IEEE Transactions on Power Electronics*, vol. 20, pp. 963-973, July 2005.
- [20] K. H. Hussein et al., "Maximum Photovoltaic Power Tracking: An Algorithm for Rapidly Changing Atmospheric Conditions," *Proc. Inst. Elect. Eng.* vol. 142, pt. G, no. 1, pp. 59–64, Jan. 1995.
- [21] W. Xiao, W. G. Dunford, "A Modified Adaptive Hill Climbing MPPT Method for Photovoltaic Power Systems," in *Proceedings of IEEE 35th Annual Power Electronics Specialists Conference*, vol. 3, pp. 1957-1963, Jun. 2004.

- [22] Fang Luo, Pengwei Xu, YongKang, Shangxu Duan. "A Variable Step Maximum Power Point Tracking Method Using Differential Equation Solution," Second IEEE Conference on Industrial Electronics and Applications, pp. 2259-2263, May 2007.
- [23] Wang Peng, et al., "A Novel Approach of Maximizing Energy Harvesting in Photovoltaic Systems Based on Bisection Search Theorem," The Applied Power Electronics Conference and Exposition (APEC2010), February 21-25, 2010, Palm Springs, CA, USA.
- [24] Seunghyun Chun, Alexis Kwasinski, "Modified Regula Falsi Optimization method approach to Digital Maximum Powerpoint Tracking for Photovoltaic Application," To be presented at The Applied Power Electronics Conference and Exposition (APEC2011), March 6-10, 2011, Fort Worth, TX USA
- [25] T. Shimizu, M. Hirakata, T. Kamezawa, and H. Watanabe, "Generation control circuit for photovoltaic modules", IEEE Transactions on Power Electronics, vol. 16, no. 3, pp. 293 - 300, May 2001.
- [26] A. Kwasinski, "Identification of Feasible Topologies for Multiple-Input dc-dc Converters," IEEE Transactions on Power Electronics, vol. 24, no. 3, pp. 856-861, March 2009.
- [27] Khaligh, A.; Jian Cao; Young-Joo Lee; , "A Multiple-Input DC–DC Converter Topology," IEEE Transactions on Power Electronics, vol.24, no.3, pp.862-868, March 2009

- [28] Li, Y.; Ruan, X.; Yang, D.; Liu, F.; K. Tse, C.; "Synthesis of Multiple-Input DC/DC Converters," IEEE Transactions on Power Electronics, vol.25, no.9, pp.2372-2385, Sept. 2010
- [29] M. G. Villalva, J. R. Gazoli, E. Ruppert F. "Comprehensive Approach to Modeling and Simulation of Photovoltaic Arrays," IEEE Transactions on Power Electronics, vol. 25, no. 5, pp. 1198--1208, May 2009.
- [30] L. Richard Burden and J. Douglas Faires, Numerical Analysis, PWSKENT (1989) ISBN 0-534-93219-3
- [31] Naghipoor, J., Ahmadian S.A., and Soheili, A.R., "An Improved Regula Falsi Method for Finding Simple Zeros of Nonlinear Equations," Applied Mathematical Sciences, vol. 2, no. 8, pp.381-386, 2008.
- [32] M. Dowell and P. Jarratt, "The Pegasus method for computing the root of an equation," BIT 12 (1972), 503–508.
- [33] R. F. King, "An improved Pegasus method for root finding," BIT 13 (1973), 423–427.
- [34] M. Dowell and D. Jarratt, "A Modified Regula Falsi Method for Computing the Root of an Equation," BIT vol. 11, no. 2, pp. 168-174, 1991.
- [35] R.F. King, "Methods without Secant steps for finding a bracketed root," Computing vol 7, no. 1, pp 49-57.
- [36] J.A. Ford, "Improved algorithms of Illinois-type for the numerical solution of nonlinear equations," Technical Report CSM-257, University of Essex (1995)

- [37] SHARP, "Data Specification Sheet," [Online]. Available : http://files.sharppusa.com/Downloads/Solar/Products/sol_dow_NE170U1.pdf
- [38] Application Report "Voltage Mode Boost Converter Small Signal Control Loop Analysis Using the TPS61030," TI Literature Number SLVA274A.
- [39] P. T. Krein, Elements of Power Electronics. New York, NY: Oxford University Press, 1998.
- [40] H. Patel and V. Agarwal "MATLAB-based modeling to study the effects of partial shading on PV array characteristics", IEEE Trans. Energy Convers., vol. 23, p.302 , 2008.
- [41] M. C. Alonso-Gracia , J. M. Ruiz and F. Chenlo "Experimental study of mismatch and shading effects in the IV characteristic of a photovoltaic module ", Solar Energy Mater. Solar Cells, vol. 90, p.329 , 2006.
- [42] M. Miyatake, T. Inada, I. Hiratsuka, H. Zhao, H. Otsuka, and M. Nakano, "Control characteristics of a Fibonacci-search-based maximum power point tracker when a photovoltaic array is partially shaded," in Proc. IEEE IPEMC, 2004, vol. 2, pp. 816–821.
- [43] K. Irisawa, T. Saito, I. Takano, and Y. Sawada, "Maximum power point tracking control of photovoltaic generation system under non-uniform insolation by means of monitoring cells," in Proc. PV Specialists Conference , pp. 1707-1710, 2000.
- [44] E. V. Solodovnik, S. Liu, and R. A. Dougal, "Power controller design for maximum power tracking in solar installations," IEEE Trans. Power Electron., vol. 19, no. 5, pp. 1295–1304, Sep. 2004.

- [45] Dhople, S.V., Ehlmann, J.L., Davoudi, A., Chapman, P.L., "Multiple-input boost converter to minimize power losses due to partial shading in photovoltaic modules," in IEEE Energy Conversion Congress and Exposition (ECCE), pp. 2633 - 2636, Sept. 2010
- [46] R. Bruendlinger, B. Bletterie, M. Milde, and H. Oldenkamp, "Maximum power point tracking performance under partially shaded PV array conditions", in Proc. 21st EUPVSEC, Dresden, Germany, pp. 2157-2160, Sept. 2006.
- [47] K.Kobayashi, I. Takano, and Y. Sawada, "A study on a two stage maximum power point tracking control of a photovoltaic system under partially shaded insolation conditions," in IEEE Power Eng. Soc.Gen.Meet., pp. 2612–2617, 2003
- [48] H. Patel and V. Agarwal, "Maximum Power Point Tracking Scheme for PV Systems Operating Under Partially Shaded Conditions," in Industrial Electronics, IEEE Transactions on, Volume 55, Issue 4, pp. 1689 – 1698, 2008
- [49] Young-Hyok Ji, Jun-Gu Kim, Sang-Hoon Park, Jae-Hyung Kim, Chung-Yuen Won, "C-language based PV array simulation technique considering effects of partial shading", Industrial Technology, 2009. ICIT 2009. IEEE International Conference on, pp.1 - 6 Feb. 2009
- [50] Young-Hyok Ji, Doo-Yong Jung, Chung-Yuen Won, Byoung-Kuk Lee, Jin-Wook Kim, "Maximum Power Point Tracking Method for PV Array under Partially Shaded Condition", IEEE Energy Conversion Congress and Exposition 2009, pp. 307 - 312, Sept. 2009

- [51] Kar, A. "A New Maximum Power Point Tracking Algorithm for PV Modules under Partial Shading and Rapidly Varying Illumination", IEEE India Conference (INDICON), pp. 1-4, Dec. 2009
- [52] Shubhajit Roy Chowdhurya, Hiranmay Saha, "Maximum power point tracking of partially shaded solar photovoltaic arrays", Solar Energy Materials and Solar Cells, vol. 94, no. 9, pp. 1441-1447, Sept. 2010
- [53] A. Kwasinski, "Identification of Feasible Topologies for Multiple-Input DC-DC Converters," IEEE Trans. Power Electronics, vol. 24, pp. 856-861, March 2009.
- [54] Y. Liu and Y. M. Chen, "A systematic approach to synthesizing multi input DC-DC converters," IEEE Trans. Power Electron., vol. 24, no. 2, pp. 116-127, Jan. 2009.
- [55] B. G. Dobbs and P. L. Chapman, "A multiple-input DC-DC converter topology," in Proc. IEEE Power Electron. Letter , vol. 1, pp. 6-9. Mar, 2003
- [56] N. D. Benavides and P. L. Chapman, "Power budgeting of a multiple input buck-boost converter," IEEE Trans. Power Electron., vol. 20, no. 6, pp. 1303-1309, Nov. 2005.
- [57] H. Matsuo, W. Lin, F. Kurokawa, T. Shigemizu, and N. Watanabe, "Characteristics of the multiple-input DC-DC converter," IEEE Trans. Ind. Appl., vol. 51, no. 3, pp. 625-631, Jun. 2004.
- [58] A. Khaligh, J. Cao, and Y. Lee, "A multiple-input DC-DC converter topology," IEEE Trans. Power Electron., vol. 24, no. 3, pp. 862-868, Mar. 2009.

- [59] Y. M. Chen, Y. C. Liu, and F. Y. Wu, "Multi-input DC/DC converter based on the multiwinding transformer for renewable energy applications," *IEEE Trans. Ind. Appl.*, vol. 38, no. 4, pp. 1096–1104, Aug. 2002.

Vita

Seunghyun Chun was born in Seoul, Korea (Republic of Korea) in 1975, to ChangHwan Chun and KeeWha Lee. After graduating from Taejeon High School, Taejeon, Korea, he attended Yonsei University, Seoul, Korea, receiving a Bachelor of Science degree in Electrical Engineering in February, 2002 and then went on to attend The University of Southern California, Los Angeles, CA, receiving a Master of Science degree in May 2004. Since then Mr. Chun has been pursuing a Ph.D. degree in the Department of Electrical and Computer Engineering at the University of Texas at Austin. He was admitted to candidacy in the Doctoral program in August 2010. After graduation he will join the School of Engineering faculty at California Baptist University, Riverside, CA as an Assistant Professor.

Permanent address : Banpo2Dong Hanshin1cha Apt. 7-201

Seoul, South Korea (Republic of Korea)

This dissertation was typed by the author.